

*Kim Georg Lind Pedersen*

# **Poor Man's Scaling for the Nonequilibrium Kondo Problem and Antiferromagnetic Correlations in Optical Lattices**

**ad finem calculations**

Master's Thesis, July 2009

Poor Man's Scaling for the Nonequilibrium Kondo Problem and Antiferromagnetic Correlations in Optical Lattices, ad finem calculations

**This report was prepared by**

Kim Georg Lind Pedersen

**Supervisors**

Jens Paaske

Georg M. Bruun

Brian M. Andersen

Theory for Nanosystems  
Niels Bohr Institute  
Copenhagen University  
Universitetsparken 5  
DK-2100 København N  
Denmark

[www.nbi.ku.dk](http://www.nbi.ku.dk)

---

Release date: July 31 2009

Edition: First

Comments: This thesis is part of the requirements to achieve the Master of Science Msc.Sc. at Copenhagen University. This thesis represents 60 ECTS points.

Rights: ©Kim Georg Lind Pedersen, 2009

Condensed matter physics has progressed enormously since the turn of the previous century, the progress being fuelled by a strong link between theory and experiment. This link has remained strong over the years, and in a way this thesis confirms this fact. The thesis contains two examples of theoretical research related to the two important sub fields of nanotechnology and cold atomic gases.

Most weight has been given to the topic of the nonequilibrium Kondo problem. This part represents a work in progress, with interesting conclusions to be drawn in this thesis and to be obtained in future work. While the work on antiferromagnetic correlations in optical lattices occupy a smaller part of the thesis, the results has been included in a paper [52] which was submitted to the Physical Review Letters at the beginning of June 2009.

The two parts share certain physical concepts. For one they are both concerned with spin, and the spin exchange interaction is in both cases on the form of the Heisenberg Hamiltonian. But rather than pursuing these accidental similarities the thesis has been split into two parts, also making it more accessible for readers only interested in one of the subjects.

I am greatly indebted to Jens Paaske, Georg Bruun and Brian M. Andersen for their pleasant and patient supervising during this last year. I would like to thank them for enlightening discussions, kind guidance and fruitful co-operation.

I would also like to thank Stephan Weiss for his patience and the interesting discussions and clarifications we have had. Last but not last my thanks also befalls Lena Secher Ejlertsen for kind help and proof reading.

# Contents

---

<b>1</b>	<b>Preface</b>	<b>i</b>
<b>I</b>	<b>Poor man's scaling for the Nonequilibrium Kondo Problem</b>	<b>1</b>
<b>2</b>	<b>Introduction</b>	<b>3</b>
<b>3</b>	<b>The Kondo Effect</b>	<b>5</b>
3.1	The equilibrium Kondo effect . . . . .	5
3.2	Nonequilibrium Kondo Effect . . . . .	13
<b>4</b>	<b>Perturbation Theory</b>	<b>19</b>
4.1	Notation . . . . .	19
4.2	Nonequilibrium Green's Functions . . . . .	20
4.3	The Conduction Electron Self-energy . . . . .	21
4.4	The Conduction Electron Self-energy to Order $J^2$ . . . . .	22
4.5	The Conduction Electron Self-energy to Order $J^3$ . . . . .	24
<b>5</b>	<b>Poor man's scaling on the Keldysh contour</b>	<b>29</b>
5.1	1-loop Calculations . . . . .	31
5.2	The Effective One-Body $S$ -matrix to Order $J$ . . . . .	32
5.3	The Effective One-Body $S$ -matrix to Order $J^2$ . . . . .	32
5.4	Variation . . . . .	37
5.5	The Scaling Equations . . . . .	38
5.6	Solving the scaling equations . . . . .	39
<b>6</b>	<b>The Nonequilibrium Kondo Problem in a Magnetic Field</b>	<b>43</b>
6.1	The Anisotropic Kondo Hamiltonian . . . . .	44
6.2	The Effective $S$ -matrix to Order $J^1$ . . . . .	45
6.3	The Effective $S$ -matrix to Order $J^2$ . . . . .	45
6.4	The Scaling Equations . . . . .	49

---

<b>7</b>	<b>Towards 2-loop Poor Man's Scaling on the Keldysh Contour</b>	<b>53</b>
7.1	Straight Terms . . . . .	54
7.2	Loop terms . . . . .	56
7.3	Scaling Equations . . . . .	57
<b>8</b>	<b>Conclusion and Outlook</b>	<b>59</b>
<b>II</b>	<b>Detection of Antiferromagnetic Correlations in Optical Lattices</b>	<b>61</b>
<b>9</b>	<b>Introduction</b>	<b>63</b>
<b>10</b>	<b>Fermions in Optical Lattices</b>	<b>65</b>
10.1	The Hubbard Model . . . . .	66
10.2	The Heisenberg Model . . . . .	68
10.3	Linear Spin Wave Theory and the Holstein-Primakoff Method . . . . .	69
<b>11</b>	<b>Density Correlation Functions</b>	<b>73</b>
11.1	Parallel Spin Noise . . . . .	73
11.2	Transverse Spin Correlations . . . . .	78
11.3	Density-Density Correlation Function . . . . .	79
<b>12</b>	<b>Results</b>	<b>81</b>
<b>13</b>	<b>Conclusion</b>	<b>85</b>
	<b>References</b>	<b>86</b>
	<b>Appendix</b>	<b>91</b>
<b>A</b>	<b>The Scaling Equations for <math>J_{\pm}</math></b>	<b>91</b>
<b>B</b>	<b>Time Ordering on the Keldysh Contour for 2-loop Calculations</b>	<b>95</b>
<b>C</b>	<b>Matlab code</b>	<b>97</b>
<b>D</b>	<b>Article</b>	<b>101</b>

## Part I

# Poor man's scaling for the Nonequilibrium Kondo Problem

# Introduction

---

A localised spin coupled to the spins of a system of conduction electrons through an antiferromagnetic Heisenberg interaction gives rise to the Kondo effect.

At temperatures and energies well above a characteristic energy scale of the system, referred to as the Kondo temperature  $T_K$ , the Kondo effect leads to a logarithmic dependence of observables with temperatures. Jun Kondo originally showed that such logarithmic dependencies even show up when performing perturbation theory to low order in the coupling strength.

Approaching  $T_K$  the system experiences a cross-over to a complex many-body state with the spin of the conduction electrons, so to say, screening the localised spin. Noziere showed that this low temperature state form is adequately described using Fermi-liquid theory with quasiparticle excitations. [3]

Originally developed in 1964 for the explanation spurred of resistance minima in dilute magnetic alloys, the equilibrium Kondo model has received overwhelming attention, leading to the development of exact solutions in the full temperature regime. The Bethe ansatz method applied by Andrei and Wiegmann [22] allows for computation of thermodynamic properties while Wilson's numerical renormalisation group method captures the features of dynamical properties. Both approaches affirm the fact that the Kondo temperature constitutes the only characteristic energy scale of the system, and thus any physical observable takes the form of a universal function of the dimensionless variable  $T/T_K$  cf. [3]

In Chapter 3 we portray the equilibrium Kondo effect in greater detail. Much weight has been given to the approximate method of Poor man's scaling originally introduced by Anderson[16] in 1970. This method is effectively resums the leading logarithmic terms of perturbation theory and captures the features of the scaling. This method has the appeal of straightforward calculations at the level of ordinary perturbation theory while still providing a fairly good approximation at temperatures above  $T_K$ . We also present a refined version of the approach based on the works by Sólyom and Zawadowski[20] where calculations is carried out to higher order in the coupling strength.

With the advent of nanotechnology the Kondo effect manifested itself in quantum dots weakly coupled to leads. Chapter 3 also describe such a quantum dot system with special care taken to the case of odd number quantum dot occupancy where the excess spin of the dot plays the role of the localised spin of a Kondo model. When below  $T_K$  the Kondo effect enhances

scattering off the dot. This enhanced scattering will sustain a current through the system even when in the Coulomb blockade regime. A wide variety has detected the Kondo effect in quantum dot systems [29], [28]. They show that the application of a bias voltage across the dot destroys the Kondo resonance. Applying a magnetic field the Kondo resonance breaks up and the problem of calculating the physics of the resonances has turned into a true nonequilibrium problem.

A wide variety of techniques has been applied to this problem. We focus on the work carried out by Rosch et al. [31], [32] and Paaske et al. [34], [35]. They have considered the effect of decoherence of the localised spin due to current through the dot. Their method is based on the pseudofermionic description of the localised spin introduced in Ref. [14], for which they propose a set of unsystematically derived scaling relations. The decoherence can then be included consistently through vertex correction of the pseudofermions.

While the pseudofermionic approach is a nice mathematical tool, the focus of this thesis will be to develop a mathematically simpler but inherently more systematic method for deriving the scaling relations. It is the hope that from such a theory the decoherence rates can be derived directly.

In Chapter 4 we carry through with a calculation of the conduction electron self-energy out of equilibrium keeping the dot spin operators as is. The result is found in compliance with calculations based on the pseudofermionic spin representation.

Chapter 5.1 we develop a Poor man's scaling approach to the nonequilibrium Kondo problem in the case of zero magnetic field. Since we are dealing with a new method which lies outside the usual calculations of nonequilibrium problems we have carried out the calculations in great detail. The method is based on the original work done in equilibrium by Sólyom and Zawadowski, and it succeeds in deriving the inherent nonequilibrium scaling equations derived more loosely in Ref. [32]. As a closing remark we also describe the method for obtaining the steady state coupling constants from the scaling as done originally in Ref. [32].

To extend this new Poor man's scaling approach to the case of non-zero magnetic field we introduce the Bloch equation describing the time-evolution of the localised spin. Chapter 6 concern the specific consequences of this idea, and include them into the developed Poor man's scaling method. In this Chapter we also hint a how decoherence may be included into the applied method.

The last Chapter concern the extension of the method to include 2-loop corrections to the scaling equations. The general idea underlining the extension is presented while we will only hint at the direct consequences of including these corrections to the scaling equation.



## The Kondo Effect

---

The main contribution to the resistivity of bulk metal comes from electrons scattering off phonons. This contribution increases enormously with temperature as more and more phonons become excited.

At extremely low temperatures when the contribution from electron-phonon interaction has mostly died out, there is still a remniscent constant contribution from electrons scattering off impurities, defects or vacancies in the lattice.

Summing up, you would expect the resistivity of a metal to be monotonically increasing with temperature.

Thus it came as a surprise when back in 1934 de Haas et al. [12] encountered a low-temperature *resistance minimum* in bulk gold. This hinted at the existence of a low-temperature contribution to resistivity hitherto unaccounted for.

Later experiments for other alloys confirmed the findings of de Haas, and allowed for the deduction of a semi-empirical formula for the unknown contribution to the resistivity [38],

$$\delta\rho(T) = n_i \ln(\varepsilon_F/T). \quad (3.1)$$

Here  $n_i$  is concentration of impurities in the metal, while  $\varepsilon_F$  is the Fermi energy. This linear relationship between resistivity and impurity concentration was even observed at the lowest attainable impurity concentrations, thus suggesting that it is a single impurity effect which does not involve inter-impurity interactions.

Experiments also showed that the susceptibility of alloys with a resistance minimum contained a Curie-Weiss term, which hinted at the presence of local magnetic moments within the alloy. [9]

### 3.1 The equilibrium Kondo effect

It took 30 years of experiments and theoretical trial and error in order to come up with an acceptable explanation. In 1964 Jun Kondo argued that electrons scattering off magnetic impurities in the metal could explain the anomalous contribution to resistivity at very low temperatures.

For his calculations Kondo applied the Hamiltonian

$$H = H_0 + H'. \quad (3.2)$$

The first term describes the unperturbed system of conduction electrons in the metal,

$$H_0 = \sum_{\mathbf{k}\sigma} \varepsilon_{\mathbf{k}} c_{\mathbf{k}\sigma}^\dagger c_{\mathbf{k}\sigma}. \quad (3.3)$$

The second term describes the exchange interaction of the impurity spin  $\mathbf{S}$  with the conduction electron spin density at the impurity site  $\mathbf{s}$ . That is

$$H' = J\mathbf{S} \cdot \mathbf{s} = \frac{1}{2}J \sum_{\mathbf{k}'\mathbf{k},\sigma'\sigma} S^i c_{\mathbf{k}'\sigma}^\dagger \tau_{\sigma'\sigma}^i c_{\mathbf{k}\sigma}. \quad (3.4)$$

Note the use of Einstein notation in the last term where repeated index  $i$  implies the summation over spacial dimensions  $x, y, z$ . The  $\tau^i$  denotes the well-known Pauli matrices

$$\tau^x = \begin{pmatrix} 0 & 1 \\ 1 & 0 \end{pmatrix}, \quad \tau^y = \begin{pmatrix} 0 & -i \\ i & 0 \end{pmatrix}, \quad \tau^z = \begin{pmatrix} 1 & 0 \\ 0 & -1 \end{pmatrix}. \quad (3.5)$$

Assume that the electronic states relevant for conduction are located symmetrically around the electron chemical potential. Physically the width  $2D$  of this conduction electron band could be determined from specific calculations of the actual bandstructure of the metal, but in reality the actual value is unimportant as long as it is large compared to the thermal smearing of the Fermi surface.

From this model Hamiltonian Kondo calculated the contribution to resistivity perturbatively in the coupling strength  $\nu_F J \ll 1$ . Including contributions beyond leading order in  $J$ , the result was,

$$\delta\rho(T) \sim n_i(\nu_F J)^2 \left[ 1 + 2J\nu_F \ln\left(\frac{D}{T}\right) \right]. \quad (3.6)$$

Here  $\nu_F$  is the density of states at the fermi surface. [13],

To order  $J^2$  the contribution to the resistivity is identical to the case of electrons scattering off a regular impurity. However to order  $J^3$  the contribution from multiple scatterings involving an intermediate spinflip of the local spin gives rise to a logarithmic dependence on temperature. Assuming an antiferromagnetic coupling (i.e.  $J > 0$ ) the contribution becomes logarithmically large at low temperatures  $T \ll D$ .

Adding this contribution and the monotonically increasing contribution from the electron-phonon interaction reproduces the resistance minimum. A fit to experimental data presented in Fig. 3.1 shows the excellent agreement with experimental data.

### 3.1.1 The Kondo Temperature

At a glance the Kondo Hamiltonian of Eq. (3.2) does not seem overly complicated. However the impurity spin operator must be handled explicitly. Because the operators does not commute, i.e.  $[S^+, S^-] = 2S_z$ , it is impossible to apply systematical methods as e.g. Wick's theorem.

Abrikosov [14] introduced a fermion representation of the local spin operators

$$S = a_\alpha^\dagger S_{\alpha,\beta} a_\beta. \quad (3.7)$$

Here the  $S_{\alpha,\beta}$  are the spin matrix elements denoting scattering from spin states  $\alpha$  to  $\beta$ . This is a valid representation assuming that the occupation number for all states sums to unity. In order to make sure this holds true, Abrikosov assumed an infinitely large chemical potential, e.g. all states are occupied, and divided the result with the total number of spin states  $(2S + 1)$ .

However unphysical this may seem, it allowed for the calculation of higher order contributions to Eq. (3.6). Considering only contributions to leading order in  $\ln(1/T)$ , the result is a geometric series which may be summed to give

$$\delta\rho(T) \sim n_i \frac{1}{\left(\ln \frac{T}{T_K}\right)^2}. \quad (3.8)$$

We have rewritten the result in terms of the *Kondo temperature*

$$T_K = D e^{-1/2\nu_F J}. \quad (3.9)$$

The result shows that at a temperature  $T = T_K$ , the resistivity diverges. This point marks the breakdown of perturbation theory. The problem of how to extend Kondo's calculations to obtain a satisfactory solution in the low temperature regime,  $T < T_K$ , is what became known as the *Kondo Problem*.

In order to attain some physical intuition about the meaning of the Kondo temperature, we consider the Hamiltonian describing the interaction of two spins

$$J\mathbf{S} \cdot \mathbf{S}. \quad (3.10)$$

For  $J > 0$  the ground state of this Hamiltonian is a spin singlet, and the triplet excitation is separated from the ground state by an energy-gap  $J$ . Thus we think of  $J$  as the binding energy of the singlet.

Replacing one of the spin operators  $\mathbf{S}$  of Eq. (3.10) with the spin density of the conduction electrons  $\mathbf{s}$  the binding energy is no longer determined by the coupling strength  $J$ , but rather the exponentially small  $T_K$ . [33]

### 3.1.2 Poor Man's Scaling

A different approach to the Kondo problem named was devised by Anderson, [16], and is generally referred to as "Poor man's scaling".

Consider Kondo's original result of Eq. (3.6). The logarithmically divergent terms  $\ln(D/T)$ , which marks the breakdown of perturbation theory, depend explicitly on the conduction bandwidth through  $\ln(D)$ . In other cases when e.g. the self-energy depends on only  $1/D$  or  $1/D^2$ , the limit of infinite bandwidth  $D \rightarrow \infty$  is taken without problems. This implies that high energy excitations are unimportant when considering the lower lying states.

On the other hand terms with  $\ln(D)$  diverges in the limit of infinite bandwidth. Hence the high energy states play a crucial role when calculating low energy states.

Anderson considered the consequences for the Kondo Model, when reducing the bandwidth  $D$  by a small amount  $\delta D$ . He applied his reasoning to the case of a spin  $S = \frac{1}{2}$  impurity spin

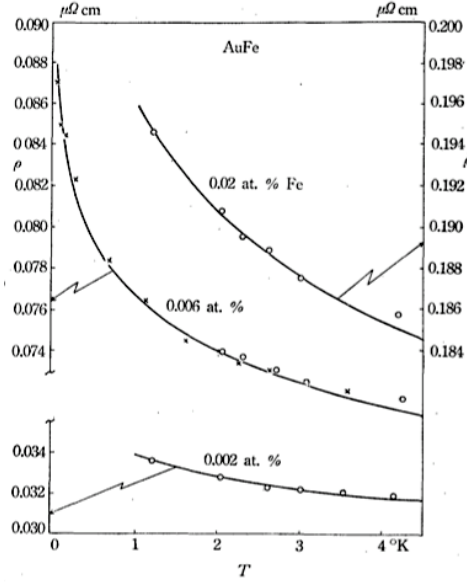


**Figure 3.1:** Comparing resistivity measurements for gold containing magnetic iron impurities, to calculations based on the perturbative expansion of the Kondo model (Reproduced from [13]).

but an anisotropic coupling  $J_x = J_y \neq J_z$ . The resulting anisotropic Kondo Model is,

$$\begin{aligned}
 H &= H_0 + H' \\
 &= \sum_{k\sigma}^{\varepsilon_k \in [-D, D]} \varepsilon_k c_{k\sigma}^\dagger c_{k\sigma} + \sum_{\substack{k_1, \sigma_1 \\ k_2, \sigma_2}} \left[ \frac{J_\pm}{2} (S_+ (s_-)_{\sigma_1 \sigma_2} + S_- (s_+)_{\sigma_1 \sigma_2}) + J_z S_z (s_z)_{\sigma_1 \sigma_2} \right] c_{k_1 \sigma_1}^\dagger c_{k_2 \sigma_2}.
 \end{aligned} \tag{3.11}$$

Here the width of the symmetric conduction electron band has been included explicitly in the Hamiltonian. Note that we have placed the zero-point of energy at the conduction electron chemical potential,  $\mu = 0$ .

The T-matrix for a system described by this Hamiltonian is,

$$T(\omega) = H' + H' G_0(\omega) T(\omega), \tag{3.12}$$

where  $G_0(\omega) = 1/(\omega - H_0)$  is the bare propagator.

The first step is to change the cut-off  $D$  by an infinitesimal amount  $\delta D$ , as depicted on Figure 3.2. Introducing a projection operator  $1 - P$  projecting onto states with only electron or hole-like excitations within the reduced band  $\varepsilon \in [-D + \delta D, D - \delta D]$  the expression for the T-matrix, Eq. (3.12), might be put on a slightly different form

$$T(\omega) = H' + H' P G_0(\omega) T(\omega) + H' (1 - P) G_0(\omega) T(\omega) \tag{3.13}$$

This is an iterative formula for calculating  $T(\omega)$  to arbitrary order. Thus to order  $n$ ,

$$\begin{aligned}
 T(\omega) &= \{ H' + H' P G_0(\omega) H' + \dots + (H' P G_0(\omega))^n H' \} \\
 &\quad + \{ H' + H' P G_0(\omega) H' + \dots + (H' P G_0(\omega))^n H' \} (1 - P) G_0(\omega) T(\omega) \\
 &\quad + (H' P G_0(\omega))^{n+1} T(\omega).
 \end{aligned} \tag{3.14}$$

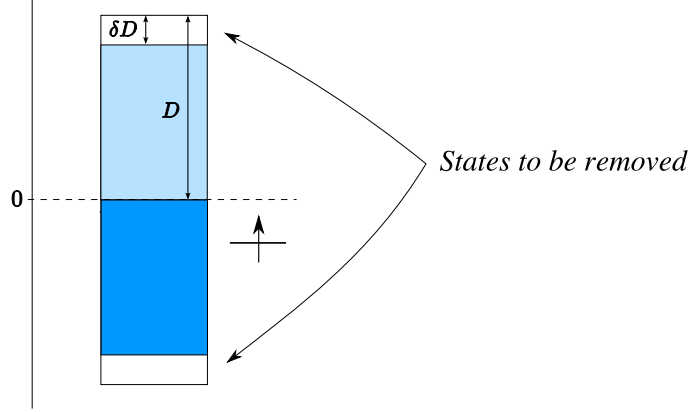


**Figure 3.2:** The conduction electron band consisting of a frozen Fermi sea (darkest blue) and unoccupied states (lighter blue). As shown the zero point of energy has been chosen at the Fermi surface.

When restricting our analysis to the weak coupling limit  $\nu_F J_{\pm}, \nu_F J_z \ll 1$  the last term of the above expression becomes negligible. Multiplying  $(1 - P)$  on both sides of this expression iterated to second order, we get

$$(1 - P)T(\omega)(1 - P) = (1 - P)H'_2(1 - P) + (1 - P)H'_2(1 - P)G_0(\omega)(1 - P)T(\omega)(1 - P), \quad (3.15)$$

where

$$H'_2 = H' + H'PG_0H'. \quad (3.16)$$

Here  $(1 - P)T(\omega)(1 - P)$  describes transitions in a Hilbert space of states within the reduced band.

Next step involves the derivation of the change in the coupling  $\delta H' = H'PG_0H'$ . The two major contributions from this calculations can be drawn as

$$\text{and} \quad (3.17)$$

In these diagrams a line denote bare propagation  $G_0$  while a vertex is an interaction  $H'$ . Lines pointing from left to right symbolise electronic states while lines pointing from right to left symbolise hole states. The thick line designate a state within the cut-off.

Details of the calculation can be found in Refs. [16], [4] and [3]. Here we just state the results. For the two diagrams of Eq. (3.17) Anderson obtained the results

$$\begin{aligned} \frac{\delta H'}{\delta D} = \frac{\nu_F}{2} \sum_{k_1\sigma_1 k_2\sigma_2} c_{k_2\sigma_2}^\dagger c_{k_1\sigma_1} & \left( \frac{1}{\omega - D + \Delta(D) + \varepsilon_{k_1}} + \frac{1}{\omega - D + \Delta(D) - \varepsilon_{k_2}} \right) \\ & \times \left\{ -J_{\pm}^2 S_z(s_z)_{\sigma_2\sigma_1} - \frac{J_{\pm}J_z}{2} (S_+(s_-)_{\sigma_2\sigma_1} + S_-(s_+)_{\sigma_2\sigma_1}) \right\} \end{aligned} \quad (3.18)$$

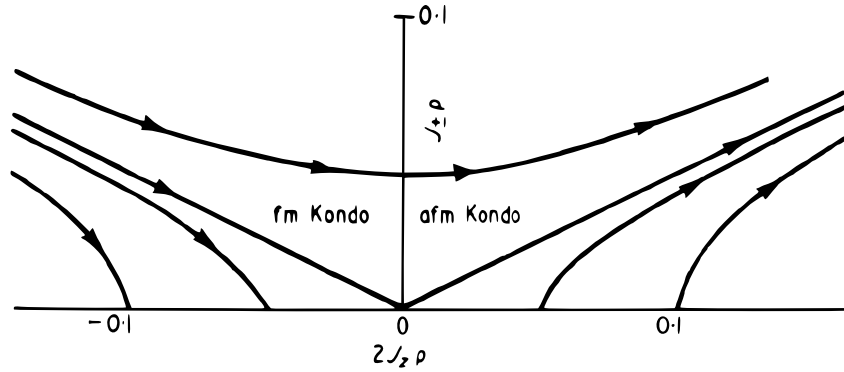


**Figure 3.3:** Scaling equations, arrows shows scaling of coupling constant when lowering  $D$ . Figure reproduced from Ref. [16].

Here  $\Delta(D)$  is a constant shift of the zero of energy. From this result we may deduce that the removal of virtual scattering to the cut-off states to lowest order has effectively changed the coupling strengths, i.e.  $J_{\pm} \rightarrow J_{\pm} + \delta J_{\pm}$  and  $J_z \rightarrow J_z + \delta J_z$ . For  $\varepsilon_{k_2}$  and  $\varepsilon_{k_1}$  close to the Fermi surface the scaling equations are

$$\frac{dJ_z}{dD} = \frac{\nu_F}{D - \omega + \Delta(D)} J_{\pm}^2, \quad (3.19a)$$

$$\frac{dJ_{\pm}}{dD} = \frac{\nu_F}{D - \omega + \Delta(D)} J_z J_{\pm}. \quad (3.19b)$$

Keep in mind that  $\delta D$  - as convention prescribes - has been taken *positive* when decreasing the bandwidth. Hence reducing  $D$  Eq. (3.19a) implies that the coupling strength  $J_z$  increases. Similarly Eq. (3.19b) shows that when  $J_z < 0$  the transverse coupling  $J_{\pm}$  increases, and for  $J_z > 0$  it decreases. Dividing Eq. (3.19a) with (3.19b) and integrating we obtain the scaling trajectories

$$J_{\pm}^2 - J_z^2 = \text{const.} \quad (3.20)$$

which corresponds to the hyperbolas of Figure 3.3. For ferromagnetic couplings, i.e.  $J_z < 0$ , all cases on or below the isotopy can be solved by scaling to the  $J_{\pm} = 0$  case. Antiferromagnetic cases above the isotopy line as well as all cases of antiferromagnetic couplings,  $J_z > 0$  scale towards the strong coupling regime.

Assuming  $\Delta \ll D$  and setting  $\omega = 0$  for the case of isotropic couplings  $J = J_{\pm} = J_z$ , the scaling equations may be put on this suggestive form

$$\frac{dJ}{d \ln D} = \nu_F J^2. \quad (3.21)$$

Integrate this expression from an initial cut-off  $D_0$  and coupling  $J$  to some intermediate cut-off  $D$  and renormalised coupling  $J$ , in order to get

$$-\frac{1}{2\nu_F J_0} - \ln D_0 = -\frac{1}{2\nu_F J} - \ln D. \quad (3.22)$$

This allow us to define an invariant of the scaling

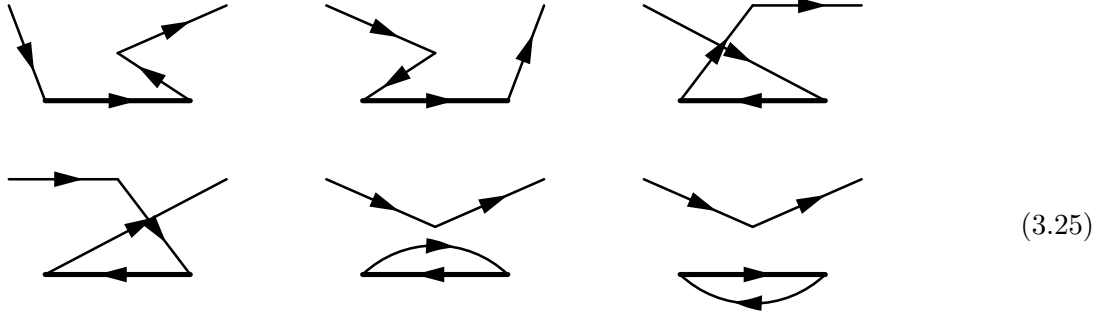
$$T_k = D e^{-1/2J\nu_F}, \quad (3.23)$$

which we recognise as the Kondo temperature of Eq. (3.9). Having reproduced the result for the Kondo temperature as found by Abrikosov, one may conclude that application of the the Poor man's scaling approach one has effectively summed the leading logarithmic terms.

If we wish to include results to higher order in the interaction  $H'$  we may expand the expression for  $(1 - P)T(\omega)(1 - P)$  to

$$H'_3 = H' + H'PG_0H' + H'PG_0PG_0H' + \dots \quad (3.24)$$

One might argue that due to the presence of the  $P$  operators, this contribution is proportional to  $(\nu_F\delta D)^2$ , but this argumentation is invalid. In the diagrammatic representation the following diagrams express the contributions to third order in the interaction proportional to  $(\delta D)^1$ .



For the purpose of determining the next order contribution to the scaling equations Sólyom and Zawadowski adopted a slightly modified version of the Poor man's scaling technique. [20]

They considered the propagation of single particle excited states. The scattering amplitude for propagation from initial state  $|i\rangle$  to the final state  $|f\rangle$  is in this case given by

$$T_{fi} = \langle f|T|i\rangle. \quad (3.26)$$

Assuming that the initial and final states both contain one excited electron

$$|i\rangle = c_{k\sigma}^\dagger|0\rangle \quad |f\rangle = c_{k'\sigma'}^\dagger|0\rangle, \quad (3.27)$$

where  $|0\rangle$  constitutes a noninteracting Fermi sea plus an impurity spin. When changing the cut-off  $D$  by  $\delta D$ , the scattering amplitude remains constant for states within the reduced cut-off. Thus the change of the bandwidth  $D$  must be compensated by a change in the coupling constant. I.e.

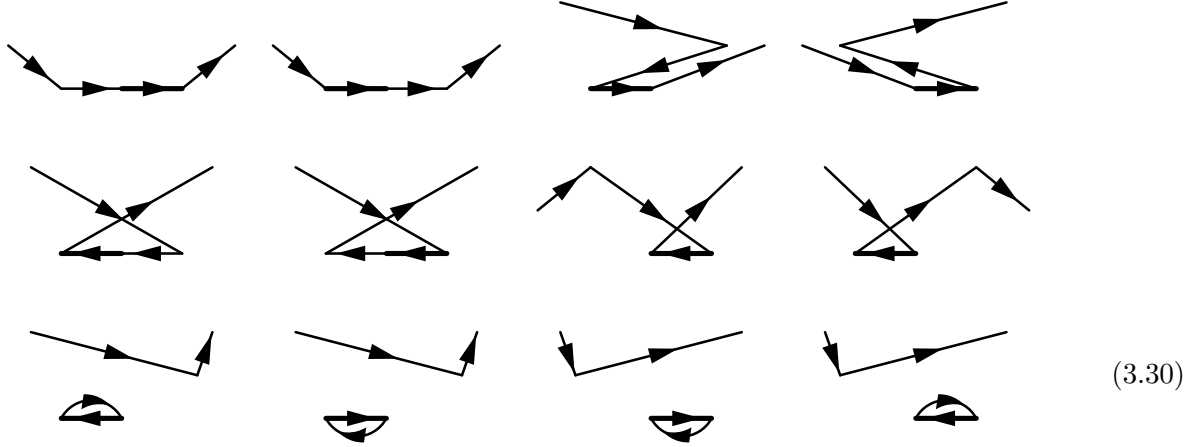
$$T_{fi}(D, J_\pm, J_z) = T_{fi}(D - \Delta D, J_\pm + \Delta J_\pm, J_z + \Delta J_z). \quad (3.28)$$

For small changes this expression can be expanded to first order giving a Callan-Symanzik like scaling equation cf. e.g. ch. 12 of Ref. [5].

$$-\frac{\partial T_{fi}}{\partial D}\Delta D + \frac{\partial T_{fi}}{\partial J_\pm}\Delta J_\pm + \frac{\partial T_{fi}}{\partial J_z}\Delta J_z = 0. \quad (3.29)$$

Calculating the derivatives, plugging into the above equation and collecting terms in front of  $S^z s^z$  and  $\frac{1}{2}(S^+ s^- + S^- s^+)$  respectively, results in two scaling relations for the coupling strengths.

This is not a rewrite of Anderson's original Poor man's scaling. When considering only propagation of single particle states the approach of Sólyom and Zawadowski includes additional diagrams. For the case of third order calculations these additional diagrams may be pictured as



Sólyom and Zawadowski stressed that the last four diagrams play a special role, as they renormalise the initial and final states. For the perturbation expansion one then has to take into account this renormalisation, and hence to third order we will instead need to consider

$$T'_{fi} = \frac{\langle f | H' + H' [1/(\omega - H_0)] T | i \rangle}{\{ \langle f | 1 + [1/(\omega - H_0)] T | f \rangle \langle i | 1 + [1/(\omega - H_0)] T | i \rangle \}^{1/2}}. \quad (3.31)$$

Calculations to second order in  $H'$  reproduce the results obtained by Anderson as the denominator of (3.31) plays no crucial role. For third order calculations this is not the case as two of the four diagrams containing a fermionic loop are cancelled by the denominator.

For some details of their calculation one may refer to Refs. [20], [21] and [3]. The results of their calculations are to third order in  $H'$ ,

$$\frac{dJ_{\pm}}{dD} = \frac{\nu_F}{D} \left[ J_{\pm} J_z - \frac{1}{4} (J_{\pm} J_z^2 + J_{\pm}^3) \nu_F \right], \quad (3.32)$$

$$\frac{dJ_z}{dD} = \frac{\nu_F}{D} \left[ J_z^2 - \frac{1}{2} J_{\pm}^2 J_z \nu_F \right]. \quad (3.33)$$

For the isotropic case the two equations both reduce to

$$\frac{dJ}{d \ln D} = \nu_F J^2 - \frac{1}{2} \nu_F^2 J^3. \quad (3.34)$$

First notice that  $\nu_F J = 2$  is a fixed point for this scaling equation. If  $\nu_F J \neq 2$  the scaling equation can be integrated from initial cut-off  $D_0$  and coupling  $J_0$  to final values  $D$  and  $J$ . This defines the constant of scaling,  $T_k$ .

$$\ln D_0 - \frac{1}{2\nu_F J_0} + \frac{1}{4} \ln \left( \frac{\nu_F J_0}{|\nu_F J_0 - 1|} \right) = \ln D - \frac{1}{2\nu_F J} + \frac{1}{4} \ln \left( \frac{\nu_F J}{|\nu_F J - 1|} \right) = \ln T_k. \quad (3.35)$$

Applying the assumption of  $\nu_F J \approx 0$  isolation of  $T_k$  yields

$$T_k = D \sqrt{2\nu_F J} e^{-1/2\nu_F J}. \quad (3.36)$$



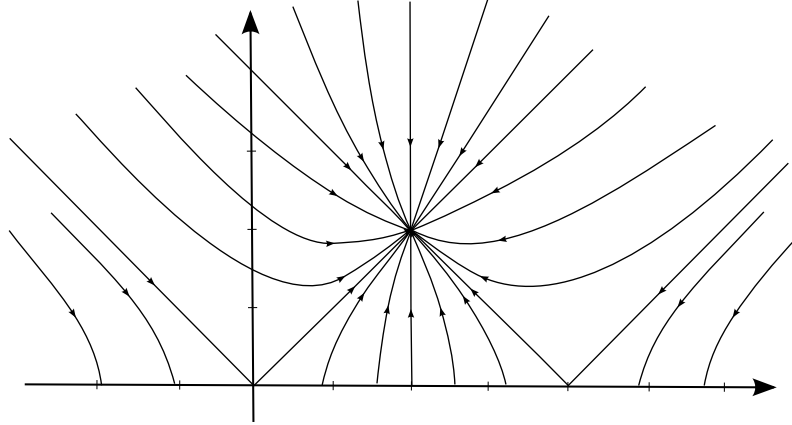


**Figure 3.4:** Scaling diagrams follow arrows as  $D$  decrease. Note the fixed point at  $J_{\pm} = J_z = 2$ . Figure reproduced from [20].

One interpretation of this “corrected” Kondo temperature is that the inclusion of third order corrections has effectively reduced the temperature at which the coupling scales to infinity, and the method breaks down. In terms of the previously calculated value for the Kondo temperature,  $T_k^{(2)}$ , the corrected Kondo temperature  $T_k^{(3)} = T_k^{(2)} \sqrt{2\nu_F J} \ll T_k^{(2)}$ . Thus  $\nu_F J$  will increase at a smaller pace. This will effectively lead to a lowering of the Kondo temperature.

In the general case of anisotropic couplings the scaling diagram of Figure 3.4 applies, all though one should keep in mind that the method is still restricted to the case of perturbatively weak couplings.

## 3.2 Nonequilibrium Kondo Effect

The birth of nanotechnology has made it possible to fabricate miniature electronic systems, which allow for minute control of the system parameters.

### 3.2.1 The Quantum Dot System

One such system is the quantum dot which constitutes electrons confined in all three dimensions. Adding electrons to the dot fill up a shell-like structure, much like atomic orbitals. The energy difference between the two highest occupied levels of the dot is denoted  $\delta E$ . The electrostatic potential  $V_G$  of a close-by gate electrode allows for shifting the levels by a constant energy.

Coupling the quantum dot to two conducting leads permit electrons to tunnel between the leads and the dot. It is normal to distinguish the leads by referring to them as the *left lead* and the *right lead*. Shift the electrochemical potentials  $\mu_L$  and  $\mu_R$  of the left and right lead respectively in order to create a bias voltage  $V_{bias} = \mu_L - \mu_R$  across the system.

Quantum dot systems may be fabricated in various ways. A quantum dot coupled to two leads may be realized as organic molecules, small clusters of atoms or carbon nanotubes coupled weakly to two massive conductors.

Another possibility considers the creation of a 2-dimensional electron gas (2DEG) on the surface between two semiconductor sheets (e.g. GaAs) using molecular beam epitaxy. By means of lithography, leads may be added on top of the semiconductors. Applying a potential to these

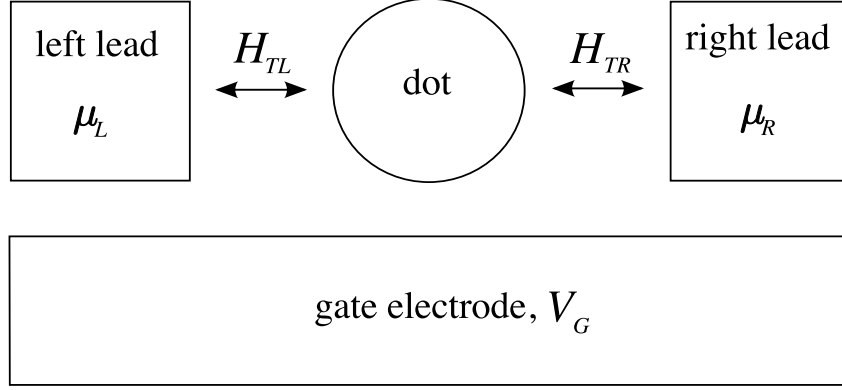


Figure 3.5: Quantum dot system

leads creates the confining potential of the dot along with tunnelling junctions to the 2DEG. Varying the potential of these leads also allow for minute control coupling strengths between the dot and left and right lead.

Consider the quantum dot in the sequential tunnelling regime, where tunnelling events onto and out of the dot are uncorrelated, allowing us to consider single tunnelling events only.

The classical electrostatic energy associated with charging the dot is

$$E(q) = \frac{q^2}{2C} - q \frac{C_G}{C} V_G, \quad (3.37)$$

where  $C = C_L + C_R + C_G$  is the total capacitance of the dot. With the discreteness of charge  $q = \hat{N}e$  the simplest Hamiltonian generating this energy spectrum is

$$H_{dot} = \sum_{n\sigma} \varepsilon_n d_{n\sigma}^\dagger d_{n\sigma} + E_C (\hat{N} - N_0)^2. \quad (3.38)$$

Here  $\hat{N} = \sum_{n\sigma} d_{n\sigma}^\dagger d_{n\sigma}$  counts the number of electrons occupying the dot,  $E_C = e^2/2C$  is the charging energy and  $N_0 = V_G C_G / Cq$  is a dimensionless measure for the gate voltage.

For simplicity the two leads are modelled as reservoirs of one-dimensional electrons with a constant density of states,  $\nu$ . Thus the Hamiltonian describing the leads is constituted by a one-dimensional free electron model,

$$H_{leads} = \sum_{\alpha k \sigma} \xi_{\alpha k} c_{\alpha k \sigma}^\dagger c_{\alpha k \sigma}, \quad \alpha = L, R. \quad (3.39)$$

Here we have introduced  $\xi_{\alpha k} = \varepsilon_k - \mu_\alpha$ . The tunnelling Hamiltonian for coupling the quantum dot to the leads,

$$H_{TL} + H_{TR} = \sum_{\alpha k n \sigma} \left[ t_\alpha c_{\alpha k \sigma}^\dagger d_{n\sigma} + t_\alpha^* d_{n\sigma}^\dagger c_{\alpha k \sigma} \right], \quad (3.40)$$

Assuming that  $N$  is a good quantum number (i.e. the dot is isolated), allow for classical analysis of the dot system. The change in electrostatic energy when adding an electron to the dot is derived from (3.38),

$$E_{N+1} - E_N = E_C \left( N + 1 - \frac{C_G V_G}{e} \right)^2 - E_C \left( N - \frac{C_G V_G}{e} \right)^2 = 2E_C \left( N + 1/2 - \frac{C_G V_G}{e} \right). \quad (3.41)$$

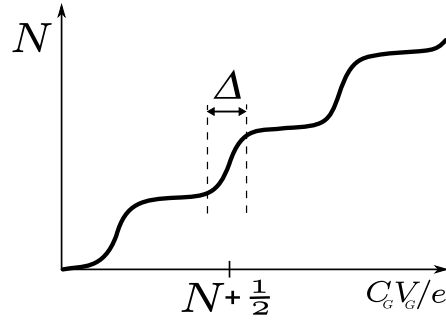


**Figure 3.6:** Occupation number  $N$  of the dot as a function of gate voltage.  $N$  remains constant except at half integer values of the dimensionless gate voltage,  $C_G V_G / e$ , of width  $\Delta \sim \max(T, \Gamma) / E_C$ .

At half integer values of the dimensional gate voltage  $C_G V_G / e$  the two dot states are degenerate, and this regime is known as a mixed-valence region. The width of this resonance is proportional to temperature, so assuming  $T \ll E_c$  the charging of the dot will follow a staircase diagram as depicted on Figure 3.6.

The quantisation of the charge on the dot has a huge effect on the conductance of the quantum dot system. Large temperatures  $T \gtrsim E_c$  smears out the staircase of Figure 3.6 resulting in a small conductance  $G_\infty \ll e^2/h$ . Lowering temperature the staircase emerges. In the mixed valence regions the conductance through the dot ultimately increases, reaching perfect conductance at zero temperature.

When the gate voltage is turned away from a mixed-valence region adding or removing an electron to the dot costs  $E_c$ , and the probability of finding such an electron in the lead is proportional to  $\exp(-E_c/T)$ . At low temperatures  $T \ll E_c$  the conductance is then exponentially suppressed, and we have established a *Coulomb blockade*.

Hence at  $T_c \ll E_C$  the conductance of the quantum dot system is a semiperiodic sequence of Coulomb blockade peaks of width  $\Delta \ll 1$  separated by large Coulomb blockade valleys.

### 3.2.2 The Kondo Effect in Quantum Dots

As the conductance of the Coulomb blockade valleys fall off exponentially with temperature, higher order scattering processes (cotunneling) become increasingly important.

For a Coulomb blockade valley with an  $N = \text{odd}$  number of electrons on the dot, the top most level of the dot is occupied by a single electron. In this case the dot net spin is  $\pm \frac{1}{2}$ , and hence the ground state is doubly degenerate.

For the antiferromagnetic Kondo spin singlet the binding energy of the Kondo spin singlet of  $\sim T_K$  is negligible when compared to the level spacing  $\delta E$ . Thus we may ignore excitations of the dot electrons to higher lying dot states.

In this case the quantum dot Hamiltonian represents a special case of the Anderson model for magnetic impurities

$$\begin{aligned}
 H &= H_d + H_U + H_e + H_{hyb} \\
 &= \sum_{\sigma} \xi_d c_{d,\sigma}^{\dagger} c_{d,\sigma} + U n_{d\uparrow} n_{d\downarrow} + \sum_{\mathbf{k},\sigma} \xi_{\mathbf{k}} c_{\mathbf{k},\sigma}^{\dagger} c_{\mathbf{k},\sigma} + \sum_{\mathbf{k},\sigma} \left( t_{\mathbf{k}} c_{d,\sigma}^{\dagger} c_{\mathbf{k},\sigma} + t_{\mathbf{k}}^* c_{\mathbf{k},\sigma}^{\dagger} c_{d,\sigma} \right). \quad (3.42)
 \end{aligned}$$

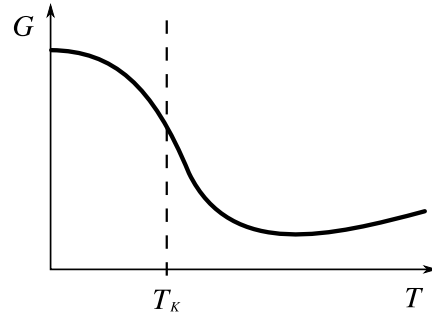


**Figure 3.7:** Differential conductance  $G$  as a function of temperature  $T$  at a zero bias voltage. Note the enhanced conductance of the system below the Kondo temperature  $T_K$ . Figure reproduced from [38].

The dot is a single level coupled to the leads through a hybridisation  $H_{hyb}$ . Note the charging energy  $H_U$  penalising double occupation of the dot.

Assuming that we are in the weak tunnelling regime, we may perform a canonical Schrieffer-Wolff transformation eliminating the zero-occupied or double-occupied states to linear order in the hybridisation. The calculations are in principle identical to the one given in section 10.1, when deriving the the Heisenberg spin model from the Hubbard Hamiltonian. For details of the calculation see Refs. [15], [10].

The resultant exchange Hamiltonian is then

$$H_S^{(2)} = \sum_{kk'\alpha\alpha'} J_{\alpha\alpha'} \mathbf{S}_d \cdot \mathbf{s}_{k\alpha, k'\alpha'} + \sum_{kk'\sigma, \alpha\alpha'} W_{\alpha\alpha'} c_{k\alpha\sigma}^\dagger c_{k'\alpha'\sigma} \quad (3.43)$$

where

$$J_{\alpha\alpha'} = 2 \left( \frac{t_\alpha t_{\alpha'}^*}{E_2 - E_1} + \frac{t_\alpha t_{\alpha'}^*}{E_0 - E_1} \right) = \frac{2U t_\alpha t_{\alpha'}^*}{(\xi_d + U)(-\xi_d)} \geq 0 \quad (3.44)$$

and

$$W_{\alpha\alpha'} = -\frac{1}{2} \left( \frac{t_\alpha t_{\alpha'}^*}{E_2 - E_1} + \frac{t_\alpha t_{\alpha'}^*}{E_1 - E_0} \right) = \frac{(2\xi_d + U)t_\alpha t_{\alpha'}^*}{2(\xi_d + U)(-\xi_d)} \geq 0 \quad (3.45)$$

Note that the first term is the antiferromagnetic Kondo Hamiltonian which describe virtual processes in which the spin of the dot changes when changing the spin of the lead electrons.

The second term describes potential scattering. We will usually assume that we are in the electron-hole symmetric regime where  $2\xi_d = -U$ , where this term becomes negligible.

In bulk metal the increased scattering of electrons due to the Kondo effect, contribute to the resistivity of the system, but for quantum dot systems the increased scattering rate means an increase in conductance through the dot. A schematic of the differential conductance at zero bias voltage is presented in Fig. 3.7.

Measurements show that the Kondo resonance lifts when a non-zero bias voltage is applied across the system. A Coulomb diamond diagram for a generic quantum dot system is shown in Figure 3.8.

The Kondo effect involves higher order scattering processes involving an intermediate spin flip of the localised spin. In a magnetic field the energy levels of the localised spin are split by a Zeeman energy. Hence we will need to apply a bias voltage for the conduction electrons to



**Figure 3.8:** Diamond diagram showing the Kondo conductance at odd electron occupancy.



**Figure 3.9:** Split Kondo peaks due to the presence of a magnetic field  $B$ . For large bias voltages  $|V| \gg T_k$  the Kondo resonance will experience a cross-over to ordinary co-tunneling.

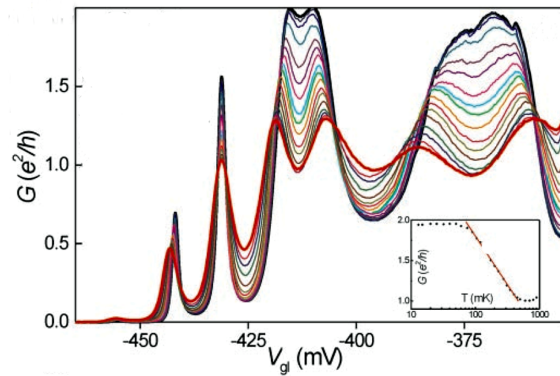


**Figure 3.10:** Differential conductance  $G$  as a function of gate voltage  $V_g$  showing how the Kondo resonance develops when lowering temperature. Figure reproduced from [29].

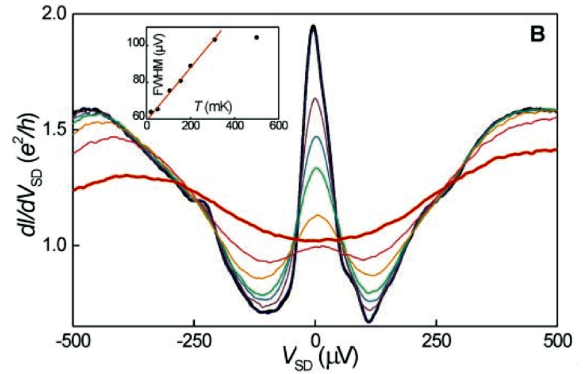


**Figure 3.11:** Differential conductance  $dI/dV$  as a function of bias voltage  $V_{sd}$ . Note the appearance of the Kondo peak at zero bias when lowering temperature below  $T_K$ . Figure reproduced from [29].

have a sufficient amount of energy for flipping the localised spin state. This effect is shown in a diamond diagram in Fig. 3.9. [39]

The experimental evidence of the Kondo effect in quantum dot systems is overwhelming. Van der Wiel et al. [29] was the first to observe Kondo resonances for a quantum dot system. Their measurements of the Kondo peak is shown in Figure 3.10 and Figure 3.11.

Nygaard et al. [28] were the first to detect the Kondo effect in a carbon nanotube coupled to two massive leads. The resulting diamond diagram of Figure 3.12 show sign of a Kondo resonance for odd dot occupancy.

### 3.2.3 The Nonequilibrium Kondo Problem

In the case of zero bias voltage the equilibrium Kondo Problem concerns itself with the extension of the weak coupling solutions for temperatures  $T < T_K$ , where the system crosses over to a strong coupling regime.

The extension of the Kondo Model to nonequilibrium including the effect of bias voltage and magnetic field on the Kondo resonance peak, constitutes the nonequilibrium Kondo Problem. As opposed to the equilibrium case you now have multiple energy scales, i.e.  $V$ ,  $B$  and  $T_K$  entering the problem. Also decoherence of the dot spin state due to the current running through the quantum dot complicates calculations.

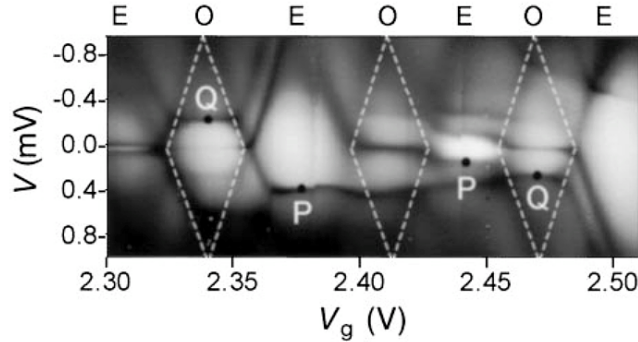


**Figure 3.12:** A measurement of the coulomb diamond diagram for a quantum dot system composed of a carbon nanotube connecting to two gold leads. The Kondo resonance is apparent when the carbon nanotube is occupied by an odd number of electrons. Figure reproduced from [28].

A variety of different approaches and theoretical frameworks has been applied to the nonequilibrium Kondo problem. To name but a few they include the Bethe ansatz for scattering states [40], the “Louvillian” theory for the real-time renormalisation group in frequency space developed in Refs. [27], [43], functional renormalisation group methods [42], and a variety of different calculational schemes [41], [26].

In Ref. [30] Coleman et al. argued that while the nonequilibrium Kondo problem was more complicated than the equilibrium case it would nevertheless experience a strong coupling cross-over at sufficiently low temperatures.

This notion was originally refuted by Rosch et al. [31] on the grounds that the decoherence of the localised spin, due to a non-zero current through the quantum dot system, would prevent a flow to strong coupling. This claim was substantiated in a series of papers, [31], [32], [34], [35]. Utilising a pseudofermionic representation of the dot spin it was shown that vertex corrections to the pseudofermionic Green’s function may introduce a decoherence rate  $\Gamma$  into the expressions for both self-energy and the Poor man’s scaling equations. The decoherence rate effectively cuts off the scaling equations for a temperature above  $T_K$ , thus preventing the flow to strong coupling.

The main goal of the following four chapters are devoted to the development of a systematic extension of Poor man’s scaling to the nonequilibrium Kondo model. In this method we will avoid the problematic<sup>1</sup> pseudofermionic representation of the dot spin. As an outlook the 2-loop calculations may facilitate the exact calculation of the decoherence rate  $\Gamma$ .

<sup>1</sup>While the pseudofermionic approach is tractable for calculational purposes, taking the limit of infinite chemical potential as mentioned in section 3.1.1 is nontrivial and can lead to unphysical results.

# Perturbation Theory

---

To start slowly we investigate how far standard perturbation theory can take us. The model system consist of a quantum dot weakly coupled to two leads. When in the electron-hole symmetric regime the contribution from potential scattering cab be safely ignored, and hence from Eq. (3.43) the time-dependent model Hamiltonian is,

$$H = H_0 + H' \quad (4.1)$$

with

$$H_0 = \sum_{\alpha k \sigma} \xi_{\alpha k} c_{\alpha k \sigma}^\dagger(\tau) c_{\alpha k \sigma}(\tau), \quad (4.2)$$

$$H' = \frac{1}{2} \sum_{\substack{\alpha' k' \sigma' \\ \alpha k \sigma}} J_{\alpha \alpha'} S^i c_{\alpha k \sigma}^\dagger(\tau) \tau_{\sigma \sigma'}^i c_{\alpha' k' \sigma'}(\tau). \quad (4.3)$$

The basic notion is to obtain an expression for the conduction electron Green's function, and expand this in powers of the interaction strength  $J$ , in order to obtain a Dyson-like equation defining the self-energy of the lead-electrons.

It is well-known that a non-zero value of the imaginary part of the retarded self-energy introduces a broadening of the spectral function. This broadening is equivalent to a finite conduction electron life-time, which is naturally interpreted as an enhanced scattering ratio. At zero bias voltage  $V = \mu_R - \mu_L = 0$  our calculations should reproduce the original results of Kondo, [13]. Hence at  $V = 0$  we would expect a non-zero imaginary part of the retarded self-energy, when extending our calculations to third order in the coupling  $\nu_F J$ .

## 4.1 Notation

The notation involved in the evaluation of Green's functions can be quite cumbersome due to the labelling of the many intermediate states. To simplify the notation we replace full sets of lead electron state variables  $\alpha k \sigma$  with Latin lowercase letters, e.g.  $a, a', a_1$  etc.. An example of use:

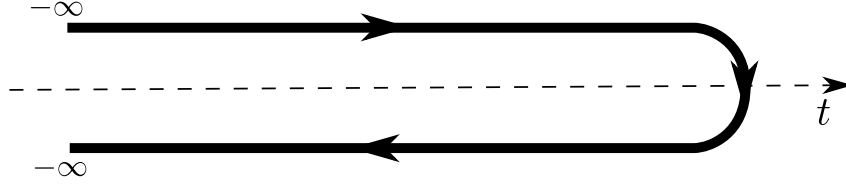


**Figure 4.1:** The Keldysh contour  $c$ . Times on the contour are normally denoted by the Greek  $\tau$ , while real times are referred as the Latin  $t$ . The contour can be divided into an upper contour,  $c_{upper}$  or  $c_1$ , and a lower contour,  $c_{lower}$  or  $c_2$ .

$$\begin{aligned} c_a(\tau) &= c_{\alpha k \sigma}(\tau), & \sum_a c_a^\dagger(\tau) &= \sum_{\alpha k \sigma} c_{\alpha k \sigma}^\dagger(\tau) \\ J_{aa'} &= J_{\alpha \alpha'}, & \sum_{aa'} J_{aa'} &= \sum_{\alpha \alpha'} J_{\alpha \alpha'} \\ \tau_{aa'}^i &= \tau_{\sigma \sigma'}^i, & \sum_{aa'} \tau_{aa'}^i &= \sum_{\sigma \sigma'} \tau_{\sigma \sigma'}^i \end{aligned}$$

Note that summation only involves the state variables explicitly contained in the summand.

## 4.2 Nonequilibrium Green's Functions

Disregarding initial correlations we consider a contour-ordered Green's function on the Keldysh contour presented in Fig. 4.1.

$$G_c(a, \tau; a', \tau') = -i \left\langle T_c (c_H(a, \tau) c_H^\dagger(a', \tau')) \right\rangle, \quad (4.4)$$

where  $T_c$  denotes time-ordering along the Keldysh contour. Subscript  $H$  reminds us that the operators are considered in the Heisenberg picture. For an introduction to nonequilibrium Green's functions consider Refs. [2], [23] or [11].

In the real-time matrix representation (also referred to as Schwinger-Keldysh space) the contour-ordered Green's function may be written

$$G_c(a, \tau; a', \tau') \rightarrow \hat{G}(a, t; a', t') = \begin{pmatrix} \hat{G}_{11}(a, t; a', t') & \hat{G}_{12}(a, t; a', t') \\ \hat{G}_{21}(a, t; a', t') & \hat{G}_{22}(a, t; a', t') \end{pmatrix}. \quad (4.5)$$

Here the matrix elements  $\hat{G}_{ij}(a, \tau; a', \tau')$  equals  $G_C(a, b)$  for  $a$  lying on the  $i$ 'th contour,  $c_i$ , and  $b$  lying on  $j$ 'th contour,  $c_j$ , with  $i, j = 1, 2$  (Consult Fig. 4.1 for definition of the different contours). Note that time arguments of the Green's function are now real times. Comparing to the well-known real-time Green's functions we may identify,

$$\hat{G}_{11}(a, t; a', t') = -i \langle T(c_H(a, t) c_H^\dagger(a', t')) \rangle, \quad (4.6a)$$

$$\hat{G}_{12}(a, t; a', t') = G^<(1, 1'), \quad (4.6b)$$

$$\hat{G}_{21}(a, t; a', t') = G^>(1, 1'), \quad (4.6c)$$

$$\hat{G}_{22}(a, t; a', t') = -i \langle \tilde{T}(c_H(a, t) c_H^\dagger(a', t')) \rangle. \quad (4.6d)$$

where  $T$  denotes standard time ordering, and  $\tilde{T}$  is reverse time ordering.



These considerations allow for a minor rewriting of Eq. (4.5),

$$\hat{G}(a, t; a', t') = \begin{pmatrix} G^<(a, t; a', t') + G^R(a, t; a', t') & G^<(a, t; a', t') \\ G^>(a, t; a', t') & G^>(a, t; a', t') - G^R(a, t; a', t') \end{pmatrix}, \quad (4.7)$$

showing that all information about the nonequilibrium Green's functions are contained in three components  $G^>$ ,  $G^<$  and  $G^R$ .

### 4.3 The Conduction Electron Self-energy

The introduction of the  $S$ -matrix

$$S = T_c e^{-i \int_c d\tau H'(\tau)}, \quad (4.8)$$

allows for a rewrite of Eq. (4.4) in the interaction picture

$$G_c(a, \tau; a', \tau') = -i \left\langle T_c S(-\infty, -\infty) c_{H_0}(a, \tau) c_{H_0}^\dagger(a', \tau') \right\rangle_0. \quad (4.9)$$

Since our dealings with operators will be restricted to the interaction picture from now on, we simplify our notation by dropping the subscript  $H_0$ .

Expansion of the  $S$ -matrix in powers of the coupling  $H'$  introduces a perturbative expansion of the Keldysh Green's function

$$\begin{aligned} G_c(a, \tau; a', \tau') &= -i \left\langle T_c c_{H_0}(a, \tau) c_{H_0}^\dagger(a', \tau') \right\rangle_0 \\ &\quad - i \left\langle T_c \left\{ -i \int_c d\tau''' H'_{H_0}(\tau''') c_{H_0}(a', \tau') c_{H_0}^\dagger(a', \tau') \right\} \right\rangle_0 \\ &\quad - \frac{i}{2!} \left\langle T_c \left\{ \left( -i \int_c d\tau'' H'_{H_0}(\tau'') \right) \left( -i \int_c d\tau''' H'_{H_0}(\tau''') \right) c_{H_0}(a, \tau) c_{H_0}^\dagger(a', \tau') \right\} \right\rangle_0 \\ &\quad + \dots \end{aligned} \quad (4.10)$$

Writing out the perturbation  $H'(\tau)$  and collecting terms similar to each other allow for a general expression for the correction to order  $J^N$ ,

$$\begin{aligned} G_c^{(N)}(a, \tau; a', \tau') &= \frac{(-i)^N}{2^N N!} \sum_{a_1 \dots a'_N} J_{a_1 a'_1} \dots J_{a_N a'_N} \int_c d\tau_1 \dots \int_c d\tau_N \left\langle T_c S^{i_1}(\tau_1) \dots S^{i_N}(\tau_N) \right\rangle_0 \\ &\quad \times \tau_{a_1 a'_1}^{i_N} \dots \tau_{a_N a'_N}^{i_1} \left\langle T_c \left\{ c_{a_1}^\dagger(\tau_1) c_{a'_1}(\tau_1) \dots c_{a_N}^\dagger(\tau_N) c_{a'_N}(\tau_N) c_a(\tau) c_{a'}^\dagger(\tau') \right\} \right\rangle_0 \end{aligned} \quad (4.11)$$

The expression looks almost deceptively simple. Except for the contour-ordered dot spin average  $\langle T_c S^{i_1}(\tau_1) \dots S^{i_N}(\tau_N) \rangle_0$  and the product of Pauli spin matrices, the expansion is identical to that of a fermionic system with pair interactions. In such an expansion the Wick contractions of  $\langle c^\dagger c \dots c_a^\dagger c_{a'} \rangle_0$  has simple Feynman diagrammatic equivalents. As of [10] the relevant diagrams are all connected to the end points either by propagators (full lines) or spin contractions (dashed

lines). Writing the expansion of Eq. (4.10) as a sum of diagrams, only including topologically identical diagrams once, one gets,

$$\begin{aligned}
 \text{Diagram 1} &= \text{Diagram 2} + \text{Diagram 3} + \text{Diagram 4} \\
 &+ \text{Diagram 5} + \text{Diagram 6} + \text{Diagram 7} + \text{Diagram 8} \quad (4.12)
 \end{aligned}$$

The first order correction to the bare propagator contain exactly one electron spin-localised spin interaction. Hence when averaging over all spin states we encounter the trace of a Pauli matrix, i.e.  $\text{Tr}\tau^i$ . By this reasoning terms to first order in the Kondo interaction does not contribute to the Green's function.

Another equally valid argument considers the average of a single spin operator  $\langle S^i \rangle$ , which due to spacial symmetry must equal zero. This consideration will be applied over and over when evaluating averages over dot spin operators.

Diagrams containing a single fermion loop also include  $\text{Tr}\tau^i = 0$  when summing spin degrees of freedom. Diagrams with a double fermion loop also vanish. Summation of the two corresponding Pauli matrices yields  $\tau_{a_1 a_2}^{i_1} \tau_{a_2 a_1}^{i_2} \propto \delta_{i_1 i_2}$ . while the contribution from the average dot spin  $\langle S^{i_1} S^{i_2} S^{i_3} \rangle \propto \varepsilon_{i_1 i_2 i_3}$ . Multiplying these two terms we get zero.

We have only drawn topologically different diagrams in Eq. (4.12). For each of the diagrams left after our initial analysis we count the number of actual diagrams. To order  $J^N$  you count  $N!$  such diagrams.

Up to order  $J^3$  the above considerations show that only diagrams with all fermion lines connected to the endpoints yield nonzero contributions. This allow us to write the expansion terms of the contour ordered Green's function as a Dyson-like equation

$$G_c^{(N)}(a, \tau; a', \tau') = G_a^{(0)}(\tau, \tau') \delta_{aa'} \int_c d\tau_1 \int_c d\tau_2 G_a^{(0)}(\tau, \tau_1) \Sigma(a, \tau_1; a', \tau_2) G_{a'}^{(0)}(\tau_2, \tau'). \quad (4.13)$$

#### 4.4 The Conduction Electron Self-energy to Order $J^2$

To order  $J^2$  the expression of the newly introduced self-energy reduces to

$$\Sigma^{(2)}(a, \tau_1; a', \tau_2) = \frac{(-i)^2}{4} \sum_{a_1} J_{aa_1} J_{a_1 a'} \langle T_c (S^i(\tau_1) S^j(\tau_2)) \rangle_0 G_{a_1}^{(0)}(\tau_1, \tau_2) \tau_{aa_1}^i \tau_{a_1 a'}^j \quad (4.14)$$

Splitting up the sum over intermediate state  $a_1$  assuming a flat band of both leads, i.e. a constant density of states  $\nu_F$ , we write

$$\sum_{a_1}(\dots) = \sum_{\alpha_1 \sigma_1 k_1}(\dots) = \sum_{\alpha_1} \sum_{\sigma_1} \nu_F \int_{-D}^D d\xi_3(\dots). \quad (4.15)$$

It turns out that the average of dot spin product is independent of the time-ordering,

$$\langle T_c (S^i(\tau_1) S^j(\tau_2)) \rangle_0 = \frac{1}{Z_{spin}} \sum_{\sigma} \langle \sigma | \frac{1}{4} \delta_{ij} + \frac{i}{2} \text{sgn}(\tau_1 - \tau_2) \varepsilon_{ijk} S^k | \sigma \rangle = \frac{1}{4} \delta_{ij}. \quad (4.16)$$

This result allows for the evaluation of

$$\sum_{ij} \sum_{\sigma_1} \langle T_c (S^i(\tau_1) S^j(\tau_3)) \rangle_0 \tau_{\sigma\sigma_1}^i \tau_{\sigma_1\sigma'}^j = \frac{3}{4} \tau_{\sigma\sigma'}^0. \quad (4.17)$$

Thus performing the analytic continuation to real-time space we get

$$\Sigma^{(2)}(a, \tau_1; a', \tau_2) = -\frac{3}{16} \delta_{\sigma\sigma'} \sum_{\alpha_1 k_1} J_{a\alpha_1} J_{\alpha_1 a'} \left[ \theta(\tau_1 - \tau_2) G_{\alpha_1 k_1}^{(0)>}(\tau_1, \tau_2) + \theta(\tau_2 - \tau_1) G_{\alpha_1 k_1}^{(0)<}(\tau_1, \tau_2) \right]. \quad (4.18)$$

From the above expression we may calculate e.g. the lesser component of the self-energy,

$$\Sigma^{(2)<}(a, t_1; a', t_2) = \frac{3}{16} \delta_{\sigma\sigma'} \sum_{\alpha_1} J_{a\alpha_1} J_{\alpha_1 a'} G_{\alpha_1}^{(0)<}(\tau_1, \tau_2). \quad (4.19)$$

We would like to transform this to frequency space. This calls for a small digression considering the interaction picture time evolution of the bare Green's functions,

$$G_{\alpha}^{(0)<}(k, t) = i f(\varepsilon_a - \mu_{\alpha}) e^{-i\varepsilon_k t}, \quad G_{\alpha}^{(0)>}(k, t) = -i(1 - f(\varepsilon_k - \mu_{\alpha})) e^{-i\varepsilon_k t}. \quad (4.20)$$

Fourier transforming this result yields

$$G_{\alpha}^{(0)<}(k, \omega) = 2\pi i f(\varepsilon_k - \mu_{\alpha}) \delta(\omega - \varepsilon_k) \quad (4.21)$$

Then calculating the  $k$ -summed Green's function  $G_{\alpha}^{(0)<}(\omega) = \sum_k^{\xi_k \in [-D, D]} G_{\alpha}^{(0)<}(k, \omega)$ , we obtain

$$G_{\alpha}^{(0)<}(\omega) = 2\pi i \nu_F \int_{-D+\mu_{\alpha}}^{D+\mu_{\alpha}} d\varepsilon f(\varepsilon - \mu_{\alpha}) \delta(\omega - \varepsilon) = 2\pi i \nu_F f(\omega - \mu_{\alpha}) \theta(D - |\omega - \mu_{\alpha}|). \quad (4.22)$$

In a similar fashion we may calculate the corresponding  $k$ -summed greater component of the Green's function

$$G_{\alpha}^{(0)>}(\omega) = 2\pi \nu_F (1 - i f(\omega - \mu_{\alpha})) \theta(D - |\omega - \mu_{\alpha}|). \quad (4.23)$$

Now we may continue the calculation of Eq. (4.19) by inserting the expression for the lesser component directly. This immediately transforms our result to frequency space in  $t_1 - t_2$ ,

$$\Sigma^{(2)<}(a, a'; \omega) = i \frac{3\pi}{8} \nu_F \delta_{\sigma\sigma'} \sum_{\alpha_1} J_{a\alpha_1} J_{\alpha_1 a'} f(\omega - \mu_{\alpha_1}) \theta(D - |\omega - \mu_{\alpha_1}|). \quad (4.24)$$

Similarly the greater component is calculated by insertion of the corresponding expression of the greater Green's function from Eq. (4.20) into Eq. (4.19). The result is

$$\Sigma^{(2)>}(a, a'; \omega) = i \frac{3\pi}{8} \nu_F \delta_{\sigma\sigma'} \sum_{\alpha_1} J_{\alpha\alpha_1} J_{\alpha_1\alpha'} (f(\omega - \mu_{\alpha_1}) - 1) \theta(D - |\omega - \mu_{\alpha_1}|). \quad (4.25)$$

Then the retarded component of the self-energy is

$$\begin{aligned} \Sigma^R(\omega) &= \int_{-\infty}^{\infty} dt e^{i\omega t} \theta(t) (\Sigma^>(t) - \Sigma^<(t)) \\ &= \int_0^{\infty} dt \int \frac{d\varepsilon}{2\pi} (\Sigma^>(\varepsilon) e^{i(\omega - \varepsilon + i0_+)t} - \Sigma^<(\varepsilon) e^{i(\omega - \varepsilon + 0_+)t}) \\ &= \int \frac{d\varepsilon}{2\pi} [\Sigma^>(\varepsilon) - \Sigma^<(\varepsilon)] \frac{i}{\omega - \varepsilon + i0_+}. \end{aligned} \quad (4.26)$$

Taking the imaginary part of Eq. (4.26), we have

$$\begin{aligned} \text{Im}\Sigma^R(a, a'; \omega) &= \frac{1}{2} (\text{Im}\Sigma^>(a, a'; \omega) - \text{Im}\Sigma^<(a, a'; \omega)) \\ &= -\frac{3\pi}{16} \nu_F \delta_{\sigma\sigma'} \sum_{\alpha_1} J_{\alpha\alpha_1} J_{\alpha_1\alpha'} \theta(D - |\omega - \mu_{\alpha_1}|). \end{aligned} \quad (4.27)$$

## 4.5 The Conduction Electron Self-energy to Order $J^3$

The third order self-energy now is

$$\begin{aligned} \Sigma^{(3)}(a, \tau_1; a', \tau_2) &= \frac{(-i)^3}{8} \sum_{a_1 a_2} J_{a a_1} J_{a_1 a_2} J_{a_2 a'} \int_c d\tau_3 \left\langle T_c \left( S^i(\tau_1) S^j(\tau_3) S^k(\tau_2) \right) \right\rangle_0 \\ &\quad \times \tau_{a a_1}^i \tau_{a_1 a_2}^j \tau_{a_2 a'}^k G_{a_1}^{(0)}(\tau_1, \tau_3) G_{a_2}^{(0)}(\tau_3, \tau_2). \end{aligned} \quad (4.28)$$

In this case the average of the dot spin product depends explicitly on the time-ordering,

$$\begin{aligned} \left\langle T_c \left( S^i(\tau_1) S^j(\tau_3) S^k(\tau_2) \right) \right\rangle_0 &= i \frac{1}{8} \text{sgn}(\tau_1 - \tau_3) \text{sgn}(\tau_3 - \tau_2) \text{sgn}(\tau_1 - \tau_2) \varepsilon_{ijk} \\ &= i \frac{1}{8} \text{spinsgn}(\tau_1, \tau_3, \tau_2) \varepsilon_{ijk}. \end{aligned} \quad (4.29)$$

This result allows us to evaluate

$$\sum_{ijk} \sum_{\sigma_1 \sigma_2} \left\langle T_c \left( S^i(\tau_1) S^j(\tau_3) S^k(\tau_2) \right) \right\rangle_0 \tau_{\sigma\sigma_1}^i \tau_{\sigma_1\sigma_2}^j \tau_{\sigma_2\sigma'}^k \propto i \frac{3}{4} \text{spinsgn}(\tau_1, \tau_3, \tau_2) \tau_{\sigma\sigma'}^0. \quad (4.30)$$

Performing the analytic continuation, evaluating the spinsgn( $\tau_1, \tau_3, \tau_2$ ) function for the different time-orderings, yields

$$\begin{aligned}
\Sigma^{(3)}(a, \tau_1; a', \tau_2) = & -\frac{3}{32}\delta_{\sigma\sigma'} \sum_{\alpha_1\alpha_2} J_{\alpha\alpha_1} J_{\alpha_1\alpha_2} J_{\alpha_2 a'} \\
& \left( \theta_c(\tau_1 - \tau_2) \left[ -\int_{-\infty}^{\tau_2} d\tau_3 G_{\alpha_1}^{(0)>}(\tau_1, \tau_3) G_{\alpha_2}^{(0)<}(\tau_3, \tau_2) \right. \right. \\
& + \int_{\tau_2}^{\tau_1} d\tau_3 G_{\alpha_1}^{(0)>}(\tau_1, \tau_3) G_{\alpha_2}^{(0)>}(\tau_3, \tau_2) \\
& \left. \left. - \int_{\tau_1}^{-\infty} d\tau_3 G_{\alpha_1}^{(0)<}(\tau_1, \tau_3) G_{\alpha_2}^{(0)>}(\tau_3, \tau_2) \right] \right. \\
& - \theta_c(\tau_2 - \tau_1) \left[ -\int_{-\infty}^{\tau_1} d\tau_3 G_{\alpha_1}^{(0)>}(\tau_1, \tau_3) G_{\alpha_2}^{(0)<}(\tau_3, \tau_2) \right. \\
& + \int_{\tau_1}^{\tau_2} d\tau_3 G_{\alpha_1}^{(0)<}(\tau_1, \tau_3) G_{\alpha_2}^{(0)<}(\tau_3, \tau_2) \\
& \left. \left. - \int_{\tau_2}^{-\infty} d\tau_3 G_{\alpha_1}^{(0)<}(\tau_1, \tau_3) G_{\alpha_2}^{(0)>}(\tau_3, \tau_2) \right] \right). \tag{4.31}
\end{aligned}$$

Using the linearity of integration one may rewrite this as

$$\begin{aligned}
\Sigma^{(3)}(a, \tau_1; a', \tau_2) = & -\frac{3}{32}\delta_{\sigma\sigma'} \sum_{\alpha_1\alpha_2} J_{\alpha\alpha_1} J_{\alpha_1\alpha_2} J_{\alpha_2 a'} \\
& \left( \theta_c(\tau_1 - \tau_2) \left[ \int_{-\infty}^{\tau_1} d\tau_3 \left\{ G_{\alpha_1}^{(0)>}(\tau_1, \tau_3) + G_{\alpha_1}^{(0)<}(\tau_1, \tau_3) \right\} G_{\alpha_2}^{(0)>}(\tau_3, \tau_2) \right. \right. \\
& - \int_{-\infty}^{\tau_2} d\tau_3 G_{\alpha_1}^{(0)>}(\tau_1, \tau_3) \left\{ G_{\alpha_2}^{(0)>}(\tau_3, \tau_2) + G_{\alpha_2}^{(0)<}(\tau_3, \tau_2) \right\} \left. \right] \\
& - \theta_c(\tau_2 - \tau_1) \left[ \int_{-\infty}^{\tau_1} d\tau_3 \left\{ G_{\alpha_1}^{(0)>}(\tau_1, \tau_3) + G_{\alpha_1}^{(0)<}(\tau_1, \tau_3) \right\} G_{\alpha_2}^{(0)<}(\tau_3, \tau_2) \right. \\
& \left. \left. - \int_{-\infty}^{\tau_2} d\tau_3 G_{\alpha_1}^{(0)<}(\tau_1, \tau_3) \left\{ G_{\alpha_2}^{(0)>}(\tau_3, \tau_2) + G_{\alpha_2}^{(0)<}(\tau_3, \tau_2) \right\} \right] \right). \tag{4.32}
\end{aligned}$$

The sum of greater and lesser components of the Green's function is normally referred to as the Keldysh component

$$G_{\alpha}^{(0)K}(t) = G_{\alpha}^{(0)>}(t) + G_{\alpha}^{(0)<}(t) = \sum_k i(2f(\varepsilon_k) - 1)e^{-i\varepsilon_k t} \tag{4.33}$$

Transferring Eq. (4.32) to Schwinger-Keldysh space, the lesser component of the Green's function is then

$$\begin{aligned}
\Sigma^{(3)<}(a, t_1; a', t_2) = & -\frac{3}{32}\delta_{\sigma\sigma'} \sum_{\alpha_1\alpha_2} J_{\alpha\alpha_1} J_{\alpha_1\alpha_2} J_{\alpha_2 a'} \\
& \times \left( \int_{-\infty}^{t_1} dt_3 G_{\alpha_1}^{(0)K}(t_1, t_3) G_{\alpha_2}^{(0)<}(t_3, t_2) - \int_{-\infty}^{t_2} dt_3 G_{\alpha_1}^{(0)<}(t_1, t_3) G_{\alpha_2}^{(0)K}(t_3, t_2) \right). \tag{4.34}
\end{aligned}$$

Note that the two integrals of the products of Green's functions looks very similar. We may employ small technical trick to deal with both integrals in single calculation. The time-dependence of the Green's functions amounts to a phase in the time-difference  $t_3 - t_2$  or  $t_1 - t_3$ . Interchanging the time-variables  $t_1$  and  $t_2$  in the second term and applying complex conjugation, we have almost reproduced the expression for the first term.

The transformation is complete if we also rename  $\alpha_1$  as  $\alpha_2$  and  $\alpha_2$  as  $\alpha_1$ . However we must remember to also interchange  $\alpha_1$  and  $\alpha_2$  in the product of coupling strengths. We may write this consideration as

$$\begin{aligned}\Sigma^{(3)<}(a, t_1; a', t_2) &= -\frac{3}{32}\delta_{\sigma\sigma'} \sum_{\alpha_1\alpha_2} \left( J_{\alpha\alpha_1} J_{\alpha_1\alpha_2} J_{\alpha_2\alpha'} K_{\alpha_1\alpha_2}(t_1, t_2) - J_{\alpha\alpha_2} J_{\alpha_2\alpha_1} J_{\alpha_1\alpha'} K_{\alpha_1\alpha_2}^*(t_2, t_1) \right) \\ &= -\frac{3}{32}\delta_{\sigma\sigma'} \sum_{\alpha_1\alpha_2} J_{\alpha\alpha_1} J_{\alpha_1\alpha_2} J_{\alpha_2\alpha'} \left( K_{\alpha_1\alpha_2}(t_1, t_2) - K_{\alpha_1\alpha_2}^*(t_2, t_1) \right)\end{aligned}\quad (4.35)$$

where the last equality derives from the fact that the Kondo model is a simplification of the more general Anderson model of Eq. (3.43), and hence the coupling strengths may be expressed as a product of tunnelling amplitudes

$$J_{\alpha\alpha_1} J_{\alpha_1\alpha_2} J_{\alpha_2\alpha'} \sim t_\alpha t_{\alpha_1}^* t_{\alpha_2} t_{\alpha_2}^* t_{\alpha'} \sim J_{\alpha\alpha_2} J_{\alpha_2\alpha_1} J_{\alpha_1\alpha'}.\quad (4.36)$$

Evaluation of the function:

$$\begin{aligned}K_{\alpha_1\alpha_2}(t_1, t_2) &= \int_{-\infty}^{t_1} dt_3 G_{\alpha_1}^{(0)K}(t_1, t_3) G_{\alpha_2}^{(0)<}(t_3, t_2) \\ &= \nu_F^2 \int_{-\infty}^{t_1} \int_{\mu_{\alpha_1}-D}^{\mu_{\alpha_1}+D} d\varepsilon \int_{\mu_{\alpha_2}-D}^{\mu_{\alpha_2}+D} d\varepsilon' (2f_{\alpha_1}(\varepsilon) - 1) e^{-i\varepsilon(t_1-t_3)} f_{\alpha_2}(\varepsilon') e^{-i\varepsilon'(t_3-t_2)} \\ &= \nu_F^2 \int_{\mu_{\alpha_1}-D}^{\mu_{\alpha_1}+D} d\varepsilon \int_{\mu_{\alpha_2}-D}^{\mu_{\alpha_2}+D} d\varepsilon' \frac{i}{\varepsilon - \varepsilon'} (2f_{\alpha_1}(\varepsilon) - 1) f_{\alpha_2}(\varepsilon') e^{-i\varepsilon'(t_1-t_2)}.\end{aligned}\quad (4.37)$$

Note that complex-conjugation along with an interchange of the times  $t_1$  and  $t_2$  in fact reproduces the original expression except for a sign-change. Thus  $K_{\alpha_1\alpha_2}(t_1, t_2) = -K_{\alpha_1\alpha_2}^*(t_2, t_1)$ .

Special care must be taken when Fourier transforming  $K_{\alpha_1\alpha_2}(t_1, t_2)$  with respect to  $t_1 - t_2$ .

$$\begin{aligned}K_{\alpha_1\alpha_2}(\omega) &= i\nu_F^2 \int_{\mu_{\alpha_2}-D}^{\mu_{\alpha_2}+D} d\varepsilon' f_{\alpha_2}(\varepsilon') 2\pi\delta(\omega - \varepsilon') \int_{\mu_{\alpha_1}-D}^{\mu_{\alpha_1}+D} d\varepsilon \frac{2f_{\alpha_1}(\varepsilon) - 1}{\varepsilon - \varepsilon'} \\ &= 2\pi i\nu_F^2 f_{\alpha_2}(\omega) \theta(D - |\omega - \mu_{\alpha_2}|) \int_{\mu_{\alpha_1}-D}^{\mu_{\alpha_1}+D} d\varepsilon \frac{2f_{\alpha_1}(\varepsilon) - 1}{\varepsilon - \varepsilon'} \\ &\approx -2\pi i\nu_F^2 f_{\alpha_2}(\omega) \theta(D - |\omega - \mu_{\alpha_2}|) \ln \left[ \frac{D^2}{T^2 + (\omega - \mu_{\alpha_1})^2} \right].\end{aligned}\quad (4.38)$$

From this result we may evaluate the Fourier transformation of the lesser component of the self-energy of order  $J^3$

$$\begin{aligned}\Sigma^{(3)<}(a, a'; \omega) &= -\frac{3}{16} \sum_{\alpha_1\alpha_2} J_{\alpha\alpha_1} J_{\alpha_1\alpha_2} J_{\alpha_2\alpha'} K_{\alpha_1\alpha_2}(\omega) \\ &\approx i\frac{3\pi}{8} \nu_F^2 \sum_{\alpha_1\alpha_2} J_{\alpha\alpha_1} J_{\alpha_1\alpha_2} J_{\alpha_2\alpha'} f(\omega - \mu_{\alpha_2}) \theta(D - |\omega - \mu_{\alpha_2}|) \ln \left[ \frac{D}{\sqrt{T^2 + (\omega - \mu_{\alpha_1})^2}} \right].\end{aligned}\quad (4.39)$$

Collecting the contributions to order  $J^2$  and  $J^3$  of the lesser component of the self-energy, we have up to third order in  $J$ .

$$\begin{aligned} \Sigma^<(a, a'; \omega) \approx & i \frac{3\pi}{8} \nu_F \sum_{\alpha_1 \alpha_2} J_{\alpha \alpha_1} J_{\alpha_1 \alpha_2} f(\omega - \mu_{\alpha_1}) \theta(D - |\omega - \mu_{\alpha_1}|) \\ & \times \left( \delta_{\alpha_2 \alpha'} + 2J_{\alpha_2 \alpha'} \nu_F \ln \left[ \frac{D}{\sqrt{T^2 + (\omega - \mu_{\alpha_2})^2}} \right] \right) \end{aligned} \quad (4.40)$$

The calculations regarding the greater component of the self-energy run along the same lines when replacing  $f_{\alpha_1}(\varepsilon')$  with  $(f_{\alpha_1}(\varepsilon') - 1)$ . This may be inferred by direct inspection of the greater and lesser components of the Green's function of Eq. (4.20).

Thus

$$\begin{aligned} \Sigma^>(a, a'; \omega) \approx & i \frac{3\pi}{8} \nu_F \sum_{\alpha_1 \alpha_2} J_{\alpha \alpha_1} J_{\alpha_1 \alpha_2} [f(\omega - \mu_{\alpha_1}) - 1] \theta(D - |\omega - \mu_{\alpha_1}|) \\ & \times \left( \delta_{\alpha_2 \alpha'} + 2J_{\alpha_2 \alpha'} \nu_F \ln \left[ \frac{D}{\sqrt{T^2 + (\omega - \mu_{\alpha_2})^2}} \right] \right). \end{aligned} \quad (4.41)$$

Using Eq. (4.26) we may calculate the imaginary part of the retarded self-energy,

$$\begin{aligned} \text{Im} \Sigma^R(a, a'; \omega) = & -\frac{3\pi}{16} \nu_F \sum_{\alpha_1 \alpha_2} J_{\alpha \alpha_1} J_{\alpha_1 \alpha_2} \theta(D - |\omega - \mu_{\alpha_1}|) \\ & \times \left( \delta_{\alpha_2 \alpha'} + 2J_{\alpha_2 \alpha'} \nu_F \ln \left[ \frac{D}{\sqrt{T^2 + (\omega - \mu_{\alpha_2})^2}} \right] \right). \end{aligned} \quad (4.42)$$

The derivation of the imaginary part of the retarded self-energy is the major result of our endeavours into old school perturbation theory.

At zero bias  $\mu_L = \mu_R = 0$  assuming vanishing  $\omega$  the  $J^3$  part of the result depends logarithmically on temperature  $\ln(D/T)$  in accordance with the equilibrium result of Eq. (3.6). At a non-zero bias  $\mu_L = -V/2$  and  $\mu_R = V/2$  the logarithmic dependence on temperature vanishes for  $T < V$ . Thus at extremely low temperatures the scattering cross-section does not diverge and we may stay in the weak couplings regime.

Paaske et al. calculated the imaginary part of the Transition matrix which in frequency space is identical to the imaginary part of the retarded self-energy. The result obtained is in complete agreement with their result cf. Eq. (71) of [34].

While we have obtained results in excellent agreement with previous calculations using different methods, we should also mention the limits of this calculation. Throughout the calculation we employed the fact that  $\langle S^i \rangle = 0$  due to the degeneracy of localised spin state. When applying a magnetic field  $B$  the degeneracy is lifted, and the dot spin average will need to be calculated by solving a quantum Boltzmann equation [34] - an approach which we will not pursue further here.





## Poor man's scaling on the Keldysh contour

---

The objective of this chapter is to extend the Poor man's scaling approach to the simplest nonequilibrium Kondo system with an applied bias voltage, but still in zero magnetic field. The general approach relies heavily on the scaling approach of Sólyom and Zawadowski covered in Chapter 3.2. While the  $T$ -matrix constituted the origin of calculation for equilibrium Poor man's scaling, we will instead consider the closely related  $S$ -matrix

$$S = T_c e^{-i \int_c d\tau V(\tau)}, \quad (5.1)$$

which leverages the calculation of non-equilibrium Green's functions through

$$G(a, \tau; a', \tau') = \left\langle T_c S c_{a'}^\dagger(\tau) c_a(\tau') \right\rangle_0. \quad (5.2)$$

Consider a perturbatively weak coupling  $\nu_F V \ll 1$  which allows for a Taylor expansion of the exponential in the  $S$ -matrix. E.g. to second order in the perturbation  $V$ , we may write

$$S = T_c \left[ 1 - i \int_c d\tau V(\tau) - \frac{1}{2} \int_c d\tau \int_c d\tau' V(\tau) V(\tau') + \mathcal{O}(V^3) \right] \quad (5.3)$$

I.e. the  $S$ -matrix splits up in contributions to increasing order in the interaction. In general the  $N$ 'th order contribution yields

$$S^{(N)} = \frac{1}{N!} T_c \left\{ \left( -i \int_c d\tau V(\tau) \right)^N \right\}. \quad (5.4)$$

Assume  $V$  to be a one-body interaction. Mathematically speaking (disregarding a shift of the ground state energy which may be incorporated in the quadratic part of the Hamiltonian),  $V$  may be put on the form

$$V(\tau) = \sum_{b, b'} F(b, b') c_b^\dagger(\tau) c_{b'}(\tau). \quad (5.5)$$

Considering the contribution from the  $N$ 'th order part of the  $S$ -matrix when calculating a nonequilibrium single particle Green's function by applying Eq. (5.2).

$$\begin{aligned} G^{(N)}(a, t; a', t') &= T_c \left\langle \left( -i \int_c d\tau V(\tau) \right)^N c_{a'}^\dagger(t') c_a(t) \right\rangle_0 \\ &= T_c \left\langle \prod_{n=1}^N \left( -i \int_c d\tau_n F(b_n, b'_n) \right) c_{b_1}^\dagger(\tau_1) b'_1(\tau_1) \cdots c_{b_N}^\dagger(\tau_N) c_{b'_N}(\tau_N) c_{a'}^\dagger(t') c_a(t) \right\rangle_0. \end{aligned} \quad (5.6)$$

Next step is to apply Wick's theorem evaluating the average  $\langle \cdots \rangle_0$ . Basically this means that  $c_{a'}^\dagger(t')$  and  $c_a(t)$  each pair with only one operator of the  $V^N$  product, while the rest of the operators from  $V^N$  pair off with each other accordingly. This is true to any order  $N > 1$  in the interaction strength. This allows for the introduction of the effective one-body  $S$ -matrix,

$$\tilde{S} = \left\langle e^{-i \int d\tau V(\tau)} \right\rangle_{(1)} \propto \int d\tau \int d\tau' c^\dagger(\tau) c(\tau'). \quad (5.7)$$

Here the average  $\langle \cdots \rangle_{(1)}$  applies Wick's theorem for  $2N - 2$  of the internal creation and annihilation operators.

Apply this reasoning to the case of the Kondo Hamiltonian. The philosophy of Poor man's scaling states that the scattering amplitudes for a system of bandwidth  $2D$  and coupling strength  $J$  may be equalled with a system of bandwidth  $2D - \delta D$  and coupling strength  $J + \delta J$ . We will here follow an approach derived from [20] to relate the scaling of  $J$  with  $D$ . Mathematically speaking the claim of poor man's scaling is

$$\tilde{S}(D, J) = \tilde{S}(D - \delta D, J + \delta J) \quad (5.8)$$

Assume  $\delta D$  and  $\delta J$  infinitesimal. By subtracting  $\tilde{S}(D - \delta D, J)$  on both sides of Eq. (5.8) and expanding to first order in both  $\delta D$  and  $\delta J$ , we have

$$\begin{aligned} \tilde{S}(D, J) - \tilde{S}(D - \delta D, J) &= \tilde{S}(D - \delta D, J + \delta J) - \tilde{S}(D - \delta D, J) \\ \frac{\partial \tilde{S}}{\partial D} \delta D &= \frac{\partial \tilde{S}}{\partial J} \delta J \\ \frac{\partial \tilde{S}}{\partial \ln D} \frac{\delta D}{D} &= \frac{\partial \tilde{S}}{\partial J} \frac{\partial J}{\partial \ln D} \frac{\delta D}{D}. \end{aligned} \quad (5.9)$$

This expression corresponds to the Callan-Symanzik like equation of Eq. (3.29) for equilibrium poor man's scaling. Assuming  $J \ll 1$  then  $\partial J / \partial \ln D$  is expanded as

$$\frac{\partial J}{\partial \ln D} = a_0 + a_1 J + a_2 J^2 + \dots \quad (5.10)$$

Similarly expanding the derivatives of the effective one-body  $S$ -matrix and collecting terms to the same order in  $J$ , allow us to determine the coefficients  $a_0, a_1$ , etc.

For  $\tilde{S}$  to second order in coupling strength  $J$  we may write out this equation to first as,

$$\left( \frac{\partial \tilde{S}^{(1)}}{\partial \ln D} \right) \frac{\delta D}{D} + \left( \frac{\partial \tilde{S}^{(2)}}{\partial \ln D} \right) \frac{\delta D}{D} = \left[ \left( \frac{\partial \tilde{S}^{(1)}}{\partial J} \right) + \left( \frac{\partial \tilde{S}^{(2)}}{\partial J} \right) \right] [a_0 + a_1 J + a_2 J^2] \frac{\delta D}{D}. \quad (5.11)$$

There is only one term proportional to  $J^0$ . Collecting these we have that

$$0 = a_0 \left( \frac{\partial \tilde{S}^{(1)}}{\partial J} \right) \frac{\delta D}{D}. \quad (5.12a)$$

Per definition the first order contribution to the effective one-body  $S$ -matrix is non-zero, and hence the prefactor  $a_0 = 0$ . We may apply this readily when collecting terms of order  $J^1$ . In this case we get that

$$\left( \frac{\partial \tilde{S}^{(1)}}{\partial \ln D} \right) \frac{\delta D}{D} = a_1 J \left( \frac{\partial \tilde{S}^{(1)}}{\partial J} \right) \frac{\delta D}{D}. \quad (5.12b)$$

To leading order  $J^2$  the final result is,

$$\left( \frac{\partial \tilde{S}^{(2)}}{\partial \ln D} \right) \frac{\delta D}{D} = a_1 J \left( \frac{\partial \tilde{S}^{(2)}}{\partial J} \right) \frac{\delta D}{D} + a_2 J^2 \left( \frac{\partial \tilde{S}^{(1)}}{\partial J} \right) \frac{\delta D}{D}. \quad (5.12c)$$

One should note the scaling equations play the role of a postulate. They include the operator form of the effective one-body  $S$ -matrix and collecting operator forms could lead to highly nontrivial scalings. In general the obtained scaling relations may contradict one another, hence disproving the initial assumption (that a change in bandwidth  $D$  can be incorporated as a rescaled coupling constant). However this does not disprove that scaling equations cannot be obtained for the problem at hand, merely that a change in bandwidth have other implications than changing the coupling constant.

While we have stressed the fact that the scaling equations are operator equations, one could repeat the argument leading to Eq. (5.9) for a scalar function depending on initial and final states of the system. However if some scalar function incorporate the scaling this behaviour should be derivable from the scaling equations for  $S$ -matrix in the first place.

## 5.1 1-loop Calculations

We will apply the reasoning of the previous section to the isotropic Kondo Hamiltonian of Eq. (4.1). The energy diagram for the system is shown in Figure 5.1 Performing the partial Wick's contraction of Eq. (5.7), on the  $N$ 'th order term of the effective one-body  $S$ -matrix yields

$$\begin{aligned} \tilde{S}^{(N)} = & \frac{1}{(2i)^N} \frac{1}{N!} T_c \left\{ \int d\tau_1 \cdots \int d\tau_N \sum_{a_1 a'_1} \cdots \sum_{a_N a'_N} J_{a_1 a'_1} \cdots J_{a_N a'_N} S^{i_1}(\tau_1) \cdots S^{i_N}(\tau_N) \right. \\ & \left. \times \tau_{a_1 a'_1}^{i_1} \cdots \tau_{a_N a'_N}^{i_N} \left\langle c_{a_1}^\dagger(\tau_1) c_{a'_1}(\tau_1) \cdots c_{a_N}^\dagger(\tau_N) c_{a'_N}(\tau_N) \right\rangle_{(1)} \right\}. \end{aligned} \quad (5.13)$$

Infinitesimal variation of the bandwidth  $D$  will only affect the  $N - 1$  Wick contracted Green's functions. Keeping only terms to first order in the infinitesimal change  $\delta D$ , yields the wanted

$$\delta_D \tilde{S}^{(N)} = \frac{\partial \tilde{S}}{\partial D} \delta D. \quad (5.14)$$

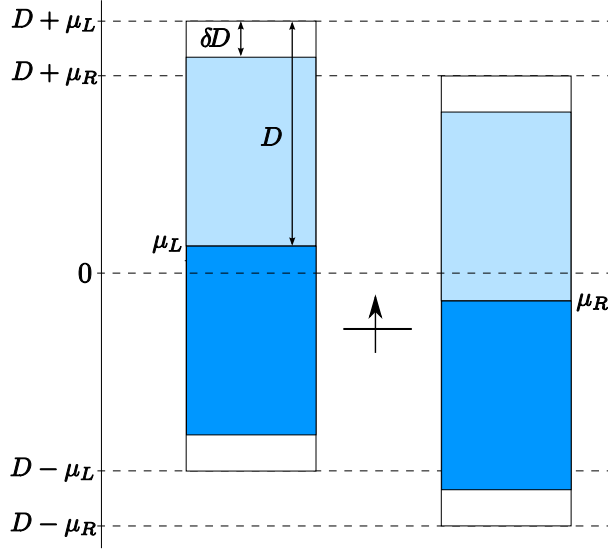


**Figure 5.1:** Energy diagram showing the left and right lead conduction electron bands.

## 5.2 The Effective One-Body $S$ -matrix to Order $J$

To order  $J^1$  we have

$$\tilde{S}^{(1)} = -i T_c \int_c d\tau H'(\tau) = -i \frac{1}{2} T_c \int_c d\tau \sum_{aa'} J_{a'a} S^i c_{a'}^\dagger \tau_{a'a}^i c_a. \quad (5.15)$$

The variation of  $\tilde{S}^{(1)}$  with bandwidth  $\delta D$  is then effectively

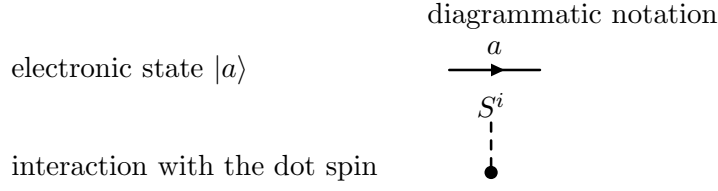
$$\delta_D \tilde{S}^{(1)} = 0. \quad (5.16)$$

## 5.3 The Effective One-Body $S$ -matrix to Order $J^2$

The contribution to order  $J^2$  is,

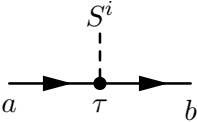
$$\begin{aligned} \tilde{S}^{(2)} &= T_c \left\{ -\frac{1}{2} \int_c d\tau \int_c d\tau' \langle H'(\tau) H'(\tau') \rangle_{(1)} \right\} \\ &= T_c \left\{ -\frac{1}{8} \int_c d\tau \int_c d\tau' \sum_{aa'} \sum_{bb'} J_{aa'} J_{bb'} S^i(\tau) S^j(\tau') \tau_{aa'}^i \tau_{bb'}^j \langle c_a^\dagger(\tau) c_a(\tau) c_b^\dagger(\tau') c_b(\tau') \rangle_{(1)} \right\}. \end{aligned} \quad (5.17)$$

Note that this expression for the one-body effective  $S$ -matrix share some similarities with the expression of Eq. (4.11) for the lead-electron Green's function. Using a similar approach we may adopt Feynman diagrammatic equivalents for Eq. (5.17) by using this small dictionary,



Then we may picture the lead-dot interaction as

$$H'(\tau) = \sum_{a'a} \text{diagram} \quad (5.18)$$

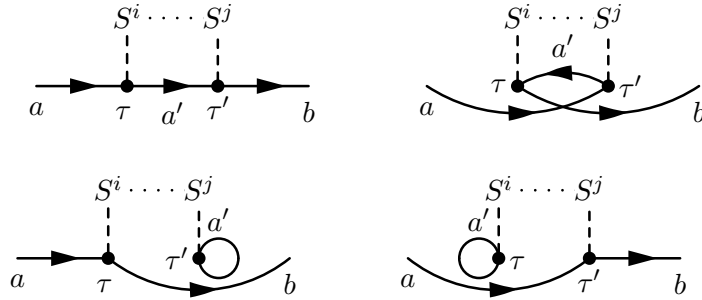



Since we are investigating  $\tilde{S}$ , all such diagrams will have a general first order structure

$$\delta_D \tilde{S} = \sum_{ab} \text{diagram} \quad (5.19)$$



The  $\delta_D S^{(2)}$  term contains two interaction points, and all diagrams will take one of the following forms:



Note again that diagrams containing a fermion loop  all vanishes, because they contain a trace over a Pauli matrix  $\text{Tr}(\tau^i) = 0$ .

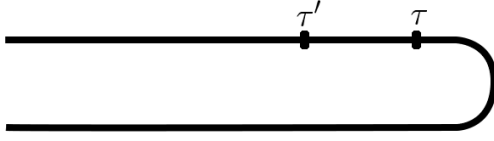
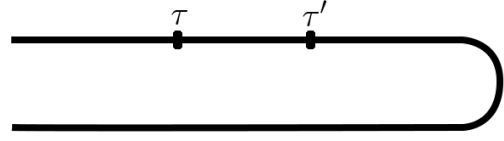
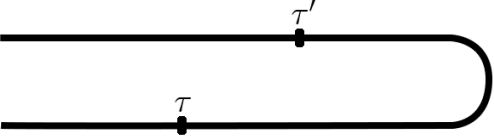
The remaining two diagrams are almost topologically equivalent. A simple renaming of state variables and times show that the two diagrams only differ by the order of dot spin operators  $S^i(\tau)S^j(\tau')$ . This is immaterial to the time ordering along the Keldysh contour, and thus the two diagrams contribute equally to the scattering amplitude.

Thus we may write Eq. (5.17) as

$$\tilde{S}^{(2)} = -\frac{i}{4} T_c \left\{ \int_c d\tau \int_c d\tau' \sum_{ab} \sum_{a'} J_{aa'} J_{a'b} \tau_{aa'}^i \tau_{a'b}^j S^i(\tau) S^j(\tau') c_a^\dagger(\tau) c_b(\tau') G_{a'}^{(0)}(\tau, \tau') \right\}. \quad (5.20)$$

### 5.3.1 Contour Ordering

Ordering along the Keldysh contour  $c$ , we encounter four different regimes depending on the values of the two time parameters  $\tau$  and  $\tau'$ . For different Keldysh contour regimes we may

5.2.1:  $\tau \in c_{upper} >_c \tau'$ 5.2.2:  $\tau \in c_{upper} <_c \tau'$ 5.2.3:  $\tau \in c_{lower} >_c \tau'$ 5.2.4:  $\tau \in c_{lower} <_c \tau'$ 

calculate  $\tilde{S}^{(2)}$  obtaining,

$$\tau \in c_{upper} >_c \tau' : -\frac{i}{4} \int_{-\infty}^{\infty} dt \int_{-\infty}^t dt' J_{aa'} J_{a'b} \tau_{a'a}^i \tau_{a'b}^j S^i(t) S^j(t') c_a^\dagger(t) c_b(t') G_a^{(0)>}(t, t'), \quad (5.21a)$$

$$\tau \in c_{upper} <_c \tau' : \frac{i}{4} \int_{-\infty}^{\infty} dt \int_t^{-\infty} dt' J_{aa'} J_{a'b} \tau_{a'a}^i \tau_{a'b}^j S^j(t') S^i(t) c_b(t') c_a^\dagger(t) G_a^{(0)<}(t, t'), \quad (5.21b)$$

$$\tau \in c_{lower} >_c \tau' : -\frac{i}{4} \int_{-\infty}^{\infty} dt \int_{-\infty}^t dt' J_{aa'} J_{a'b} \tau_{a'a}^i \tau_{a'b}^j S^i(t) S^j(t') c_a^\dagger(t) c_b(t') G_a^{(0)>}(t, t'), \quad (5.21c)$$

$$\tau \in c_{lower} <_c \tau' : \frac{i}{4} \int_{-\infty}^{\infty} dt \int_t^{-\infty} dt' J_{aa'} J_{a'b} \tau_{a'a}^i \tau_{a'b}^j S^j(t') S^i(t) c_b(t') c_a^\dagger(t) G_a^{(0)<}(t, t'). \quad (5.21d)$$

Based on the result obtained from the analytic continuation it is possible to write  $\tilde{S}^{(2)}$  on Schwinger-Keldysh component form

$$\tilde{S}^{(2)} = \begin{pmatrix} \tilde{S}_{11}^{(2)} & \tilde{S}_{12}^{(2)} \\ \tilde{S}_{21}^{(2)} & \tilde{S}_{22}^{(2)} \end{pmatrix} \quad (5.22)$$

### 5.3.2 Diagonal Components

Consider the  $\tilde{S}_{11}^{(2)}$  component with both events  $\tau$  and  $\tau'$  residing on the upper contour. From Eq. (5.21a) and Eq. (5.21b) we obtain the expression,

$$\begin{aligned} \tilde{S}_{11}^{(2)} = & -\frac{i}{4} \sum_{ab} \sum_{a'} J_{aa'} J_{a'b} \tau_{a'a}^i \tau_{a'b}^j \int_{-\infty}^{\infty} dt \left\{ \int_{-\infty}^t dt' S^i S^j c_a^\dagger(t) c_b(t') G_{a'}^{(0)>}(t, t') \right. \\ & \left. + \int_t^{\infty} dt' S^j S^i [-c_b(t') c_a^\dagger(t)] G_{a'}^{(0)<}(t, t') \right\}. \end{aligned} \quad (5.23)$$

In order to simplify this result, we will need to perform the  $t'$  integral and sum the Green's functions over the momentum interval of  $a'$ . In an effort to keep the expression as simple as possible we only write out the  $a'$  sum, so

$$\tilde{S}_{11}^{(2)} = -\frac{i}{4} \sum_{ab} \sum_{\alpha' \sigma'} J_{a\alpha'} J_{\alpha'b} \tau_{\alpha'a}^i \tau_{\alpha'b}^j K_{a,b,\alpha'}(t), \quad (5.24)$$

with

$$K_{a,b,\alpha'}(t) = \int_{-\infty}^{\infty} dt \sum_{k'}^{\varepsilon_{k'} - \mu_{\alpha'} \in [-D, +D]} \left\{ \int_{-\infty}^t dt' S^i S^j c_a^\dagger(t) c_b(t') i(f_{\alpha'}(\varepsilon_{k_1}) - 1) e^{-i\varepsilon_{k'}(t-t')} \right. \\ \left. + \int_t^{\infty} dt' S^j S^i [-c_b(t') c_a^\dagger(t)] i f_{\alpha'}(\varepsilon_{k'}) e^{-i\varepsilon_{k'}(t-t')} \right\}. \quad (5.25)$$

where we have inserted the actual expression for the greater and lesser components of the Green's function from Eq. (4.20). Explicit extraction of the time-evolution of  $c_b(t') = c_b e^{-i\varepsilon_b t'}$  allow us to evaluate the  $t'$  integrals,

$$K_{a,b,\alpha'}(t) = \nu_F \int_{-\infty}^{\infty} dt \int_{-D}^D d\xi \left\{ S^i S^j c_a^\dagger(t) c_b e^{-i\varepsilon_b t} \frac{(f(\xi) - 1)}{\xi + \mu_{\alpha'} - \varepsilon_b - i0_+} \right. \\ \left. - S^j S^i [-c_b c_a^\dagger(t)] e^{-i\varepsilon_b t} \frac{f(\xi)}{\xi + \mu_{\alpha'} - \varepsilon_b + i0_+} \right\} \quad (5.26)$$

Note the change of variables  $\xi = \varepsilon_{k'} - \mu_{\alpha'}$  performed after the time-integration. In the limit of zero-temperature the fermi-functions may be replaced by step-functions, and the evaluation of the energy-integrals yields

$$\text{Re}K_{a,b,\alpha'}(t) = \nu_F \int_{-\infty}^{\infty} dt \left\{ \left( \frac{1}{4} \delta_{ij} + \frac{i}{2} \varepsilon_{ijk} S^k \right) c_a^\dagger(t) c_b(t) \ln \left( \frac{\varepsilon_b - \mu_{\alpha'}}{D - \varepsilon_b + \mu_{\alpha'}} \right) \right. \\ \left. - \left( \frac{1}{4} \delta_{ij} - \frac{i}{2} \varepsilon_{ijk} S^k \right) [-c_b(t) c_a^\dagger(t)] \ln \left( \frac{\varepsilon_b - \mu_{\alpha'}}{D + \varepsilon_b - \mu_{\alpha'}} \right) \right\}. \quad (5.27)$$

And in the case when  $\varepsilon_b - \mu_{\alpha'} \in [-D, D]$  the imaginary part of  $K$  is non-zero,

$$i\text{Im}K_{a,b,\alpha'}(t) = i\pi\nu_F \int_{-\infty}^{\infty} dt \left\{ S^i S^j c_a^\dagger(t) c_b(t) (f_{\mu_{\alpha'}}(\varepsilon_b) - 1) \right. \\ \left. + S^j S^i [-c_b(t) c_a^\dagger(t)] f_{\mu_{\alpha'}}(\varepsilon_b) \right\}. \quad (5.28)$$

While this is a relevant contribution to the effective one-body  $S$ -matrix is almost independent of bandwidth  $D$ . Differentiating with respect to  $D$  yields a non-zero result only when exactly  $\varepsilon_b - \mu_{\alpha'} = D$ . Thus we will only calculate the real part of  $K$ , i.e. the imaginary part of the effective one-body  $S$ -matrix to order  $J^2$ .

Hence in the last term of Eq. (5.27) we may replace  $c_b c_a^\dagger = \delta_{ab} - c_a^\dagger c_b$ . This leaves us with three qualitatively different contributions to the  $\tilde{S}_{11}^{(2)}$  component of the  $S$ -matrix.

$$i\text{Im}\tilde{S}_{11}^{(2)} = \tilde{S}_{cn.st.}^{(2)} + \tilde{S}_{pot.}^{(2)} + \tilde{S}_{ex.}^{(2)} \quad (5.29)$$

The least important contributions arise from the  $\delta_{ab}$  term appearing when interchanging the field operators. In this case the integrand is time-independent and evaluating the integral yields infinity. From Eq. (5.27) the contribution yields

$$\tilde{S}_{cn.st.}^{(2)} = \frac{i}{4} \nu_F \int_{-\infty}^{\infty} dt \sum_a \sum_{\alpha'\sigma'} J_{a\alpha'} J_{\alpha'a} \tau_{a\sigma'}^i \tau_{\sigma'a}^j \left( \frac{1}{4} \delta_{ij} - \frac{i}{2} \varepsilon_{ijk} S^k \right) \ln \left( \frac{\varepsilon_a - \mu_{\alpha'}}{D + \varepsilon_a - \mu_{\alpha'}} \right). \quad (5.30)$$

For the part on the form of potential scattering,

$$\tilde{S}_{pot.}^{(2)} = -\frac{3i}{8} \sum_{ab} \sum_{\alpha'\sigma'} J_{a\alpha'} J_{\alpha'b} \tau_{ab}^0 \int_{-\infty}^{\infty} dt c_a^\dagger(t) c_b(t) \ln \left( \frac{D + \xi_b - \mu_{\alpha'}}{D - \xi_b + \mu_{\alpha'}} \right) \quad (5.31)$$

Last and most importantly the exchange interaction yields

$$\tilde{S}_{ex.}^{(2)} = \frac{i}{4} \nu_F \sum_{ab} \sum_{\alpha'} J_{a\alpha'} J_{\alpha'b} \tau_{ab}^k S^k \int_{-\infty}^{\infty} dt c_a^\dagger(t) c_b(t) \ln \left( \frac{(\xi_b - \mu_{\alpha'})^2}{D^2 - (\xi_b - \mu_{\alpha'})^2} \right). \quad (5.32)$$

For the other diagonal component  $\tilde{S}_{22}^{(2)}$  with both times  $\tau$  and  $\tau'$  residing on the lower contour, we may use Eq. (5.21c) and Eq. (5.21d), to write

$$\begin{aligned} \tilde{S}_{22}^{(2)} = & -\frac{i}{4} \sum_{ab} \sum_{a'} J_{aa'} J_{a'b} \tau_{a'a}^i \tau_{a'b}^j S^i S^j \int_{-\infty}^{\infty} dt \left\{ \int_{\infty}^t dt' S^i S^j c_a^\dagger(t) c_b(t') G_{a'}^{(0)>}(t, t') \right. \\ & \left. + \int_t^{-\infty} dt' S^j(t') S^i(t) \left[ -c_b(t') c_a^\dagger(t) \right] G_{a'}^{(0)<}(t, t') \right\}. \end{aligned} \quad (5.33)$$

Note the striking similarity with the expression for the  $\tilde{S}_{11}^{(2)}$  component of Eq. (5.23). Expanding the above expression it follows that

$$\text{Im} \tilde{S}_{22}^{(2)} = -\text{Im} \tilde{S}_{11}^{(2)}. \quad (5.34)$$

### 5.3.3 Off-Diagonal Components

For the off-diagonal components we have,

$$\tilde{S}_{12}^{(2)} = \frac{i}{4} \sum_{ab} \sum_{a'} J_{aa'} J_{a'b} \tau_{a'a}^i \tau_{a'b}^j \int_{-\infty}^{\infty} dt \int_{-\infty}^{\infty} dt' S^j S^i \left[ c_b(t') c_a^\dagger(t) \right] i f_{\mu_{a'}}(\varepsilon_{a'}) e^{-i\varepsilon_{a'}(t-t')}. \quad (5.35)$$

Extract the time-evolution of  $c_b(t')$  and performing the  $t'$ -integral to obtain

$$\begin{aligned} \tilde{S}_{12}^{(2)} = & -\frac{\pi}{2} \sum_{ab} \sum_{\alpha'\sigma'} J_{a\alpha'} J_{\alpha'b} \tau_{\sigma'a}^i \tau_{\sigma'b}^j S^j S^i \int_{-\infty}^{\infty} dt c_b c_a^\dagger(t) \nu_F \int_{-D}^D d\xi f(\xi) \delta(\xi + \mu_{\alpha'} - \varepsilon_b) e^{-i(\xi + \mu_{\alpha'})t} \\ = & -\frac{\pi}{2} \nu_F \sum_{ab} \sum_{\alpha'\sigma'} J_{a\alpha'} J_{\alpha'b} \tau_{\sigma'a}^i \tau_{\sigma'b}^j S^j S^i \int_{-\infty}^{\infty} dt c_b(t) c_a^\dagger(t) f_{\mu_{\alpha'}}(\varepsilon_b) \theta(D - |\varepsilon_b - \mu_{\alpha'}|). \end{aligned} \quad (5.36)$$

Similarly for the  $\tilde{S}_{21}^{(2)}$  component

$$\begin{aligned} \tilde{S}_{21}^{(2)} = & -\frac{i}{4} \sum_{ab} \sum_{a'} J_{aa'} J_{a'b} \tau_{aa'}^i \tau_{a'b}^j \int_{-\infty}^{\infty} dt \int_{-\infty}^{\infty} dt' S^i S^j c_a^\dagger(t) c_b(t') i (f_{\mu_{a'}}(\varepsilon_{a'}) - 1) e^{-i\varepsilon_{a'}(t-t')} \\ = & -\frac{\pi}{2} \sum_{ab} \sum_{\alpha'\sigma'} J_{a\alpha'} J_{\alpha'b} \tau_{\sigma'a}^i \tau_{\sigma'b}^j \int_{-\infty}^{\infty} dt c_a^\dagger(t) c_b(t) (f_{\mu_{\alpha'}}(\varepsilon_b) - 1) \theta(D - |\varepsilon_b - \mu_{\alpha'}|). \end{aligned} \quad (5.37)$$

The off-diagonal terms resemble the terms arising from the real part of the diagonal components, which we ignored by arguing that non-zero results only occurred for two exact values of  $\varepsilon_b$ . While the argumentation might have seemed a bit hand-waving we will carry out explicit calculation for the off-diagonal terms in the next section.



## 5.4 Variation

The next step is to calculate the variation of the components of the effective one-body  $S$ -matrix with bandwidth  $D$ . For the diagonal components we argued that

$$\delta_D \tilde{S}_{11}^{(2)} = i\delta_D \text{Im} \tilde{S}_{11}^{(2)} = \delta_D \tilde{S}_{cnst.}^{(2)} + \delta_D \tilde{S}_{pot.}^{(2)} + \delta_D \tilde{S}_{ex.}^{(2)} \quad (5.38)$$

The total variation can thus be calculated by varying each term with respect to  $D$ . You may remember that the first term  $S_{cnst.}^{(2)}$  yielded infinity. Unfortunately these infinities survive the variation of  $D$ . However the  $S_{cnst.}^{(2)}$  contain no field operators, and hence when calculating a Green's function from e.g. Eq. (5.6) the two external vertices must be joined. Thus  $S_{cnst.}^{(2)}$  include only disconnected diagrams. Variation of this term thus cuts out the infinitely many disconnected diagrams living in the cut-off states.

For the pure potential scattering part, we have that

$$\delta_D \tilde{S}_{pot.}^{(2)} = \frac{3i}{8} \sum_{ab} \sum_{\alpha'\sigma'} J_{a\alpha'} J_{\alpha'b} \tau_{ab}^0 \int_{-\infty}^{\infty} dt c_a^\dagger(t) c_b(t) \frac{\varepsilon_b - \mu_{\alpha'}}{D^2 - (\varepsilon_b - \mu_{\alpha'})^2} \delta D. \quad (5.39)$$

By applying an argument similar to that of Anderson [16] we may argue that this contribution yields zero when averaging over either all energies  $\varepsilon_b$  or over all bandwidths  $D$ . Thus we will ignore this part in the coming calculations.

For the exchange coupling,

$$\delta \tilde{S}_{ex.}^{(2)} = -\frac{i}{4} \nu_F \sum_{ab} \sum_{\alpha'} J_{a\alpha'} J_{\alpha'b} \tau_{ab}^k S^k \int_{-\infty}^{\infty} dt c_a^\dagger(t) c_b(t) \frac{2D}{D^2 - (\xi_b - \mu_{\alpha'})^2} \delta D. \quad (5.40)$$

For the off-diagonal components we get

$$\delta_D \tilde{S}_{12}^{(2)} = -\frac{1}{4} \nu_F \pi \sum_{ab} \sum_{\alpha'\sigma'} J_{a\alpha'} J_{\alpha'b} \tau_{\sigma'a}^i \tau_{\sigma'b}^j S^j S^i \int_{-\infty}^{\infty} dt c_b(t) c_a^\dagger(t) f_{\mu_{\alpha'}}(\varepsilon_b) \delta(D - |\varepsilon_b - \mu_{\alpha'}|). \quad (5.41)$$

Likewise we get for the remaining off-diagonal component

$$\delta_D \tilde{S}_{21}^{(2)} = \frac{i}{4} \sum_{ab} \sum_{\alpha'\sigma'} J_{a\alpha'} J_{\alpha'b} \tau_{a\sigma'}^i \tau_{\sigma'b}^j \int_{-\infty}^{\infty} dt c_a^\dagger(t) c_b(t) (f_{\mu_{\alpha'}}(\varepsilon_b) - 1) \delta(D - |\varepsilon_b - \mu_{\alpha'}|). \quad (5.42)$$

As mentioned earlier this is an important result because it shows that two off-diagonal components are virtually independent of the bandwidth  $D$ . Only for the single incoming energy close to the band edge where  $D = \varepsilon_b - \mu_{\alpha'} > 0$  we get a contribution. If we ignore this minute contribution the Schwinger-Keldysh representation of the variation of the effective one-body  $S$ -matrix is diagonal. A diagonal form is tractable because the Schwinger-Keldysh representation of the  $S$ -matrix to order  $J^1$  is

$$\tilde{S}^{(1)} = -\frac{i}{2} T_c \left\{ \int_c d\tau \int_c d\tau' \sum_{aa'} J_{a'a} S^i c_{a'}^\dagger(\tau) \tau_{a'a}^i c_a(\tau') \delta_c(\tau - \tau') \right\} = \begin{pmatrix} \tilde{S}_{11}^{(1)} & 0 \\ 0 & \tilde{S}_{22}^{(1)} \end{pmatrix}. \quad (5.43)$$

By reversing the argument we may turn the diagonal Schwinger Keldysh representation of the  $S$ -matrix back into a contour ordered integral thus obtaining,

$$\delta_D \tilde{S}^{(2)} = -\frac{i}{2} \nu_F \sum_{ab} \sum_{\alpha'} J_{a\alpha'} J_{\alpha'b} \tau_{ab}^i S^i \int_c dt c_a^\dagger(t) c_b(t) \frac{D}{D^2 - (\xi_b - \mu_{\alpha'})^2} \delta D. \quad (5.44)$$

### 5.4.1 An easier method for variation

We might add a small technical comment to the variation of the effective one-body  $S$ -matrix. We calculated the variations  $\delta\tilde{S}^{(2)}$  in two steps by first deriving an expression for  $\tilde{S}^{(2)}$ , and then varying the bandwidth. We may easily combine these two steps into one. Considering e.g. Eq. (5.26) we evaluate an integral on the form

$$\int_{-D}^D d\xi f(\xi). \quad (5.45)$$

Applying the variation of  $D$  directly to this expression yields

$$\begin{aligned} \delta_D \int_{-D}^D d\xi f(\xi) &= \delta_D \int_{-1}^1 dx D f(xD) \\ &= \int_{-1}^1 dx \{f(xD) + xD f'(xD)\} \delta D \\ &= [f(D) + f(-D)] \delta D. \end{aligned} \quad (5.46)$$

The last expression is much easier to evaluate, and in general we will adopt the notation,

$$\int_{\square} d\xi f(\xi) = [f(D) + f(-D)] \delta D = \delta_D \int_{-D}^D d\xi f(\xi). \quad (5.47)$$

Here the two boxes on the integral sign refer to integration over intervals of size  $\delta D$  at the band-edges  $\xi = \pm D$ .

## 5.5 The Scaling Equations

Note that from an operator point of view Eq. (5.44) is identical to the expression for the  $J^1$  order part of the  $S$ -matrix. We are now ready to plug the results into the scaling equation, Eq. (5.11). To order  $J^1$  we plug the result of Eq. (5.16) into the expression of Eq. (5.12b) obtaining,

$$\left( \frac{\partial \tilde{S}^{(1)}}{\partial \ln D} \right) \frac{\delta D}{D} = 0 = a_1 J \left( \frac{\partial \tilde{S}^{(1)}}{\partial J} \right) \frac{\delta D}{D}. \quad (5.48)$$

Hence  $a_1 = 0$  as expected, and the leading order contribution to the scaling of  $J$  is thus of order  $J^2$ . Applying this fact to the scaling equation Eq. (5.12c) the result is

$$\left( \frac{\partial \tilde{S}^{(2)}}{\partial \ln D} \right) \frac{\delta D}{D} = a_2 J^2 \left( \frac{\partial \tilde{S}^{(1)}}{\partial J} \right), \quad (5.49)$$

which with inserted values looks like

$$T_c \left\{ -\frac{i}{2} \int_c d\tau \sum_{ab} \left( \sum_{\alpha'} \nu_F J_{a\alpha'} J_{\alpha'b} \frac{2D^2}{D^2 - (\xi_b - \mu_{\alpha'})^2} - \delta J^2 \right) S_a^i c_a^\dagger(\tau) \tau_{ab}^i c_b(\tau) \right\} \frac{\delta D}{D} = 0. \quad (5.50)$$

The renormalised couplings depend explicitly on the energy of the initial state,  $\varepsilon_b$ . When the initial state energy is close to the Fermi surface far from the band edge, the energy-dependent

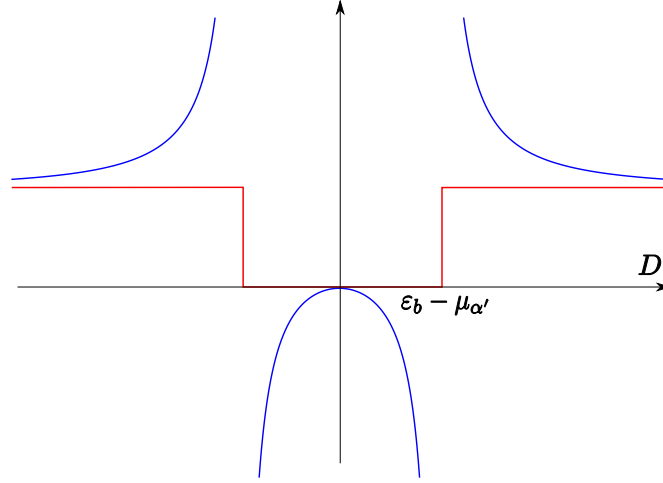


**Figure 5.2:** Plot showing the function  $f(D) = D^2 / (D^2 - (\varepsilon_b - \mu_{\alpha'}))$  (blue line), alongside the Heaviside step function  $\theta(D - |\varepsilon_b - \mu_{\alpha'}|)$  (red line).

part of the renormalized coupling is negligible. While for energies far beyond the band-edge, the bandwidth can be ignored. These considerations rely on the prefactor

$$\frac{D^2}{D^2 - (\varepsilon_b - \mu_{\alpha'})^2} \approx \begin{cases} 1 & \text{for } \varepsilon_b \approx \mu_{\alpha'} \\ 0 & \text{for } |\varepsilon_b - \mu_{\alpha'}| \gg D \end{cases} \quad (5.51)$$

Thus we might interpret the energy-dependence as a Heaviside step function cutting off states with an initial energy beyond the band-edge of the intermediate state  $a'$ . While this seems plausible for states far away from the band edge, it is quite clear from Fig. 5.2 that the approximation fails miserably when considering states close to the edge of the band with the coupling actually diverging.

As considered in the coming section 5.6 the scaling equations will be applied starting from initial bandwidth  $D_0$  and scaling to some exponentially small bandwidth. Thus for a fixed energy  $\varepsilon_b$  the corresponding couplings  $J(\varepsilon_b)$  will initially increase as is the case for equilibrium. When at some point  $\varepsilon_b > D + \mu_{\alpha'}$  the coupling constants will instead decrease when decreasing the bandwidth. At zero bandwidth the argument is that the effect of the prefactor in Eq. (5.51) is in fact identical to that of the Heaviside step function.

Thus if approximating the energy-dependence as a Heaviside step function the final scaling relation takes the form of

$$\frac{\partial J_{\alpha\beta}}{\partial \ln D} = 2\nu_F \sum_{\alpha'} J_{\alpha\alpha'} J_{\alpha'\beta} \theta(D - |\xi_b - \mu_{\alpha'}|). \quad (5.52)$$

Which corresponds to the results of Paaske et al. in [34] and [35] in the case of zero decoherence rate  $\Gamma = 0$ .

## 5.6 Solving the scaling equations

We may end this chapter by showing how the steady state values of the coupling constants can be obtained from the scaling relations in the case of a non-zero decoherence rate. Assuming

that the coupling constants  $g = \nu_F J$  are perturbatively small Ref. [34] obtain the following scaling equations in the simplest case of zero magnetic field,

$$\frac{\partial g_{\alpha\alpha'}}{\partial \ln D}(\varepsilon) = \sum_{\beta} g_{\alpha\beta} g_{\beta\alpha'} \theta_{\Gamma}(D - |\varepsilon - \mu_{\beta}|). \quad (5.53)$$

Here we have defined the smeared step function

$$\theta_{\Gamma}(D - |\varepsilon - \mu - \beta|) = \theta(D - \sqrt{\Gamma^2 + (\varepsilon - \mu_{\beta})^2}). \quad (5.54)$$

In these scaling equations the couplings  $g$  depend explicitly on energy  $\varepsilon$ . Thus we will need to identify the relevant energy argument for the coupling strengths occurring on the right hand side of the equations. Assuming that by applying Eq. (5.53) we will succeed in reaching zero temperature without leaving the weak coupling regime. At this point step functions will force the the energy  $\varepsilon$  to lie within a distance  $\Gamma$  to the chemical potential included in the step function. Thus we end up with the following four scaling equations

$$\frac{\partial g_{LL}(\varepsilon)}{\partial \ln D} = g_{LL}(\mu_L) g_{LL}(\mu_L) \theta_{\Gamma}(D - |\varepsilon - \mu_L|) + g_{LR}(\mu_R) g_{RL}(\mu_R) \theta_{\Gamma}(D - |\varepsilon - \mu_R|) \quad (5.55a)$$

$$\frac{\partial g_{LR}(\varepsilon)}{\partial \ln D} = g_{LL}(\mu_L) g_{LR}(\mu_L) \theta_{\Gamma}(D - |\varepsilon - \mu_L|) + g_{LR}(\mu_R) g_{RR}(\mu_R) \theta_{\Gamma}(D - |\varepsilon - \mu_R|) \quad (5.55b)$$

$$\frac{\partial g_{RL}(\varepsilon)}{\partial \ln D} = g_{RL}(\mu_L) g_{LL}(\mu_L) \theta_{\Gamma}(D - |\varepsilon - \mu_L|) + g_{RR}(\mu_R) g_{RL}(\mu_R) \theta_{\Gamma}(D - |\varepsilon - \mu_R|) \quad (5.55c)$$

$$\frac{\partial g_{RR}(\varepsilon)}{\partial \ln D} = g_{RL}(\mu_L) g_{LR}(\mu_L) \theta_{\Gamma}(D - |\varepsilon - \mu_L|) + g_{RR}(\mu_R) g_{RR}(\mu_R) \theta_{\Gamma}(D - |\varepsilon - \mu_R|) \quad (5.55d)$$

In order to complete the scaling we need to solve this set of coupled differential equations for  $g_{\alpha'\alpha}(\varepsilon)$ . With the couplings  $g_{\alpha'\alpha}(\varepsilon)$  depending on both bandwidth  $D$  and incoming energy  $\varepsilon$  the solution of Eq. (5.55) takes two logical step. First step is to determine the  $D$  dependence at the value of the relevant chemical potential. Do this by fixing the energy-dependence of the coupling constants at the relevant chemical potentials and plug into Eq. (5.55). This leaves us with the following six equations,

$$\frac{\partial g_{LL}(\mu_L)}{\partial \ln D} = g_{LL}(\mu_L) g_{LL}(\mu_L) + g_{LR}(\mu_R) g_{RL}(\mu_R) \theta_{\Gamma}(D - V) \quad (5.56a)$$

$$\frac{\partial g_{RL}(\mu_L)}{\partial \ln D} = g_{RL}(\mu_L) g_{LL}(\mu_L) + g_{RR}(\mu_R) g_{RL}(\mu_R) \theta_{\Gamma}(D - V) \quad (5.56b)$$

$$\frac{\partial g_{RL}(\mu_R)}{\partial \ln D} = g_{RL}(\mu_L) g_{LL}(\mu_L) \theta_{\Gamma}(D - V) + g_{RR}(\mu_R) g_{RL}(\mu_R) \quad (5.56c)$$

$$\frac{\partial g_{LR}(\mu_R)}{\partial \ln D} = g_{LL}(\mu_L) g_{LR}(\mu_L) \theta_{\Gamma}(D - V) + g_{LR}(\mu_R) g_{RR}(\mu_R) \quad (5.56d)$$

$$\frac{\partial g_{LR}(\mu_L)}{\partial \ln D} = g_{LL}(\mu_L) g_{LR}(\mu_L) + g_{LR}(\mu_R) g_{RR}(\mu_R) \theta_{\Gamma}(D - V) \quad (5.56e)$$

$$\frac{\partial g_{RR}(\mu_R)}{\partial \ln D} = g_{RL}(\mu_L) g_{LR}(\mu_L) \theta_{\Gamma}(D - V) + g_{RR}(\mu_R) g_{RR}(\mu_R) \quad (5.56f)$$

Here we replaced the chemical potentials within the step function by the bias voltage  $V = \mu_L - \mu_R$ . While an analytic solution of this set of coupled differential equations is tractable, especially in some limiting cases, the calculations can be rather lengthy. Instead we will solve Eq.

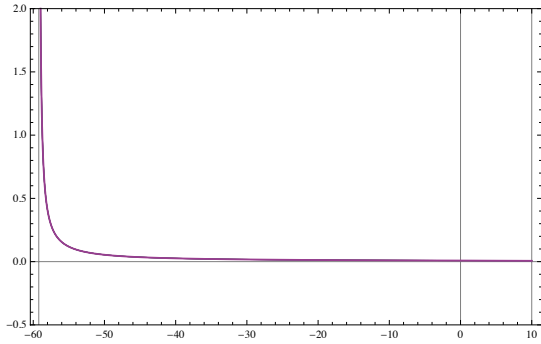


**Figure 5.3:** The running coupling strength as a function of bandwidth  $D$  for a system without decoherence. The system parameters are  $W_0 = \ln D_0 = 10$ ,  $V = 3$ ,  $t_L = t_R = 0.08$ .

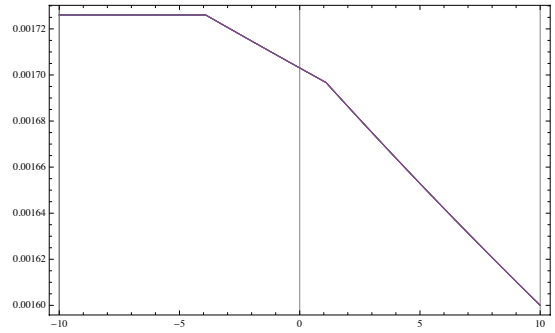


**Figure 5.4:** A close-up of the running couplings in the interval  $[-W_0, W_0]$  after introducing a decoherence rate  $\Gamma = 0.02$ .

(5.56) numerically yielding the coupling strengths  $g_{\alpha\beta}(\mu_\beta)$  as functions of  $W = \ln D$ . Starting from an initially large bandwidth  $D^0$  and small coupling strengths  $g_{\alpha\beta}^0$  we reduce the bandwidth until we reach either zero or the Kondo temperature  $T_K$  earmarked by the divergence of the running couplings. For a given set of initial parameters with symmetric couplings Fig. 5.3 depicts the divergence of the coupling constants at the Kondo temperature, while Fig. 5.4 shows the coupling strengths with incoming energy at the chemical potentials as functions of bandwidth  $D$ . Note the discontinuity due to the step functions turning different terms on and off in Eq. (5.56).

For the case of a vanishing decoherence rate  $\Gamma = 0$  an example result for the coupling strengths  $g$  as a function of bandwidth  $D$  is provided in Figure 5.3. The initial system parameters is given as  $W_0 = \ln D_0 = 10$ ,  $V = 3$ , and  $t_L = t_R = 0.08$ . The initial couplings are given in terms of the tunnelling coefficients  $t_L$  and  $t_r$  in accordance with Eq. (3.43). Note that in this case the couplings diverge at a bandwidth  $\sim T_K$  as argued in Ref. [30].

However introducing a nonzero decoherence rate  $\Gamma > T_K$  the couplings remain small for exponentially small temperatures as predicted in Ref. [31]. The turning on and off performed by the step functions of Eq. (5.56) can be seen e.g. by examining the resulting coupling strengths in the energy window  $[-W_0, W_0]$  as presented in Figure 5.4.

Having calculated the coupling strengths as functions of bandwidth at the relevant chemical potential we may insert those functions into Eq. (5.55). The generated set of equations only depend on the incoming energy  $\varepsilon$  through the arguments of the smeared step functions. Starting the scaling procedure with initial parameters  $D^0$  and  $g_{\alpha\beta}^0$  the set of equations are solved numerically for each of the relevant incoming energies  $\varepsilon$  as shown in Figure 5.5. Note that as  $D$  approaches the Kondo temperature the constant coupling increases as we would expect and peaks form at the chemical potentials  $\varepsilon = \pm V/2$ .

Our initial sample system parameters were chosen symmetric in couplings so  $t_R = t_L$ , and hence the different coupling strengths followed the same scaling flow. The result of the scaling from initially asymmetric system parameters  $t_L \neq t_R$  is shown in Figure 5.6 for the coupling  $g_{LR}(\varepsilon)$ . In this case the initial asymmetry manifests itself even after scaling to exponentially small temperatures.

Having obtained the coupling constant at steady state after scaling to approximately zero temperature relevant physical quantities can be calculated accordingly. The current through the dot can be derived from the equation of motion for the charge density as done in Refs. [32],[34].

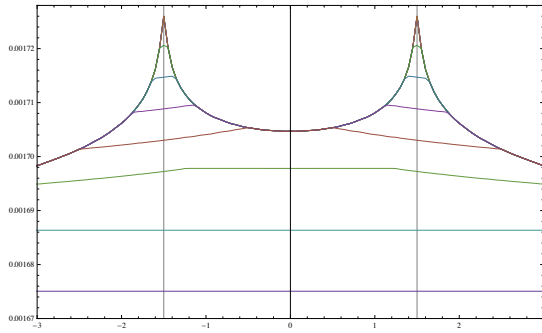


**Figure 5.5:** Running couplings as a function of incoming energy for various stages of the scaling, starting at  $D_0$  and ending at  $D = e^{-300W_0} \approx 0$

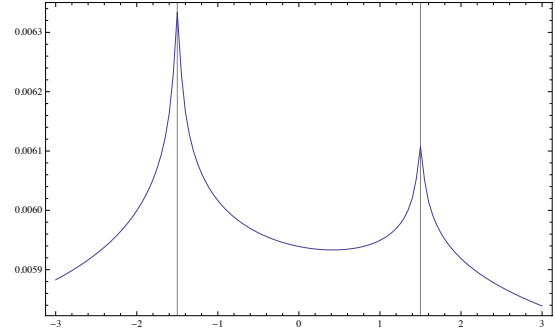


**Figure 5.6:**  $g_{LR}(\varepsilon_b)$  for an asymmetric system with  $W_0 = \ln D_0 = 10$ ,  $V = 3$ ,  $t_L = 0.06$ ,  $t_R = 0.08$  and decoherence  $\Gamma = 0.02$

Here the energy-dependence of the couplings needs to be taken into account accordingly. For a simplified approach considering a quantum dot system strongly coupled to one lead and weakly to the other one can consider the imaginary part of the  $T$  matrix as done in Ref. [37].

# The Nonequilibrium Kondo Problem in a Magnetic Field

---

Having reproduced the scaling equations obtained from direct calculation of the imaginary part of the self-energy by applying a Poor man's scaling approach to the reduced one-body  $S$ -matrix, we turn our attention to a more difficult problem.

Applying a magnetic field,  $\mathbf{B}$ , to the quantum dot system, introduces a Zeeman shift of the electrons in the leads as well as the dot spin. A Hamiltonian describing this system is

$$H(\tau) = H_0(\tau) + H_B(\tau) + H'(\tau), \quad (6.1)$$

where as usual  $H_0(\tau)$  is the unperturbed lead electron Hamiltonian while  $H'(\tau)$  is the Kondo exchange interaction. The perturbation due to a uniform magnetic field  $\mathbf{B}$  is

$$H_B(\tau) = \mathbf{B} \cdot [\gamma_l \mathbf{s}(\tau) + \gamma_d \mathbf{S}(\tau)] = \gamma_l \sum_{\alpha k \sigma \sigma'} B^i c_{\alpha k \sigma}^\dagger(\tau) \tau_{\sigma \sigma'}^i c_{\alpha k \sigma'}(\tau) + \gamma_d B^i S^i(\tau), \quad (6.2)$$

where  $\gamma_l$  and  $\gamma_d$  are the gyromagnetic ratio for lead electrons and dot spin respectively. There is a direct relation between the  $g$ -factor and the gyromagnetic ratio

$$\gamma_d = -\frac{gd\mu_B}{\hbar}, \quad \text{and} \quad \gamma_l = -\frac{gl\mu_B}{2\hbar}. \quad (6.3)$$

The first term of Eq. (6.2) is on a form similar to that of the unperturbed Hamiltonian for the lead-electrons. Thus the effect of this term is to add  $\gamma_l|B|$  to the unperturbed energy of electronic states with spin parallel to the applied magnetic field, and subtracting a similar amount to the energy of electronic states with a spin anti-parallel to the applied field.

However simple this adjustment of the lead electron energy levels we will not consider it here, thus restricting ourselves to the case of a small field  $\frac{\mu_B gl}{\hbar}|B| \ll D$ . The second part of Eq. (6.2) considers only the dot spin,

$$H_{B_d}(\tau) = \gamma_d B^i S^i(\tau). \quad (6.4)$$

In the interaction picture this as a part of the unperturbed Hamiltonian, it simply governs the time-dependence of the dot spin operator,

$$\dot{S}_j(t) = -i[H_{B_d}, S^j(t)] = -i\gamma_d[B_i S^i(t), S^j(t)] = \gamma_d B_i \epsilon_{ijk} S^k(t). \quad (6.5)$$

Taking the  $B$ -field parallel to the  $z$ -direction, we may put Eq. (6.5) on a simpler form by rewriting the spin creation and annihilation operators

$$\dot{S}^+(t) = \dot{S}_x(t) + i\dot{S}_y(t) = -i\gamma_d B S^+(t), \quad (6.6a)$$

$$\dot{S}^-(t) = \dot{S}_x(t) - i\dot{S}_y(t) = i\gamma_d B S^-(t). \quad (6.6b)$$

Integrating both terms results in a simple harmonic time dependence of these operators

$$S^+(t) = S^+ e^{-iBt}, \quad (6.7a)$$

$$S^-(t) = S^- e^{iBt}, \quad (6.7b)$$

$$S^z(t) = S^z. \quad (6.7c)$$

Actually this approach has already been applied to the similar problems as e.g. a nuclear spin in a magnetic field, with the nuclear magnetisation playing the role of the dot spin. In that case the equivalent Eq. (6.5) is known as the Bloch equations cf. Ref. [6] without spin relaxation. If we would later need to include the case of spin relaxation of the dot spin due the full Bloch equations are

$$\dot{S}_x(t) = \gamma B_z S^y(t) - \Gamma_2 S^x(t), \quad (6.8a)$$

$$\dot{S}_y(t) = -\gamma B_z S^x(t) - \Gamma_2 S^y(t), \quad (6.8b)$$

$$\dot{S}_z(t) = \Gamma_1 (S^z(t) - S^z). \quad (6.8c)$$

Where we have introduced the average spin relaxation rates  $\Gamma_1$  and  $\Gamma_2$ . The solution of the above equation can be stated in terms of the usual Bloch equation solutions if adding or subtracting an imaginary component to the  $B$ -field,

$$S^+(t) = S^+ e^{-i(B-i\Gamma_2)t}, \quad (6.9a)$$

$$S^-(t) = S^- e^{i(B+i\Gamma_2)t}, \quad (6.9b)$$

$$S^z(t) = S^z e^{-\Gamma_1 t}. \quad (6.9c)$$

Thus carrying out the calculations applying the solutions of the non-relaxing Bloch equations, it is not impossible to add the decoherence rates at a later time.

## 6.1 The Anisotropic Kondo Hamiltonian

With the introduction of a uniform magnetic field, the system is no longer isotropic. Hence we have no longer any reason to expect the interaction to be independent of spacial orientation. This may also be inferred from Eq. (6.7), which naturally separates the direction of the  $B$ -field from the directions perpendicular to it. This means that in this case our interaction is described by the anisotropic Kondo model. The full system Hamiltonian is then

$$H(\tau) = H_0(\tau) + H'(\tau), \quad (6.10)$$



with

$$H_0 = \sum_a (\varepsilon_a - \mu_a) c_a^\dagger(\tau) c_a + \gamma_d B_i S_i, \quad (6.11)$$

$$\begin{aligned} H'(\tau) &= \sum_{a'a} J_{a'a}^i S^i s_{a'a}^i \\ &= \sum_{a'a} \frac{1}{2} J_{a'a}^\pm [S^+ s_{a'a}^- + S^- s_{a'a}^+] + J_{a'a}^z S^z s_{a'a}^z, \end{aligned} \quad (6.12)$$

where we have assumed that  $J^\pm = J_x = J_y$ .

In order to obtain the scaling relations for the couplings constants  $J^\pm$  and  $J_z$ , we will need to calculate the reduced one-body  $S$ -matrix with band-width  $D$ .

## 6.2 The Effective S-matrix to Order $J^1$

As for the effective one-body  $S$ -matrix to order  $J^1$  we may repeat the argument of the previous chapter, so

$$\delta_D \tilde{S}^{(1)} = \delta_D T_c \left\{ -i \int_c d\tau H'(\tau) \right\} = \delta_D T_c \left\{ -i \frac{1}{2} \int_c d\tau \sum_{aa'} J_{a'a}^i S^i c_a^\dagger \tau_{a'a}^i c_a \right\} = 0. \quad (6.13)$$

## 6.3 The Effective S-matrix to Order $J^2$

As for the effective one-body  $S$ -matrix to order  $J^2$  we have that

$$\tilde{S}^{(2)} = \left\langle T_c \left\{ -\frac{1}{2} \int_c d\tau \int_c d\tau' H'(\tau) H'(\tau') \right\} \right\rangle_{(1)}. \quad (6.14)$$

The first step is simply to calculate the product  $H'(\tau)H'(\tau')$ . Since we are considering the anisotropic Kondo model this includes quite a bit of bookkeeping. When taking into account that  $S^x(\tau)S^x(\tau') = S^y(\tau)S^y(\tau') = 0$ , the result of the multiplication is,

$$\begin{aligned} H'(\tau)H'(\tau') &= \sum_{a'a'b'b} \left\{ \frac{1}{4} J_{a'a}^\pm J_{b'b}^\pm [S^+(\tau)S^-(\tau') s_{a'a}^-(\tau) s_{b'b}^+(\tau') + S^-(\tau)S^+(\tau') s_{a'a}^+(\tau) s_{b'b}^-(\tau')] \right. \\ &\quad + \frac{1}{2} J_{a'a}^\pm J_{b'b}^z [S^+(\tau)S^z(\tau') s_{a'a}^-(\tau) s_{b'b}^z(\tau') + S^-(\tau)S^z(\tau') s_{a'a}^+(\tau) s_{b'b}^z(\tau')] \\ &\quad + \frac{1}{2} J_{a'a}^z J_{b'b}^\pm [S^z(\tau)S^-(\tau') s_{a'a}^z(\tau) s_{b'b}^+(\tau') + S^z(\tau)S^+(\tau') s_{a'a}^z(\tau) s_{b'b}^-(\tau')] \\ &\quad \left. + J_{a'a}^z J_{b'b}^z [S^z(\tau)S^z(\tau') s_{a'a}^z(\tau) s_{b'b}^z(\tau')] \right\}. \end{aligned} \quad (6.15)$$

Next step is to apply the time-ordering to this expression. Here it is convenient that the lead electron spin operators as well as dot spin operators are bosonic with respect to the time ordering  $T_c$ , i.e.  $S^i S^j = S^j S^i$ .

Renaming both times and state variables accordingly we encounter four different terms under the time-ordering

$$\begin{aligned} S^{(2)} &= T_c \left\{ -\frac{1}{2} \int d\tau \int d\tau' H'(\tau) H'(\tau') \right\} \\ &= S_z^{(2)} + S_{pot.}^{(2)} + S_-^{(2)} + S_+^{(2)}, \end{aligned} \quad (6.16)$$

with

$$S_z^{(2)} = -\frac{1}{2} T_c \sum_{a'ab'b} \int_c d\tau \int_c d\tau' \frac{1}{2} J_{a'a}^\pm J_{b'b}^\pm S^+(\tau) S^-(\tau') s_{a'a}^-(\tau) s_{b'b}^+(\tau'), \quad (6.17)$$

$$S_{pot.}^{(2)} = -\frac{1}{2} T_c \sum_{a'ab'b} \int_c d\tau \int_c d\tau' J_{a'a}^z J_{b'b}^z S^z(\tau) S^z(\tau') s_{a'a}^z(\tau) s_{b'b}^z(\tau'), \quad (6.18)$$

$$S_-^{(2)} = -\frac{1}{2} T_c \sum_{a'ab'b} \int_c d\tau \int_c d\tau' J_{a'a}^\pm J_{b'b}^\pm S^+(\tau) S^z(\tau') s_{a'a}^-(\tau) s_{b'b}^z(\tau'), \quad (6.19)$$

$$S_+^{(2)} = -\frac{1}{2} T_c \sum_{a'ab'b} \int_c d\tau \int_c d\tau' J_{a'a}^\pm J_{b'b}^\pm S^-(\tau) S^z(\tau') s_{a'a}^+(\tau) s_{b'b}^z(\tau'). \quad (6.20)$$

Where we in the naming of the different terms anticipate the nature of their contributions to the overall  $S$ -matrix.

Focusing on the first contribution  $S_z^{(2)}$ , next step is to apply the averaging function  $\langle \dots \rangle_{(1)}$  transforming the  $S$ -matrix into the one-body reduced  $S$ -matrix. Remembering that we may write the lead electron spin operators in terms of common creation and annihilation operators,

$$s_{a'a}^+(\tau) = s_{a'a}^x(\tau) + i s_{a'a}^y(\tau) = c_{a'\uparrow}^\dagger(\tau) c_{a\downarrow}(\tau) \quad (6.21a)$$

$$s_{a'a}^-(\tau) = s_{a'a}^x(\tau) - i s_{a'a}^y(\tau) = c_{a'\downarrow}^\dagger(\tau) c_{a\uparrow}(\tau) \quad (6.21b)$$

Here we have introduced the notation  $c_{a\sigma}^\dagger = \delta_{\sigma,\sigma_a} c_{\alpha_a k_a \sigma_a}^\dagger$ . We get that

$$\begin{aligned} \tilde{S}_z^{(2)} &= -\frac{1}{2} \left\langle T_c \sum_{a'ab'b} \int_c d\tau \int_c d\tau' \frac{1}{2} J_{a'a}^\pm J_{b'b}^\pm S^+(\tau) S^-(\tau') s_{a'a}^-(\tau) s_{b'b}^+(\tau') \right\rangle_{(1)} \\ &= \frac{1}{4} T_c \sum_{a'ab} \int_c d\tau \int_c d\tau' \left\{ J_{a'a}^\pm J_{ab}^\pm S^+(\tau) S^-(\tau') \langle c_{a\uparrow}(\tau) c_{a\uparrow}^\dagger(\tau') \rangle c_{a'\downarrow}^\dagger(\tau) c_{b\downarrow}(\tau') \right. \\ &\quad \left. + J_{ba}^\pm J_{b'b}^\pm S^+(\tau) S^-(\tau') \langle c_{b\downarrow}(\tau') c_{b\downarrow}^\dagger(\tau) \rangle c_{b'\uparrow}^\dagger(\tau') c_{a\uparrow}(\tau) \right\}. \end{aligned} \quad (6.22)$$

Replace the average with the appropriate Green's function and rename both state variables  $a$ ,  $b$  etc. and time variables  $\tau$  and  $\tau'$  in order to reduce the above to

$$\begin{aligned} \tilde{S}_z^{(2)} &= -\frac{i}{4} T_c \sum_{a'ab} \int_c d\tau \int_c d\tau' \left\{ J_{a'a}^\pm J_{ab}^\pm S^+(\tau) S^-(\tau') G_a^{(0)}(\tau, \tau') c_{a'\downarrow}^\dagger(\tau) c_{b\downarrow}(\tau') \right. \\ &\quad \left. + J_{a'a}^\pm J_{ab}^\pm S^+(\tau') S^-(\tau) G_a^{(0)}(\tau, \tau') c_{a'\uparrow}^\dagger(\tau) c_{b\uparrow}(\tau') \right\}. \end{aligned} \quad (6.23)$$

The two terms of the last expression have two subtle differences. One is that the time-labels for the dot spin operator are interchanged, and the other is that the lead electron spin reads  $\downarrow$

in one term and  $\uparrow$  in the other. To reduce the amount of calculation one term is immediately extrapolable having calculated the other term. Thus we split

$$\tilde{S}_z^{(2)} = \tilde{S}_{z\downarrow}^{(2)} + \tilde{S}_{z\uparrow}^{(2)} \quad (6.24)$$

### 6.3.0.1 Contour Ordering

The Schwinger-Keldysh representation of  $\tilde{S}_z^{(2)}$  from Eq. (6.23) is

$$\tilde{S}_z^{(2)} = \begin{pmatrix} \tilde{S}_{z,11}^{(2)} & \tilde{S}_{z,12}^{(2)} \\ \tilde{S}_{z,21}^{(2)} & \tilde{S}_{z,22}^{(2)} \end{pmatrix}. \quad (6.25)$$

Starting with the diagonal components, we concentrate on  $\tilde{S}_{z,11}^{(2)}$  i.e. with both times residing on the upper part of the Keldysh contour. For the first term of Eq. (6.24) we have that

$$\tilde{S}_{z\downarrow,11}^{(2)} = -\frac{i}{4} \sum_{a'ab} J_{a'a}^{\pm} J_{ab}^{\pm} \int_{-\infty}^{\infty} dt \left\{ \int_{-\infty}^t dt' S^+(t) S^-(t') G_a^{(0)>}(t, t') c_{a'\downarrow}^{\dagger}(t) c_{b\downarrow}(t') \right. \\ \left. + \int_t^{\infty} dt' S^-(t') S^+(t) G_a^{(0)<}(t, t') \left[ -c_{b\downarrow}(t') c_{a'\downarrow}^{\dagger}(t) \right] \right\}. \quad (6.26)$$

While this expression looks somewhat similar to Eq. (5.23) of the previous chapter, there is a couple of important differences.

The first major difference involves the integration over the intermediate time  $t'$ . While the creation and annihilation operators follow the usual interaction picture time-evolution, the dot spin operators evolve according to Eq. (6.7). Extraction of the total time evolution allows us to evaluate,

$$\int_{-\infty}^t dt' \left\{ e^{-i\gamma_d B(t'-t)} e^{-i\varepsilon_{a\uparrow}(t-t')} e^{-i\varepsilon_{b\downarrow} t'} e^{i\varepsilon_{a'\downarrow} t} \right\} = \frac{e^{-i\varepsilon_{b\downarrow} t} e^{i\varepsilon_{a'\downarrow} t}}{i(-\gamma_d B + \varepsilon_{a\uparrow} - \varepsilon_{b\downarrow} - i0^+)} \quad (6.27)$$

and

$$\int_t^{\infty} dt' \left\{ e^{-i\gamma_d B(t'-t)} e^{-i\varepsilon_{a\uparrow}(t-t')} e^{-i\varepsilon_{b\downarrow} t'} e^{i\varepsilon_{a'\uparrow} t} \right\} = -\frac{e^{-i\varepsilon_{b\downarrow} t} e^{i\varepsilon_{a'\downarrow} t}}{i(-\gamma_d B + \varepsilon_{a\uparrow} - \varepsilon_{b\downarrow} + i0^+)} \quad (6.28)$$

Note that the  $B$ -field strength conveniently enters the denominator on the same terms as the bias voltage. As before the remaining  $t$ -dependence can be absorbed as the time-evolution of the creation and annihilation operators.

We are now at a stage where we may apply the spin ordering, using that

$$S^+ S^- = \frac{1}{2} + S^z, \quad S^- S^+ = \frac{1}{2} - S^z.$$

The result of these manipulations is

$$\tilde{S}_{z\downarrow,11}^{(2)} = -\frac{i}{4} \sum_{a'ab} J_{a'a}^{\pm} J_{ab}^{\pm} \int_{-\infty}^{\infty} dt \left\{ \frac{(\frac{1}{2} + S^z) (f_{\mu_a}(\varepsilon_a) - 1) c_{a'\downarrow}^{\dagger}(t) c_{b\downarrow}(t)}{-\gamma_d B + \varepsilon_{a\uparrow} - \varepsilon_{b\downarrow} - i0^+} \right. \\ \left. - \frac{(\frac{1}{2} - S^z) f_{\mu_a}(\varepsilon_a) (c_{a'\downarrow}^{\dagger}(t) c_{b\downarrow}(t) - \delta_{ab})}{-\gamma_d B + \varepsilon_{a\uparrow} - \varepsilon_{b\downarrow} + i0^+} \right\}, \quad (6.29)$$

and by the reasoning of section 5.4.1, we may calculate the variation of this expression, as

$$\delta_D \tilde{S}_{z\downarrow,11}^{(2)} = -\frac{i\nu_F}{4} \sum_{a'b} \sum_{\alpha} J_{a'\alpha}^{\pm} J_{\alpha b}^{\pm} \int_{-\infty}^{\infty} dt \int_{\square} d\xi \left\{ \frac{(\frac{1}{2} + S^z) (f(\xi) - 1) c_{a'\downarrow}^{\dagger}(t) c_{b\downarrow}(t)}{-\gamma_d B + \xi + \mu_{\alpha} - \varepsilon_{b\downarrow} - i0^+} - \frac{(\frac{1}{2} - S^z) f(\xi) (c_{a'\downarrow}^{\dagger}(t) c_{b\downarrow}(t) - \delta_{ab})}{-\gamma_d B + \xi + \mu_{\alpha} - \varepsilon_{b\downarrow} + i0^+} \right\}. \quad (6.30)$$

Again there is a contribution from the real part of Eq. (6.30), when exactly we have that  $-\gamma_d B \pm D + \mu_{\alpha} - \varepsilon_{b\downarrow} = 0$ . As explained in the analysis of the previous chapter this term is unimportant to the scaling and thus will it not be included in the calculation.

The imaginary part can be split in three different contributions

$$\delta_D \tilde{S}_{z\downarrow,11}^{(2)} = i\delta_D \text{Im} \tilde{S}_{z\downarrow,11}^{(2)} = \delta_D \tilde{S}_{\downarrow, \text{cnst.}}^{(2)} + \delta_D \tilde{S}_{\downarrow, \text{pot.}}^{(2)} + \delta_D \tilde{S}_{\downarrow, \text{ex.}}^{(2)}. \quad (6.31)$$

The first term  $\delta_D \tilde{S}_{\downarrow, \text{cnst.}}^{(2)}$  again evaluates to infinity. Like earlier most of these infinities end up being cancelled by similar terms of the  $\delta_D \tilde{S}_{z\downarrow,22}^{(2)}$  component. But we will not delve into a detailed analysis of this term here.

The potential scattering term  $\delta_D \tilde{S}_{\downarrow, \text{pot.}}^{(2)}$  stemming from the factor  $\frac{1}{2}$  in the spin sum, yields

$$\delta_D \tilde{S}_{\downarrow, \text{pot.}}^{(2)} = \frac{i\nu_F}{8} \sum_{a'b} \int_{-\infty}^{\infty} dt \sum_{\alpha} J_{a'\alpha}^{\pm} J_{\alpha b}^{\pm} c_{a'\downarrow}^{\dagger}(t) c_{b\downarrow}(t) \times \left\{ \frac{\delta D}{D - \gamma_d B + \mu_{\alpha} - \varepsilon_{b\downarrow}} + \frac{\delta D}{-D - \gamma_d B + \mu_{\alpha} - \varepsilon_{b\downarrow}} \right\}. \quad (6.32)$$

The exchange term then is

$$\delta_D \tilde{S}_{\downarrow, \text{ex.}}^{(2)} = \frac{i\nu_F}{4} \sum_{a'b} \int_{-\infty}^{\infty} dt \sum_{\alpha} J_{a'\alpha}^{\pm} J_{\alpha b}^{\pm} S^z c_{a'\downarrow}^{\dagger}(t) c_{b\downarrow}(t) \times \left\{ \frac{\delta D}{D - \gamma_d B + \mu_{\alpha} - \varepsilon_{b\downarrow}} - \frac{\delta D}{-D - \gamma_d B + \mu_{\alpha} - \varepsilon_{b\downarrow}} \right\}. \quad (6.33)$$

This concludes the evaluation of the  $\tilde{S}_{z\downarrow,1}^{(2)}$ . Calculations very similar to the ones we have just carried out yield for the remaining term of Eq. (6.24),  $\tilde{S}_{z\uparrow,11}^{(2)}$ ,

$$\delta_D \tilde{S}_{\uparrow, \text{pot.}}^{(2)} = \frac{i\nu_F}{8} \sum_{a'b} \int_{-\infty}^{\infty} dt \sum_{\alpha} J_{a'\alpha}^{\pm} J_{\alpha b}^{\pm} c_{a'\uparrow}^{\dagger}(t) c_{b\uparrow}(t) \times \left\{ \frac{1}{D + \gamma_d B + \mu_{\alpha} - \varepsilon_{b\uparrow}} + \frac{1}{-D + \gamma_d B + \mu_{\alpha} - \varepsilon_{b\uparrow}} \right\}. \quad (6.34)$$

And for the exchange term we have

$$\delta_D \tilde{S}_{\uparrow, \text{ex.}}^{(2)} = -\frac{i\nu_F}{4} \sum_{a'b} \int_{-\infty}^{\infty} dt \sum_{\alpha} J_{a'\alpha}^{\pm} J_{\alpha b}^{\pm} S^z c_{a'\uparrow}^{\dagger}(t) c_{b\uparrow}(t) \times \left\{ \frac{1}{D + \gamma_d B + \mu_{\alpha} - \varepsilon_{b\uparrow}} - \frac{1}{-D + \gamma_d B + \mu_{\alpha} - \varepsilon_{b\uparrow}} \right\} \quad (6.35)$$

We may evaluate the remaining diagonal component  $\tilde{S}_{z,11}^{(2)}$  in the matrix-representation of the effective  $S$ -matrix with both operators residing on the lower Keldysh contour. For the

$$\begin{aligned} \tilde{S}_{z,22}^{(2)} = & -\frac{i}{4} \sum_{a'a'b} J_{a'a}^{\pm} J_{ab}^{\pm} \int_{\infty}^{-\infty} dt \left\{ \int_{\infty}^t dt' S^{-}(t) S^{+}(t') G_a^{(0)>}(t, t') c_{a'\downarrow}^{\dagger}(t) c_{b\downarrow}(t') \right. \\ & \left. + \int_t^{-\infty} dt' S^{+}(t') S^{-}(t) G_a^{(0)<}(t, t') \left[ -c_{b\downarrow}(t') c_{a'\downarrow}^{\dagger}(t) \right] \right\} \quad (6.36) \end{aligned}$$

Using similar arguments as in the previous chapter one may convince oneself that with regard to the scaling  $\delta_D \tilde{S}_{z,22}^{(2)} = -\delta_D \tilde{S}_{z,11}^{(2)}$ , and likewise  $\delta_D \tilde{S}_{z,22}^{(2)} = -\delta_D \tilde{S}_{z,11}^{(2)}$

As for the off-diagonal Schwinger-Keldysh components,

$$\begin{aligned} \delta_D \tilde{S}_{z,12}^{(2)} &= \frac{i}{4} \sum_{a'\alpha b} J_{a'a}^{\pm} J_{ab}^{\pm} \int_{-\infty}^{\infty} dt \int_{\square} d\xi \int_{\infty}^{-\infty} dt' S^{-}(t') S^{+}(t) c_{b\downarrow}(t) c_{a'\downarrow}^{\dagger}(t) i f(\xi) e^{-i(\xi+\mu_{\alpha})(t-t')} \\ &= -\frac{\pi}{2} \sum_{a'\alpha b} J_{a'a}^{\pm} J_{ab}^{\pm} \int_{-\infty}^{\infty} dt \int_{\square} d\xi \int_{\infty}^{-\infty} dt' S^{-}(t') S^{+}(t) c_{b\downarrow}(t) c_{a'\downarrow}^{\dagger}(t) f(\xi) \delta(\xi + \gamma_d B + \mu_{\alpha} - \varepsilon_b) \\ &= \begin{cases} \text{non-zero,} & \text{for } \xi + \gamma_d B + \mu_{\alpha} - \varepsilon_b = 0 \\ 0, & \text{else} \end{cases} \end{aligned}$$

And these terms can again be ignored for most energies.

## 6.4 The Scaling Equations

For the  $\tilde{S}_z^{(2)}$  component of the effective one-body  $S$ -matrix we may repeat the scaling procedure of section 5.5.

The prefactor of the potential scattering terms is of the same form as in the previous chapter, and on the average of either incoming energies  $\varepsilon_b$  or bandwidth  $D$  such terms yield zero. Thus the final expression for the change of the  $S$ -matrix with bandwidth

$$\begin{aligned} \delta_D \tilde{S}_z^{(2)} &= -\frac{i\nu_F}{2} \sum_{a'b} \int_c d\tau \sum_{\alpha} J_{a'\alpha}^{\pm} J_{\alpha b}^{\pm} S^z \\ &\times \left\{ \frac{c_{a'\uparrow}^{\dagger}(\tau) c_{b\uparrow}(\tau)}{D^2 - (-\gamma_d B - \mu_{\alpha} + \varepsilon_{b\uparrow})^2} - \frac{c_{a'\downarrow}^{\dagger}(\tau) c_{b\downarrow}(\tau)}{D^2 - (\gamma_d B - \mu_{\alpha} + \varepsilon_{b\downarrow})^2} \right\} D \delta D \quad (6.37) \end{aligned}$$

By plugging into the Callan-Symanzik like scaling equations of the previous Chapter 5 and collecting terms on similar operator forms yield a spin dependent scaling equation for the coupling constant

$$\frac{\delta J_{\alpha'\beta}^{z\sigma}}{\delta \ln D} = \nu_F \sum_{\alpha} J_{\alpha'\alpha}^{\pm} J_{\alpha\beta}^{\pm} \frac{D^2}{D^2 - (\varepsilon_{\sigma b} - \mu_{\alpha} + \sigma \gamma_d B)^2} \quad (6.38a)$$

Similar derivations for the  $\delta_D \tilde{S}_+^{(2)}$  and  $\delta_D \tilde{S}_-^{(2)}$  terms has been sketched in Appendix A. The resulting scaling equation is

$$\frac{\delta J_{\alpha'\beta}^{\pm}}{\delta \ln D} = \frac{1}{2} \nu_F \sum_{\alpha} \left( J_{\alpha'\alpha}^z J_{\alpha\beta}^{\pm} + J_{\alpha'\alpha}^{\pm} J_{\alpha\beta}^z \right) \left( \frac{D^2}{D^2 - (\varepsilon_b - \mu_{\alpha})^2} + \frac{D^2}{D^2 - (\varepsilon_b - \mu_{\alpha} - \gamma_d B)^2} \right) \quad (6.38b)$$

Our reasoning about the magnetic field breaking the spacial symmetry of the problem has proven important. The scaling relations for the different coupling strengths either transverse to or parallel with the magnetic field scale differently with bandwidth  $D$ . This is equivalent to Anderson's original treatment of the anisotropic Kondo model [16]. However in Anderson's case it was the initial difference between the transverse and parallel coupling strengths that broke the spacial symmetry.

Let us first consider the result in the limit of a vanishing magnetic field,  $B \approx 0$ . Here the scaling equations reduce to

$$\frac{\delta J_{\alpha'\beta}^{z\sigma}}{\delta \ln D} = \nu_F \sum_{\alpha} J_{\alpha'\alpha}^{\pm} J_{\alpha\beta}^{\pm} \frac{D^2}{D^2 - (\varepsilon - \mu_{\alpha})^2} \quad (6.39a)$$

and

$$\frac{\delta J_{\alpha'\beta}^{\pm}}{\delta \ln D} = \nu_F \sum_{\alpha} \left( J_{\alpha'\alpha}^z J_{\alpha\beta}^{\pm} + J_{\alpha'\alpha}^{\pm} J_{\alpha\beta}^z \right) \frac{D^2}{D^2 - (\varepsilon - \mu_{\alpha})^2} \quad (6.39b)$$

First we note that in the isotropic case setting  $J^{\pm} = J^z$ , the scaling equations are identical to the results of the previous calculations Eq. (5.52), when inserting the appropriate step functions. If we instead assume that the coupling to one of the leads are extraordinarily poor, e.g.  $t_R^z, t_R^{\pm} \approx 0$  meaning that  $J_{LR}^i, J_{RR}^i \approx 0$ . As previously mentioned this limit is identical to the Kondo problem of dilute alloys. For incoming energies close to the chemical potential  $\varepsilon_L \approx \mu_L$  the scaling equations are

$$\frac{\delta J_{LL}^{z\sigma}}{\delta \ln D} = \nu_F J_{LL}^{\pm} J_{LL}^{\pm} \quad (6.40a)$$

$$\frac{\delta J_{LL}^{\pm}}{\delta \ln D} = \nu_F J_{LL}^{\pm} J_{LL}^z, \quad (6.40b)$$

reproducing the results of Anderson's original calculation of Eq. (3.19).

The final test for the equations is against the results of Rosch et al. [32]. Replacing the  $D^2/(D^2 - K^2)$  by the Heaviside step functions  $\theta(D - |K|)$  as discussed in the previous chapter, we obtain the results

$$\frac{\delta J_{\alpha'\beta}^{z\sigma}}{\delta \ln D} = \nu_F \sum_{\alpha} J_{\alpha'\alpha}^{\pm} J_{\alpha\beta}^{\pm} \theta(D - |\varepsilon_{\sigma b} - \mu_{\alpha} + \sigma \gamma_d B|) \quad (6.41a)$$

$$\frac{\delta J_{\alpha'\beta}^{\pm}}{\delta \ln D} = \frac{1}{2} \nu_F \sum_{\alpha} \left( J_{\alpha'\alpha}^z J_{\alpha\beta}^{\pm} + J_{\alpha'\alpha}^{\pm} J_{\alpha\beta}^z \right) \left( \theta(D - |\varepsilon_b - \mu_{\alpha}|) + \theta(D - |\varepsilon_b - \mu_{\alpha} - \gamma_d B|) \right) \quad (6.41b)$$

Assume that  $J_{LL} = J_{LR} = J_{RL} = J_{RR}$  for both superscript  $z$  and  $\pm$ , and choose the zero of energy such that  $\mu_L = V/2$  and  $\mu_R = -V/2$ . Consider only incoming energies  $|\varepsilon_b| < D$ . Inserting the energy-arguments of the running coupling constants taken at the Fermi level (remembering that we must include the shift due to magnetic field), the scaling equations can be written on the simpler form, which compares fairly well with the scaling equations of Rosch

et al. cf. Eq. (5) in Ref. [32]. The result is

$$\frac{\delta J^{z\sigma}(\varepsilon_b)}{\delta \ln D} = \nu_F \sum_{\beta} J^{\pm} (\beta V/2 + \sigma \gamma_l B)^2 \theta(\varepsilon_{\sigma b} + \beta V/2 + \sigma \gamma_l B) \quad (6.42a)$$

$$\begin{aligned} \frac{\delta J^{\pm}(\varepsilon_b)}{\delta \ln D} &= \frac{1}{2} \nu_F \sum_{\beta=-1,1} \sum_{\sigma} J^{z\sigma} (\beta V/2) J^{\pm} (\beta V/2 + \sigma \gamma_l B) \\ &\quad \times [\theta(\varepsilon_b + \beta V/2) + \theta(\varepsilon_b + \beta V/2 - \gamma_d B)] \end{aligned} \quad (6.42b)$$

Where we have remembered that  $J^z = J^{z\uparrow} + J^{z\downarrow}$ . This concludes the investigation of the 1-loop scaling equations for both non-zero magnetic field and bias voltage.





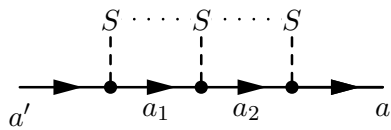
# Towards 2-loop Poor Man's Scaling on the Keldysh Contour

---

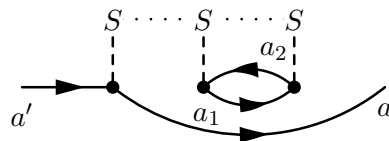
Emboldened by the success we will use this chapter to touch upon calculations for the 2-loop corrections to the scaling equations for the case of zero magnetic field. In this case we may build upon the results of Chapter 5.1, and to third order in the coupling strength,

$$\begin{aligned} \tilde{S}^{(3)} = \frac{1}{(2i)^3} \frac{1}{3!} T_c \left\{ \int_c d\tau \int_c d\tau' \int_c d\tau'' \sum_{aa'} \sum_{de} \sum_{bb'} J_{aa'} J_{ed} J_{bb'} S^i(\tau) S^j(\tau') S^k(\tau'') \right. \\ \left. \times \tau_{aa'}^i \tau_{ed}^j \tau_{bb'}^k \left\langle c_a^\dagger(\tau) c_{a'}(\tau) c_e^\dagger(\tau') c_d(\tau') c_b^\dagger(\tau'') c_{b'}(\tau'') \right\rangle_{(1)} \right\}, \end{aligned} \quad (7.1)$$

which imply that  $\tilde{S}^{(3)}$  is represented by Feynman diagrams containing three interaction points. This amounts to two topologically different diagrams, where we have left out diagrams containing a single fermion loop. The “straight” diagram of Figure 7.1.1 has  $3! = 6$  alterations, hence



7.1.1: Example of straight diagram



7.1.2: Example of loop diagram

contributing to the  $S$ -matrix with,

$$\begin{aligned}
\tilde{S}_{straight}^{(3)} &= \frac{i}{8} \sum_{ab'} \sum_{de} J_{ae} J_{de} J_{eb'} \tau_{ad}^i \tau_{de}^k \tau_{eb'}^j T_c \int_c d\tau \int_c d\tau' \int_c d\tau'' S^i(\tau) S^j(\tau') S^k(\tau'') \\
&\quad \times c_a^\dagger(\tau) c_{b'}(\tau') \langle T_c c_d(\tau) c_d^\dagger(\tau'') \rangle \langle T_c c_e(\tau'') c_e^\dagger(\tau') \rangle \\
&= -\frac{i}{8} \sum_{ab'} \sum_{de} J_{ae} J_{de} J_{eb'} \tau_{ad}^i \tau_{de}^k \tau_{eb'}^j T_c \int_c d\tau \int_c d\tau' \int_c d\tau'' S^i(\tau) S^j(\tau') S^k(\tau'') \\
&\quad \times c_a^\dagger(\tau) c_{b'}(\tau') G_d^{(0)}(\tau, \tau'') G_e^{(0)}(\tau'', \tau').
\end{aligned} \tag{7.2}$$

The “loop” diagram of Figure 7.1.2 has 3 representation thus contributing with a total of

$$\begin{aligned}
\tilde{S}_{loop}^{(3)} &= \frac{i}{16} \sum_{ab'} \sum_{de} J_{ab'} J_{de} J_{ed} \tau_{ab'}^i \tau_{de}^k \tau_{ed}^j T_c \int_c d\tau \int_c d\tau' \int_c d\tau'' S^i(\tau) S^j(\tau') S^k(\tau'') \\
&\quad \times c_a^\dagger(\tau) c_{b'}(\tau') \langle T_c c_d(\tau') c_d^\dagger(\tau'') \rangle \langle T_c c_e(\tau'') c_e^\dagger(\tau') \rangle \\
&= -\frac{i}{16} \sum_{ab'} \sum_{de} J_{ab'} J_{de} J_{ed} \tau_{ab'}^i \tau_{de}^k \tau_{ed}^j T_c \int_c d\tau \int_c d\tau' \int_c d\tau'' S^i(\tau) S^j(\tau') S^k(\tau'') \\
&\quad \times c_a^\dagger(\tau) c_{b'}(\tau') G_d^{(0)}(\tau', \tau'') G_e^{(0)}(\tau'', \tau')
\end{aligned} \tag{7.3}$$

## 7.1 Straight Terms

### 7.1.1 Contour Ordering

Because we only seek to sketch the necessary calculations we will not consider the different Schwinger-Keldysh components of the contour-ordered  $S$ -matrix. Instead we will adhere to a more sloppy notation that does not distinguish between terms with field operators residing on the same contour or terms with field operators residing on different contour.

Keeping this in mind we proceed with the contour-ordering of the “straight” terms. Since three different time-parameters are involved we end up with a total of 6 different terms cf. Appendix B, all of the form

$$S_{straight}^{(3)} = -\frac{i}{8} \sum_{ab'} \sum_{de} J_{ae} J_{de} J_{eb'} \tau_{ad}^i \tau_{de}^k \tau_{eb'}^j \left( \int_{-\infty}^{\infty} dt + \int_{\infty}^{-\infty} dt \right) \sum_n^6 K_n \tag{7.4}$$

With

$$\tau'' < \tau' < \tau : K_1 = \int_{-\infty}^t dt' \int_{-\infty}^{t'} dt'' S^k S^j S^i c_{b'}(t') c_a^\dagger(t) G_d^{(0)>}(t, t'') G_e^{(0)<}(t'', t') \tag{7.5}$$

$$\tau' < \tau'' < \tau : K_2 = \int_{-\infty}^t dt' \int_{t'}^t dt'' S^j S^k S^i c_{b'}(t') c_a^\dagger(t) G_d^{(0)>}(t, t'') G_e^{(0)>}(t'', t') \tag{7.6}$$

$$\tau' < \tau < \tau'' : K_3 = \int_{-\infty}^t dt' \int_t^{-\infty} dt'' S^j S^i S^k c_{b'}(t') c_a^\dagger(t) G_d^{(0)<}(t, t'') G_e^{(0)>}(t'', t') \tag{7.7}$$

$$\tau'' < \tau < \tau' : K_4 = \int_t^{-\infty} dt' \int_{-\infty}^t dt'' S^k S^i S^j c_a^\dagger(t) c_{b'}(t') G_d^{(0)>}(t, t'') G_e^{(0)<}(t'', t') \quad (7.8)$$

$$\tau < \tau'' < \tau' : K_5 = \int_t^{-\infty} dt' \int_t^{t'} dt'' S^i S^k S^j c_a^\dagger(t) c_{b'}(t') G_d^{(0)<}(t, t'') G_e^{(0)<}(t'', t') \quad (7.9)$$

$$\tau < \tau' < \tau'' : K_6 = \int_t^{-\infty} dt' \int_{t'}^{-\infty} dt'' S^i S^j S^k c_a^\dagger(t) c_{b'}(t') G_d^{(0)<}(t, t'') G_e^{(0)>}(t'', t') \quad (7.10)$$

### 7.1.2 Spin sums

No more tricks can be invoked to reduce this mammoth expression, and we resort as always to straight-forward calculations.

Let us begin by contracting the spin sums. From the common prefactor we see that  $\sum_{de} \tau_{ad}^i \tau_{de}^k \tau_{eb'}^j = (\tau^i \tau^k \tau^j)_{ab'}$ , and thus

$$\tau^i \tau^k \tau^j = \delta_{kj} \tau^i - \varepsilon_{kjm} \varepsilon_{imn} \tau^n + i \varepsilon_{ikj} \tau^0 = \delta_{kj} \tau^i + \delta_{ki} \tau^j - \delta_{ji} \tau^k + i \varepsilon_{ikj} \tau^0 \quad (7.11)$$

We disregard the last imaginary term as it correspond to a potential scattering term. When combining the three first terms of Eq. (7.11) with any permutation of  $S^i S^j S^k$ , we end up with terms like

$$\sum_j S^j S^i S^j = -\frac{1}{4} S^i \quad \text{and} \quad \sum_j S^j S^j S^i = \frac{3}{4} S^i \quad (7.12)$$

and

$$\tau^i \tau^k \tau^j S^k S^j S^i = \tau^i S^j S^j S^i + \tau^j S^i S^j S^i - \tau^k S^k S^i S^i = \frac{3}{4} \tau^i S^i - \frac{1}{4} \tau^i S^i - \frac{3}{4} \tau^i S^i = -\frac{1}{4} \tau^i S^i \quad (7.13)$$

Likewise the two last terms yield,

$$\tau^i \tau^k \tau^j S^j S^k S^i = \frac{7}{4} \tau^i S^i \quad (7.14)$$

$$\tau^i \tau^k \tau^j S^j S^i S^k = -\frac{1}{4} \tau^i S^i \quad (7.15)$$

Hence in general  $K_1, \dots, K_6 \propto S^i$  by construction.

### 7.1.3 Time integrals

Having dealt with the spin sums we turn to the evaluation of the time integrals. First we may write out the bare Green's functions

$$\begin{aligned} K_1 &= - \int_{-\infty}^t dt' \int_{-\infty}^{t'} dt'' \frac{1}{4} S^i c_{b'}(t') c_a^\dagger(t) (1 - f(\xi_d)) e^{-i\varepsilon_d(t-t'')} f(\xi_e) e^{-i\varepsilon_e(t''-t')} \\ &= -\frac{1}{4} S^i (1 - f(\xi_d)) f(\xi_e) e^{-i\xi_d t} \int_{-\infty}^t dt' c_{b'}(t') c_a^\dagger(t) e^{i\xi_e t'} \int_{-\infty}^{t'} dt'' e^{-it''(\varepsilon_e - \varepsilon_d)} \\ &= -\frac{i}{4} S^i (1 - f(\xi_d)) f(\xi_e) e^{-i\varepsilon_d t} \frac{1}{\varepsilon_e - \varepsilon_d + i0_+} \int_{-\infty}^t dt' c_{b'}(t') c_a^\dagger(t) e^{i\varepsilon_e t'} \end{aligned} \quad (7.16)$$

Extracting the time-evolution of the field operators we obtain

$$\begin{aligned} K_1 &= -\frac{i}{4} S^i c_{b'} c_a^\dagger e^{-i\varepsilon_a t} (1 - f(\xi_d)) f(\xi_e) e^{-i\varepsilon_d t} \frac{1}{\varepsilon_e - \varepsilon_d + i0_+} \int_{-\infty}^t dt' e^{it'(\varepsilon_d + \varepsilon_{b'})} \\ &= -\frac{1}{4} S^i c_{b'}(t) c_a^\dagger(t) (1 - f(\xi_d)) f(\xi_e) \frac{1}{\varepsilon_e - \varepsilon_d + i0_+} \frac{1}{\varepsilon_d + \varepsilon_{b'} - i0_+} \end{aligned} \quad (7.17)$$

The rest of  $K_2$  through  $K_6$  yield similar results.

### 7.1.4 Energy Integrals

Ignoring any imaginary parts of  $K_1$  the necessary energy integrals in general looks like

$$\begin{aligned} \int_{-D}^T d\xi \int_T^D d\xi' \frac{1}{\xi' - \xi + \text{const.}} \frac{1}{\xi + \text{const.}} &\sim \int_{-D}^T d\xi \ln \left( \frac{D - \xi + \text{const.}}{T - \xi + \text{const.}} \right) \frac{1}{\xi + \text{const.}} \\ &\sim \text{const.} + \ln^2(D) \end{aligned} \quad (7.18)$$

Varying such terms with bandwidth  $D$  one will obtain an overall contribution to the effective  $S$ -matrix of,

$$\delta_D \tilde{S}_{\text{straight}}^{(3)} \sim J^3 \mathbf{S} \cdot \mathbf{s} \ln(D) \frac{\delta D}{D} \quad (7.19)$$

## 7.2 Loop terms

### 7.2.1 Contour Ordering

Similarly we may evaluate the loop terms. Performing the contour ordering, we again end up with six terms of the form

$$\tilde{S}_{\text{loop}}^{(3)} = -\frac{i}{16} \sum_{aa'} \sum_{de} J_{aa'} J_{de} J_{ed} \tau_{aa'}^i \tau_{de}^k \tau_{ed}^j \left( \int_{-\infty}^{\infty} dt + \int_{\infty}^{-\infty} dt \right) \sum_n^6 K'_n \quad (7.20)$$

with

$$t'' < t' < t : K'_1 = \int_{-\infty}^t dt' \int_{-\infty}^{t'} dt'' S^k S^j S^i c_a^\dagger(t) c_{a'}(t) G_d^{(0)>}(t', t'') G_e^{(0)<}(t'', t') \quad (7.21a)$$

$$t' < t'' < t : K'_2 = \int_{-\infty}^t dt' \int_{t'}^t dt'' S^j S^k S^i c_a^\dagger(t) c_{a'}(t) G_d^{(0)<}(t', t'') G_e^{(0)>}(t'', t') \quad (7.21b)$$

$$t' < t < t'' : K'_3 = \int_{-\infty}^t dt' \int_t^{t''} dt'' S^j S^i S^k c_a^\dagger(t) c_{a'}(t) G_d^{(0)<}(t', t'') G_e^{(0)>}(t'', t') \quad (7.21c)$$

$$t'' < t < t' : K'_4 = \int_t^{t''} dt' \int_{-\infty}^{t'} dt'' S^k S^i S^j c_a^\dagger(t) c_{a'}(t) G_d^{(0)>}(t', t'') G_e^{(0)<}(t'', t') \quad (7.21d)$$

$$t < t'' < t' : K'_5 = \int_t^{t''} dt' \int_t^{t'} dt'' S^i S^k S^j c_a^\dagger(t) c_{a'}(t) G_d^{(0)>}(t', t'') G_e^{(0)<}(t'', t') \quad (7.21e)$$

$$t < t' < t'' : K'_6 = \int_t^{t''} dt' \int_{t'}^{t''} dt'' S^i S^j S^k c_a^\dagger(t) c_{a'}(t) G_d^{(0)<}(t', t'') G_e^{(0)>}(t'', t') \quad (7.21f)$$

### 7.2.2 Spin sums

From the common prefactor we see that  $\sum_{de} \tau_{aa'}^i \tau_{de}^k \tau_{ed}^j$ . The last two spin operators may be contracted to

$$\sum_{\sigma} (\tau^k \tau^j)_{\sigma\sigma} = \sum_{\sigma} \delta_{kj} \tau_{\sigma\sigma}^0 + i \sum_{\sigma} \varepsilon_{kjm} \tau_{\sigma\sigma}^m = 2\delta_{kj} \quad (7.22)$$

Combining this result with the dot spin operators contained in  $K'_1, \dots, K'_6$ ,

$$\sum_j S^j S^i S^j = -\frac{1}{4} S^i \quad \sum_j S^j S^j S^i = \frac{3}{4} S^i \quad (7.23)$$

Hence we may again construct  $K'_1, \dots, K'_6 \propto S^i$ .

### 7.2.3 Time integrals

This step involves the evaluation of terms like  $\int_{-\infty}^{t'} dt'' G_d^{(0)>}(t', t'') G_e^{(0)<}(t'', t')$  defined in the previous section. Again we only consider the contribution from  $K'_1$ . The remaining terms will be on the same general form,

$$\begin{aligned} I'_1 &= \int_{-\infty}^{t'} dt'' G_d^{(0)>}(t', t'') G_e^{(0)<}(t'', t') \\ &= (1 - f(\xi_d)) f(\xi_e) \int_{-\infty}^{t'} dt'' e^{-i\varepsilon_d(t' - t'')} e^{-i\varepsilon_e(t'' - t')} \\ &= \frac{i}{\varepsilon_e - \varepsilon_d + i0_+} (1 - f(\xi_d)) f(\xi_e) \end{aligned} \quad (7.24)$$

### 7.2.4 Energy integrals

Ignoring the imaginary part of  $I'_1$ , and we must evaluate the energy-integrals on the form,

$$\begin{aligned} \int_T^D d\xi' \int_{-D}^T d\xi \frac{1}{\xi - \xi' + const.} &\sim \int_T^D \ln \left( \frac{T - \xi' + const.}{-D - \xi' + const.} \right) \\ &\sim const. + \ln(D) \end{aligned} \quad (7.25)$$

And variation of the bandwidth then yields the result,

$$\delta_D \tilde{S}_{loop}^{(3)} \sim J^3 \mathbf{S} \cdot \mathbf{s} \frac{\delta D}{D} \quad (7.26)$$

## 7.3 Scaling Equations

We may sum up the result of our rather handwaving calculations in the equation,

$$\delta_D \tilde{S}^{(3)} \sim J^3 \mathbf{S} \cdot \mathbf{s} \frac{\delta D}{D} + J^3 \mathbf{S} \cdot \mathbf{s} \ln(D) \frac{\delta D}{D} \quad (7.27)$$

From Chapter 5 we recall that (in our sloppy notation),

$$\left( \frac{\partial \tilde{S}^{(2)}}{\partial J} \right) \sim J \mathbf{S} \cdot \mathbf{s} \ln(D) \quad (7.28)$$

The scaling equations then take the form,

$$\left(\frac{\partial \tilde{S}^{(2)}}{\partial \ln D}\right) \frac{\delta D}{D} + \left(\frac{\partial \tilde{S}^{(3)}}{\partial \ln D}\right) \frac{\delta D}{D} s = \left[ \left(\frac{\partial \tilde{S}^{(1)}}{\partial J}\right) + \left(\frac{\partial \tilde{S}^{(2)}}{\partial J}\right) \right] [a_2 J^2 + a_3 J^3] \frac{\delta D}{D}. \quad (7.29)$$

To order  $J^2$  the scaling equations stay the same as in Chapter 5. To order  $J^3$  we obtain the relation

$$\begin{aligned} a_2 J^2 \left(\frac{\partial \tilde{S}^{(2)}}{\partial J}\right) + a_3 J^3 \left(\frac{\partial \tilde{S}^{(1)}}{\partial J}\right) &= \left(\frac{\partial \tilde{S}^{(3)}}{\partial \ln D}\right) \frac{\delta D}{D} && \Leftrightarrow \\ a_2 \ln(D) + a_3 &= J^3 + J^3 \ln(D) && (7.30) \end{aligned}$$

In the equilibrium calculation of Sóllyom and Zawadowski the two logarithmic terms cancel, leaving the coefficient  $a_3$  to be determined only by the contribution from the third order loop terms. We could but it would most certainly be interesting to investigate this relationship further.

The ignored imaginary contributions to  $K_1$  and  $K'_1$  may also yield interesting results. As the loop terms take the form of conduction electron vertex correction one may hope to obtain a Korenga like spin relaxation term. However we are still unsure of how such a term may enter the scaling equations, and further research would probably try to investigate this.

## Conclusion and Outlook

---

To conclude, we have succeeded in applying a simple but still systematic extension of the Poor man's scaling approach to the nonequilibrium Kondo problem, and we have shown that this method leads to the scaling equations proposed by Rosch et al. cf. Ref. [32].

The main advantage of this approach is that the localised spin operators are treated directly without any modifications. In a pseudofermionic approach one has to consider the two-particle interaction of conduction electrons and pseudofermions, and hence include vertex corrections to the pseudofermion Green's function. Using Poor man's scaling this problem is reduced to a simpler one-body-plus-spin vertex problem. Furthermore the presented approach has the advantage that it is free of the spurious complications in the projection to single occupancy which is inherent to the pseudofermionic approach.

The simplicity of the presented approach make it possible to include higher order corrections in the perturbation expansion of the  $S$ -matrix. We have hinted at how 2-loop corrections will improve to the scaling equation in much the same way as the original equilibrium results of Sólyom and Zawadowski cf. [20].

Detailed calculations of the 2-loop corrections are thus good candidates for future work on this Poor man's scaling approach. Another candidate for future is the inclusion of the spin state decoherence rates mentioned shortly in chapter 6 into the scaling equations allowing for a direct comparison to the results of Ref. [32].





## Part II

# Detection of Antiferromagnetic Correlations in Optical Lattices



# Introduction

---

Richard P. Feynman originally proposed the idea of quantum computer as a powerful simulator in which a highly controllable quantum system can be used to simulate the dynamical behaviour of another complex quantum system. [50]

Quantum gases in optical lattices can be considered an example of such a quantum simulator. The general idea is that using counterpropagating laser beams one can construct a periodic lattice potential. Load a fermionic quantum gas into the lattice in order to create a quantum system analogous to that of a metal. However for the Fermi gas we may control both the lattice potential and the interatomic interactions.

Experimental techniques such as X-ray spectroscopy or neutron scattering usually used to probe properties of metals and crystals, cannot be used in optical lattice experiments because of the weakness of the lattice potential. Instead Altman et al. [47] has proposed a different technique based on the detection of two-particle density-density correlation function. In Chapter 10 we shortly present the general idea of such two-particle correlations. In a magnetic field one may consider a Fermi gas composed of equal amounts of identical atoms in two different hyperfine states. It is shown how the anisotropic Heisenberg Hamiltonian can be extracted from the system Hamiltonian.

For antiferromagnetic coupling and in a three dimensional lattice the atomic spin states will order below a critical temperature. At low temperatures the excitations of this antiferromagnetically ordered are spin waves. The theory of linear spin wave theory is reproduced at the end of Chapter 10.

To detect the onset of antiferromagnetic ordering one will have to consider certain two-particle correlation functions. In Chapter 11 we will consider three candidates for such functions and calculate their high-temperature and low-temperature behaviour.

The final Chapter 12 shows the results of numerical computation of the high-temperature and low-temperature approximations for all three correlation functions. We also shortly discuss whether or not the computed correlations are within the reach of current experiments.

The work presented in this part of the thesis has been included in the article of Ref. [52] currently submitted to Physical Review Letters. The article has also been attached as Appendix D.



# Fermions in Optical Lattices

---

We begin with a brief description of the model optical lattice system.

Two counter-propagating laser beams create a standing electromagnetic wave. Atoms placed in such a standing electromagnetic wave will experience a periodic potential determined by the intensity of the wave cf. Ref. [50]. If thermal fluctuations are small enough compared to the magnitude of the periodic potential the atoms may order in the periodic potential minima created by the laser beams.

An external magnetic field cause a hyperfine splitting of the atom energy levels. We will in general assume that the atoms occupy only one of two possible different hyperfine energy levels cf. Ref. [50]. Load such a two-component Fermi gas into a cubic periodic potential constructed from three sets of counter-propagating laser beams placed at directions perpendicular to each other. With the number of atoms matching the number of lattice sites the system may enter the Mott phase with a single atom placed at each lattice site.

We will in general assume that the two hyperfine split levels have a relative magnetic moment of  $\Delta m = 1/2$ , and in this case we denote the levels spin  $\uparrow$  and spin  $\downarrow$ . A lattice system inhabited by such spin  $1/2$  particles may be expected to show certain features of magnetic ordering when below the critical Neel temperature,  $T_N$ . [6]

Because of the weakness of the optical lattice potential usual techniques for investigating the magnetic properties such as neutron scattering or muon spin spectroscopy are inappropriate. Instead the system may be investigated using time-of-flight (TOF) measurements. Here the Fermi gas is released from the optical lattice by turning off the lattice potential and then allowed to expand for some time. Using a quadratic array of detectors the density of the expanding atomic cloud can then be measured cf. Ref. [50]. Utilising a Stern-Gerlach technique one may also hope to obtain the spin-resolved density of the cloud [52].

From such measurements it is possible to extract two-particle correlation functions. An example of the obtained two dimensional density profile for the expanding cloud is shown in Figure 10.1(a), while the two-particle density-density correlation function is presented in Figure 10.1(c). The data is from the first experiment by Rom et al. [48] measuring the fermionic anti-bunching dips for fermionic atoms in an optical lattice. The anti-bunching is a feature of the

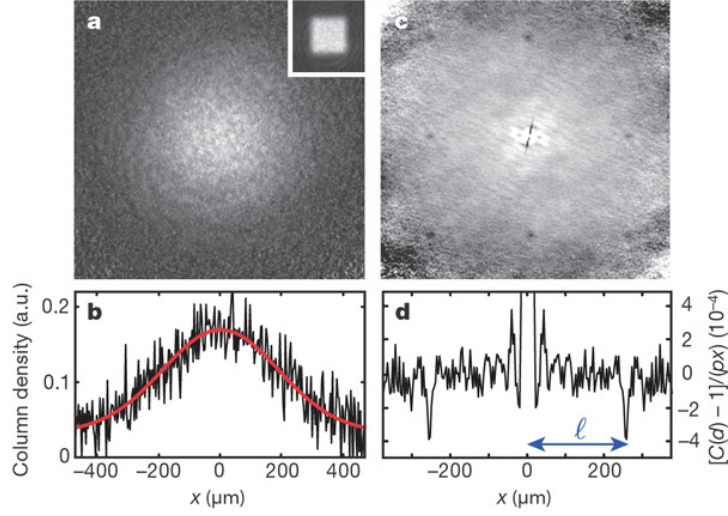


**Figure 10.1:** (a) A 2D image of the particle density taken after release of the trap and subsequent expansion of the gas. (c) The two-particle density-density correlation function obtained from the first plot. Dips in the correlation function show fermionic anti-bunching due to the Hanbury-Brown-Twiss effect. Figure reproduced from [48].

Pauli statistics of fermions, and we will encounter such dips later when calculating the relevant correlations functions for antiferromagnetic interactions between the atoms.

## 10.1 The Hubbard Model

We will in the following consider the system Hamiltonian for  $N$  fermionic atoms in an optical lattice with  $N_0$  lattice sites  $I$ . As of Refs. [45], [46] by expansion of the field operators in Wannier states the system Hamiltonian can be approximated by the Hubbard Hamiltonian if keeping only the lowest vibrational Wannier states,

$$H = H_K + H_U, \quad (10.1)$$

with

$$H_K = - \sum_{l,l',\sigma} t_{\sigma,l-l'} c_{l\sigma}^\dagger c_{l'\sigma} - \mu \sum_{l,\sigma} c_{l\sigma}^\dagger c_{l\sigma} \quad (10.2)$$

$$H_U = U \sum_l n_{l\uparrow} n_{l\downarrow}. \quad (10.3)$$

The  $H_K$  describes hopping between sites, while  $H_U$  penalise the double occupancy of a single lattice site. In an optical lattice this double occupancy energy shift can be tuned by the laser intensity.

When  $U \gg |t_{l-l',\sigma}|$  the penalty for having two particles occupy the same lattice site is significantly larger than the energy required for hopping between lattice sites. At a half-filled band ( $N = N_0$ ) the Mott phase with each lattice state occupied by a single atom is  $2^N$ -fold degenerate. The objective of the following calculation will be to investigate the Mott phase

taking into account double exchange interactions. We can project the Hilbert space of Eq. (10.1) into the Hilbert space of the Mott phase configuration using the projection operator,

$$P = \prod_l (1 - n_{l\uparrow} n_{l\downarrow}). \quad (10.4)$$

The operator  $Q = 1 - P$  will then project into states with at least one doubly occupied site. Now introduce  $Q$  and  $P$  in the Schrödinger equation

$$\begin{aligned} H\Psi &= E\Psi, & \Leftrightarrow \\ H(P+Q)\Psi &= E(P+Q)\Psi. \end{aligned} \quad (10.5)$$

We isolate  $Q\Psi$ , multiplying Eq. (10.5) with  $Q$  from the left, and remembering that the projection operators are idempotent (i.e.  $QQ = Q$  and  $PP = P$ ),

$$\begin{aligned} (QHQ - E)Q\Psi &= -QHP\Psi & \Leftrightarrow \\ Q\Psi &= -(QHQ - E)^{-1}QHP\Psi. \end{aligned} \quad (10.6)$$

Insert this into Eq. (10.5) and multiply with  $P$  from the left to obtain

$$[PHP - PHQ(QHQ - E)^{-1}QHP] P\Psi = EP\Psi. \quad (10.7)$$

Note that in the Mott insulator state of the Hubbard Model

$$PHP = PH_U P = 0, \quad (10.8)$$

so

$$PHQ = PH_K Q, \quad QHP = QH_K P. \quad (10.9)$$

We will apply Eq. (10.7) to second order in  $t_{\sigma,l-l'}$ . Note that  $(QHQ - E)^{-1}$  is of 0th order in  $t_{\sigma,l-l'}$  and can be replaced by  $U$ , while both  $PH_K Q$  and  $QHP = QH_K P$  are of first order in  $t_{\sigma,l-l'}$ . To second order in  $t_{\sigma,l-l'}$ , we have the effective Hamiltonian

$$H_{eff} = -\frac{(PH_K Q)(QH_K P)}{U} = -P \frac{H_K^2}{U} P \quad (10.10)$$

$$= \sum_{l_1, l'_1, l_2, l'_2} \sum_{\sigma_1, \sigma_2} t_{\sigma_1, l_1 - l'_1} t_{\sigma_1, l_2 - l'_2} P c_{l_1 \sigma_1}^\dagger c_{l'_1 \sigma_1} c_{l_2 \sigma_2}^\dagger c_{l'_2 \sigma_2} P. \quad (10.11)$$

Note that because  $P$  is multiplied on both sides, a particle annihilated at  $l'_2$  must reappear at the same place. Considering  $t_{\sigma, l-l} = 0$  we must have that  $l'_2 = l_1$  and  $l_2 = l'_1$ . This means that

$$\begin{aligned} PH_K^2 P &= \sum_{l_1, l_2} \sum_{\sigma_1, \sigma_2} t_{\sigma_1, l_1 - l_2} t_{\sigma_2, l_2 - l_1} P c_{l_1 \sigma_1}^\dagger c_{l_2 \sigma_1} c_{l_2 \sigma_2}^\dagger c_{l_1 \sigma_2} P \\ &= \sum_{l_1, l_2} \sum_{\sigma_1, \sigma_2} t_{\sigma_1, l_1 - l_2} t_{\sigma_2, l_2 - l_1} P c_{l_1 \sigma_1}^\dagger c_{l_1 \sigma_2} P \cdot P c_{l_2 \sigma_1} c_{l_2 \sigma_2}^\dagger P. \end{aligned} \quad (10.12)$$

Now use that

$$c_{l\sigma_1}^\dagger c_{l\sigma_2} = \frac{1}{2} \delta_{\sigma_1 \sigma_2} (n_{l\uparrow} + n_{l\downarrow}) + \mathbf{s}_l \cdot \boldsymbol{\sigma}_{\sigma_2 \sigma_1}, \quad (10.13)$$

$$c_{l\sigma_1} c_{l\sigma_2}^\dagger = \delta_{\sigma_1 \sigma_2} \left( 1 - \frac{n_{l\uparrow} + n_{l\downarrow}}{2} \right) - \mathbf{s}_l \cdot \boldsymbol{\sigma}_{\sigma_1 \sigma_2}, \quad (10.14)$$

where  $\mathbf{S}_l$  denotes particle spin. Insert it into Eq. (10.12) to obtain

$$\begin{aligned}
PH_K^2P &= \sum_{l_1, l_2} \sum_{\sigma_1, \sigma_2} t_{\sigma_1, l_1 - l_2} t_{\sigma_2, l_2 - l_1} \left( \frac{\delta_{\sigma_1 \sigma_2}}{2} + \mathbf{s}_{l_1} \cdot \sigma_{\sigma_2 \sigma_1} \right) \left( \frac{\delta_{\sigma_1 \sigma_2}}{2} - \mathbf{s}_{l_2} \cdot \sigma_{\sigma_1 \sigma_2} \right) \\
&= \sum_{l_1, l_2} \sum_{\sigma} |t_{\sigma, l_1 - l_2}|^2 \left( \frac{1}{2} + \mathbf{s}_{l_1} \cdot \sigma_{\sigma \sigma} \right) \left( \frac{1}{2} - \mathbf{s}_{l_2} \cdot \sigma_{\sigma \sigma} \right) \\
&\quad + \sum_{l_1, l_2} \sum_{\sigma_1 \neq \sigma_2} t_{\sigma_1, l_1 - l_2} t_{\sigma_2, l_2 - l_1} (\mathbf{s}_{l_1} \cdot \sigma_{\sigma_2 \sigma_1}) (-\mathbf{s}_{l_2} \cdot \sigma_{\sigma_1 \sigma_2}). \tag{10.15}
\end{aligned}$$

If  $t_{\downarrow, l-l'} = \alpha t_{\uparrow, l-l'}$  we may evaluate the terms of Eq. (10.15).

$$\begin{aligned}
PH_K^2P &= \sum_{l_1, l_2} (1 + \alpha^2) |t_{\uparrow, l_1 - l_2}|^2 \left( \frac{1}{4} - s_{l_1}^z s_{l_2}^z \right) + \sum_{l_1, l_2} (1 - \alpha^2) |t_{\uparrow, l_1 - l_2}|^2 \frac{1}{2} (s_{l_1}^z - s_{l_2}^z) \\
&\quad + \sum_{l_1, l_2} 2\alpha |t_{\uparrow, l_1 - l_2}|^2 \left( -s_{l_1}^x s_{l_2}^x - s_{l_1}^y s_{l_2}^y \right) \\
&= \sum_{l_1, l_2} |t_{\uparrow, l_1 - l_2}|^2 \left[ (1 + \alpha^2) \left( \frac{1}{4} - s_{l_1}^z s_{l_2}^z \right) - 2\alpha (s_{l_1}^x s_{l_2}^x + s_{l_1}^y s_{l_2}^y) \right]. \tag{10.16}
\end{aligned}$$

Here one may note that the  $s_{l_1}^z - s_{l_2}^z$  term disappear when summing symmetrically over lattice sites  $l_1$  and  $l_2$ . Inserting the result for  $PH_K^2P$  into Eq. (10.10), we obtain an effective Hamiltonian,

$$H_{eff} = \frac{1}{U} \sum_{l_1, l_2} |t_{\uparrow, l_1 - l_2}|^2 \left[ (1 + \alpha^2) \left( -\frac{1}{4} + s_{l_1}^z s_{l_2}^z \right) + 2\alpha (s_{l_1}^x s_{l_2}^x + s_{l_1}^y s_{l_2}^y) \right]. \tag{10.17}$$

If we introduce the coupling strength

$$J_{l_1, l_2}^z = \frac{1}{U} (1 + \alpha^2) |t_{\uparrow, l_1 - l_2}|^2, \quad J_{l_1, l_2}^{xy} = \frac{2}{U} \alpha |t_{\uparrow, l_1 - l_2}|^2. \tag{10.18}$$

We may note that  $J_{l_1, l_2}^z \geq J_{l_1, l_2}^{xy}$  for any real value of  $\alpha$ . The equality is true when  $\alpha = 1$ . Now assume that nearest neighbour interactions are dominant and the particle interaction is isotropic throughout the lattice (i.e. all values of  $|t_{\uparrow, l_1 - l_2}|^2$  are equal if  $l_1$  and  $l_2$  are nearest neighbours and zero otherwise). Then we have for  $\alpha > 0$  effectively reduced our Hubbard Hamiltonian to the antiferromagnetic anisotropic Heisenberg Model:

$$H_{eff} = 2 \sum_{\langle l_1, l_2 \rangle} \left[ J^z s_{l_1}^z s_{l_2}^z + J^{xy} (s_{l_1}^x s_{l_2}^x + s_{l_1}^y s_{l_2}^y) - \frac{1}{4} J^z \right], \tag{10.19}$$

where  $\langle l_1, l_2 \rangle$  denotes summing all nearest neighbour pairs exactly once. Note that when  $J_{l_1, l_2}^z = J_{l_1, l_2}^{xy}$  this reduces to the isotropic Heisenberg Model.

## 10.2 The Heisenberg Model

Let us restate our conclusions. When considering particles of spin  $\mathbf{s}$  trapped in an optical lattice of size  $N$ , so that each lattice site  $i$  is occupied by exactly one particle, we may describe this system using the anisotropic Heisenberg Model.

$$H_{eff} = J \sum_{\langle l_1, l_2 \rangle} \left[ d s_{l_1}^z s_{l_2}^z + (s_{l_1}^x s_{l_2}^x + s_{l_1}^y s_{l_2}^y) \right], \tag{10.20}$$



where the anisotropy  $d \geq 1$ . The spin operator for a site  $l$  is  $s_l$ .

For a three dimensional system the Heisenberg system will undergo a phase transition to an antiferromagnetically ordered state at the Neel temperature  $T_N$  cf. [8]. In the following we will investigate this system further considering both the antiferromagnetically ordered state present at low temperature  $T < T_N$ .

### 10.3 Linear Spin Wave Theory and the Holstein-Primakoff Method

To describe the low temperature state, we apply spin wave theory which concerns small collective spin modes present in the antiferromagnetically ordered spin lattice. For simplicity we will restrict the presentation to a  $D$ -dimensional cubic lattice with lattice constant  $a$ . In this case each lattice site has  $z = 2D$  nearest neighbours.

Divide the lattice into two sublattices, such that sites on one sublattice only has nearest neighbours belonging to the other sublattice. Notationally sites on one sublattice are referenced by  $l$  and sites on the other sublattice by  $j$ . Assuming that spins are aligned in the  $z$ -direction (this might not be the case when  $d = 1$ ), we take spins on the  $j$  sites to be aligned so  $s_{jz} \approx s$ , while spin on  $l$  sites have  $s_{lz} \approx -s$ .

Stating the Bose operators of linear spin wave theory,

$$s_{jz} = s - a_j^\dagger a_j, \quad (10.21a)$$

$$s_{lz} = -s + b_l^\dagger b_l, \quad (10.21b)$$

$$s_{j+} = s_{jx} + i s_{jy} = \sqrt{2s} a_j - \frac{1}{\sqrt{2s}} a_j^\dagger a_j a_j, \quad (10.21c)$$

$$s_{j-} = s_{jx} - i s_{jy} = \sqrt{2s} a_j^\dagger - \frac{1}{\sqrt{2s}} a_j^\dagger a_j^\dagger a_j, \quad (10.21d)$$

$$s_{l+} = \sqrt{2s} b_l^\dagger - \frac{1}{\sqrt{2s}} b_l^\dagger b_l^\dagger b_l, \quad (10.21e)$$

$$s_{l-} = \sqrt{2s} b_l - \frac{1}{\sqrt{2s}} b_l^\dagger b_l b_l. \quad (10.21f)$$

Using these operators we hope to diagonalize the Heisenberg Hamiltonian of Eq. (10.20). Plain insertion of the operators yields,

$$\begin{aligned} H &= J \sum_{\langle l,j \rangle} \left\{ d s_{jz} s_{lz} + \frac{1}{2} s_{j+} s_{l-} + \frac{1}{2} s_{j-} s_{l+} \right\} \\ &= J \sum_{\langle l,j \rangle} \left\{ d (s - a_j^\dagger a_j) (-s + b_l^\dagger b_l) + \frac{1}{2} (\sqrt{2s} a_j - \frac{1}{\sqrt{2s}} a_j^\dagger a_j a_j) (\sqrt{2s} b_l - \frac{1}{\sqrt{2s}} b_l^\dagger b_l b_l) \right. \\ &\quad \left. + \frac{1}{2} (\sqrt{2s} a_j^\dagger - \frac{1}{\sqrt{2s}} a_j^\dagger a_j^\dagger a_j) (\sqrt{2s} b_l^\dagger - \frac{1}{\sqrt{2s}} b_l^\dagger b_l^\dagger b_l) \right\} \quad (10.22) \end{aligned}$$

$$= -\frac{1}{2} d J z N s^2 + d J z s \sum_j a_j^\dagger a_j + d J z s \sum_l b_l^\dagger b_l + J s \sum_{\langle l,j \rangle} (a_j b_l + a_j^\dagger b_l^\dagger) + \mathcal{O}(a^3). \quad (10.23)$$

Introduce the standard Fourier transform of the Bose operators,

$$a_{\mathbf{u}} = \sqrt{\frac{2}{N}} \sum_j e^{-i\mathbf{u}\cdot R_j} a_j, \quad (10.24)$$

$$b_{\mathbf{u}} = \sqrt{\frac{2}{N}} \sum_l e^{i\mathbf{u}\cdot R_l} b_l. \quad (10.25)$$

Here the sum only considers states within the first Brillouin zone of each sublattice. Now simplify Eq. (10.22) ignoring terms to cubic order in the Bose operators

$$\begin{aligned} H &\approx -dJzNs^2 + dJzs \sum_{\mathbf{u}} \left( a_{\mathbf{u}}^\dagger a_{\mathbf{u}} + b_{\mathbf{u}}^\dagger b_{\mathbf{u}} \right) + Js \sum_{\mathbf{u}} \left( a_{\mathbf{u}} b_{\mathbf{u}} + a_{\mathbf{u}}^\dagger b_{\mathbf{u}}^\dagger \right) \left( e^{i\sum_i u_i a} + e^{i\sum_i -u_i a} \right) \\ &= -dJzNs^2 + Js z \sum_{\mathbf{u}} \left\{ d \left( a_{\mathbf{u}}^\dagger a_{\mathbf{u}} + b_{\mathbf{u}}^\dagger b_{\mathbf{u}} \right) + \gamma_{\mathbf{u}} \left( a_{\mathbf{u}} b_{\mathbf{u}} + a_{\mathbf{u}}^\dagger b_{\mathbf{u}}^\dagger \right) \right\}. \end{aligned} \quad (10.26)$$

In the last term  $\gamma_{\mathbf{u}} = D^{-1} \left( e^{i\sum_i u_i a} + e^{i\sum_i -u_i a} \right) = D^{-1} \sum_{i=1}^D \cos u_i$ . The form of Eq. (10.26) is diagonalized by a Bogoliubov transformation [10]. First we introduce a new set of Bose operators,

$$\begin{aligned} a_{\mathbf{u}} &= \alpha_{\mathbf{u}} \cosh \Theta_{\mathbf{u}} - \beta_{\mathbf{u}}^\dagger \sinh \Theta_{\mathbf{u}}, \\ b_{\mathbf{u}} &= -\alpha_{\mathbf{u}}^\dagger \sinh \Theta_{\mathbf{u}} + \beta_{\mathbf{u}} \cosh \Theta_{\mathbf{u}}, \end{aligned} \quad (10.27)$$

where  $\Theta_{\mathbf{u}}$  is determined by  $\tanh 2\Theta_{\mathbf{u}} = \gamma_{\mathbf{u}}/d$ . Rewriting Eq. (10.26) in terms of the transformed Bose operators,

$$H = \sum_{\mathbf{u}} \omega_{\mathbf{u}} (\alpha_{\mathbf{u}}^\dagger \alpha_{\mathbf{u}} + \beta_{\mathbf{u}}^\dagger \beta_{\mathbf{u}}) + \text{const}. \quad (10.28)$$

Here the eigenenergy  $\omega_{\mathbf{u}} = Jzs\sqrt{d^2 - \gamma_{\mathbf{u}}^2}$ .

### 10.3.1 The Spin-Spin Correlation Function $\langle S_z S_z \rangle$

Spin wave theory allows us to perform direct calculations in the low temperature region. As done by [51], we can calculate the spin-spin correlation function  $\langle S_z S_z \rangle$  assuming  $s = \frac{1}{2}$ . First consider the summed operator

$$S_z = \sum_j s_{jz} + \sum_l s_{lz} = -\sum_j a_j^\dagger a_j + \sum_l b_l^\dagger b_l. \quad (10.29)$$

Insert Eq. (10.24), Eq. (10.25) and perform the Bogoliubov transformation on  $S_z$  to obtain

$$\begin{aligned} S_z &= \sum_{\mathbf{u}} b_{\mathbf{u}}^\dagger b_{\mathbf{u}} - a_{\mathbf{u}}^\dagger a_{\mathbf{u}} \\ &= \sum_{\mathbf{u}} (-\alpha_{\mathbf{u}} \sinh \Theta_{\mathbf{u}} + \beta_{\mathbf{u}}^\dagger \cosh \Theta_{\mathbf{u}}) (-\alpha_{\mathbf{u}}^\dagger \sinh \Theta_{\mathbf{u}} + \beta_{\mathbf{u}} \cosh \Theta_{\mathbf{u}}) \\ &\quad - \sum_{\mathbf{u}} (\alpha_{\mathbf{u}}^\dagger \cosh \Theta_{\mathbf{u}} - \beta_{\mathbf{u}} \sinh \Theta_{\mathbf{u}}) (\alpha_{\mathbf{u}} \cosh \Theta_{\mathbf{u}} - \beta_{\mathbf{u}}^\dagger \sinh \Theta_{\mathbf{u}}) \\ &= \sum_{\mathbf{u}} \left[ \alpha_{\mathbf{u}}^\dagger \alpha_{\mathbf{u}} (-\cosh^2 \Theta_{\mathbf{u}} + \sinh^2 \Theta_{\mathbf{u}}) + \beta_{\mathbf{u}}^\dagger \beta_{\mathbf{u}} (\cosh^2 \Theta_{\mathbf{u}} - \sinh^2 \Theta_{\mathbf{u}}) \right] \\ &= \sum_{\mathbf{u}} \left[ \beta_{\mathbf{u}}^\dagger \beta_{\mathbf{u}} - \alpha_{\mathbf{u}}^\dagger \alpha_{\mathbf{u}} \right]. \end{aligned} \quad (10.30)$$

To quadratic order in the Bose operators we evaluate  $\langle S_z S_z \rangle$ , i.e.

$$\begin{aligned}
\langle S_z S_z \rangle &= \sum_{\mathbf{u}\mathbf{v}} \left\langle (\beta_{\mathbf{u}}^\dagger \beta_{\mathbf{u}} - \alpha_{\mathbf{u}}^\dagger \alpha_{\mathbf{u}}) (\beta_{\mathbf{v}}^\dagger \beta_{\mathbf{v}} - \alpha_{\mathbf{v}}^\dagger \alpha_{\mathbf{v}}) \right\rangle \\
&= \sum_{\mathbf{u}\mathbf{v}} \left[ \langle \beta_{\mathbf{u}}^\dagger \beta_{\mathbf{u}} \beta_{\mathbf{v}}^\dagger \beta_{\mathbf{v}} \rangle + \langle \alpha_{\mathbf{u}}^\dagger \alpha_{\mathbf{u}} \alpha_{\mathbf{v}}^\dagger \alpha_{\mathbf{v}} \rangle - \langle \beta_{\mathbf{u}}^\dagger \beta_{\mathbf{u}} \alpha_{\mathbf{v}}^\dagger \alpha_{\mathbf{v}} \rangle - \langle \alpha_{\mathbf{u}}^\dagger \alpha_{\mathbf{u}} \beta_{\mathbf{v}}^\dagger \beta_{\mathbf{v}} \rangle \right] \\
&= 2 \sum_{\mathbf{u}\mathbf{v}} \left[ \langle \beta_{\mathbf{u}}^\dagger \beta_{\mathbf{u}} \rangle \langle \beta_{\mathbf{v}}^\dagger \beta_{\mathbf{v}} \rangle + \langle \beta_{\mathbf{u}}^\dagger \beta_{\mathbf{v}} \rangle \langle \beta_{\mathbf{u}} \beta_{\mathbf{v}}^\dagger \rangle - \langle \beta_{\mathbf{u}}^\dagger \beta_{\mathbf{u}} \rangle \langle \alpha_{\mathbf{v}}^\dagger \alpha_{\mathbf{v}} \rangle - \langle \beta_{\mathbf{u}}^\dagger \alpha_{\mathbf{v}} \rangle \langle \beta_{\mathbf{u}} \alpha_{\mathbf{v}}^\dagger \rangle \right] \\
&= 2 \sum_{\mathbf{u}} [n_{\mathbf{u}} - n_{\mathbf{u}}^2] \\
&= 2 \sum_{\mathbf{u}} \frac{1}{1 - e^{\beta\omega_{\mathbf{u}}}} \left[ \frac{e^{\beta\omega_{\mathbf{u}}}}{1 - e^{\beta\omega_{\mathbf{u}}}} \right] \\
&= \sum_{\mathbf{u}} \frac{1}{2 \sinh^2(\frac{1}{2}\beta\omega_{\mathbf{u}})}. \tag{10.31}
\end{aligned}$$

This final result shows that at low temperatures  $T \ll \max(\omega_{\mathbf{u}})$ , we have  $\langle S_z S_z \rangle \approx 0$ . This result will be used in the coming section when we will consider two-particle density correlation function.



# Density Correlation Functions

---

As mentioned earlier TOF experiments may probe density correlation functions on the general form,

$$C(\mathbf{k}', \mathbf{k}) = \langle A(\mathbf{k})B(\mathbf{k}') \rangle - \langle A(\mathbf{k}) \rangle \langle B(\mathbf{k}') \rangle, \quad (11.1)$$

with  $A(\mathbf{k})$  and  $B(\mathbf{k}')$  being some atomic density functions. In the experiments of Refs. [48], [49] the density-density correlation function were extracted, and in this case  $A(\mathbf{k}) = B(\mathbf{k}) = \sum_{\sigma} n_{\sigma}(\mathbf{k})$ .

While the objective of these calculation is to find an analytic expression for various correlation functions in a three dimensional optical lattice, we will keep the calculations as generally as possible only applying the restrictions of dimensions or spin when necessary.

## 11.1 Parallel Spin Noise

The objective of this chapter will be to calculate both low-temperature and high-temperature approximations of three different correlation functions. The first correlation function of our choice is the parallel spin noise

$$C_{||}(\mathbf{k}, \mathbf{k}') = \langle \hat{n}_{\mathbf{k}\uparrow} \hat{n}_{\mathbf{k}'\downarrow} \rangle - \langle \hat{n}_{\mathbf{k}\uparrow} \rangle \langle \hat{n}_{\mathbf{k}'\downarrow} \rangle = \langle c_{\mathbf{k}\uparrow}^{\dagger} c_{\mathbf{k}\uparrow} c_{\mathbf{k}'\downarrow}^{\dagger} c_{\mathbf{k}'\downarrow} \rangle - \frac{1}{4} = C'_{||}(\mathbf{k}, \mathbf{k}') - \frac{1}{4}. \quad (11.2)$$

Where we have introduced the notation  $C'_{||}(\mathbf{k}, \mathbf{k}') = \langle \hat{n}_{\mathbf{k}\uparrow} \hat{n}_{\mathbf{k}'\downarrow} \rangle$ . Insert the Fourier transformation of the field operators

$$c_{\mathbf{k}}^{\dagger} = \frac{1}{\sqrt{N}} \sum_i e^{-i\mathbf{k}\mathbf{r}_i} c_i^{\dagger},$$

$$c_{\mathbf{k}} = \frac{1}{\sqrt{N}} \sum_i e^{i\mathbf{k}\mathbf{r}_i} c_i,$$

in order to obtain

$$C'_{||}(\mathbf{k}, \mathbf{k}') = \frac{1}{N^2} \sum_{ijlm} e^{-i\mathbf{k}(\mathbf{r}_i - \mathbf{r}_j)} e^{-i\mathbf{k}'(\mathbf{r}_l - \mathbf{r}_m)} \langle c_{j\uparrow}^{\dagger} c_{i\uparrow} c_{m\downarrow}^{\dagger} c_{l\downarrow} \rangle. \quad (11.3)$$

Only terms of either  $i = j$ ,  $m = l$  or  $i = m$ ,  $j = l$  will contribute to the sum. This leaves us with the preliminary result

$$C'_{||}(\Delta\mathbf{k}) = \frac{1}{N^2} \sum_{ij} \left\{ \langle c_{i\uparrow}^\dagger c_{i\uparrow} c_{j\downarrow}^\dagger c_{j\downarrow} \rangle + \langle c_{i\uparrow}^\dagger c_{j\uparrow} c_{j\downarrow}^\dagger c_{i\downarrow} \rangle e^{-i\Delta\mathbf{k}\mathbf{r}_i} e^{i\Delta\mathbf{k}\mathbf{r}_j} \right\}. \quad (11.4)$$

Here we have introduced the relative momentum vector  $\Delta\mathbf{k} = \mathbf{k} - \mathbf{k}'$ .

### 11.1.1 High Temperature Approximation

Our first concern will be the high temperature behaviour of Eq. (11.4). Introduce an average  $\sum_\nu \langle \nu | \dots e^{-\beta H_\nu} | \nu \rangle / Z$  over all possible spin configurations  $\nu$  of the lattice, in order to reexpress Eq. (11.4) as,

$$\begin{aligned} C'_{||}(\Delta\mathbf{k}) &= \frac{1}{Z} \sum_\nu \langle \nu | \hat{n}_{\mathbf{k}\uparrow} \hat{n}_{\mathbf{k}'\downarrow} e^{-\beta H_\nu} | \nu \rangle \\ &= \frac{1}{Z} \frac{1}{N^2} \langle \nu | \sum_{ij} \left\{ c_{i\uparrow}^\dagger c_{i\uparrow} c_{j\downarrow}^\dagger c_{j\downarrow} + c_{i\uparrow}^\dagger c_{j\uparrow} c_{j\downarrow}^\dagger c_{i\downarrow} e^{-i\Delta\mathbf{k}\mathbf{r}_i} e^{i\Delta\mathbf{k}\mathbf{r}_j} \right\} e^{-\beta H_\nu} | \nu \rangle. \end{aligned} \quad (11.5)$$

We will calculate this expression to first order in the Hamiltonian  $H$ . The first order expansion of the exponential yields,

$$e^{-\beta H} = 1 - \beta J \sum_{\langle n,m \rangle} (s_{mx}s_{nx} + s_{my}s_{ny} + ds_{mz}s_{nz}) = 1 - \beta(H_{xy} + H_z). \quad (11.6)$$

Where we have introduced

$$\begin{aligned} H_{xy} &= J \sum_{\langle n,m \rangle} (s_{mx}s_{nx} + s_{my}s_{ny}) \\ &= \frac{1}{4} J \sum_{\langle m,n \rangle} \left[ \left( c_{m\downarrow}^\dagger c_{m\uparrow} + c_{m\uparrow}^\dagger c_{m\downarrow} \right) \left( c_{n\downarrow}^\dagger c_{n\uparrow} + c_{n\uparrow}^\dagger c_{n\downarrow} \right) - \left( c_{m\downarrow}^\dagger c_{m\uparrow} - c_{m\uparrow}^\dagger c_{m\downarrow} \right) \left( c_{n\downarrow}^\dagger c_{n\uparrow} - c_{n\uparrow}^\dagger c_{n\downarrow} \right) \right] \\ &= \frac{1}{2} J \sum_{\langle m,n \rangle} \left( c_{m\downarrow}^\dagger c_{m\uparrow} c_{n\uparrow}^\dagger c_{n\downarrow} + c_{m\uparrow}^\dagger c_{m\downarrow} c_{n\downarrow}^\dagger c_{n\uparrow} \right). \end{aligned} \quad (11.7)$$

Note that  $H_{xy}$  is responsible for flipping the spins of nearest neighbour pairs. The remaining term  $H_z$  is,

$$H_z = dJ \sum_{\langle n,m \rangle} s_{mz}s_{nz} = \frac{1}{4} dJ \sum_{\langle m,n \rangle} (n_{n\uparrow} - n_{n\downarrow})(n_{m\uparrow} - n_{m\downarrow}). \quad (11.8)$$

Hence it simply counts the direct spin-correlations. For the partition function  $Z$  to first order in  $\beta J$ ,

$$Z = \sum_\nu \langle \nu | e^{-\beta H} | \nu \rangle \approx \langle \nu | 1 - \beta J \sum_{\langle n,m \rangle} (s_{mx}s_{nx} + s_{my}s_{ny} + ds_{mz}s_{nz}) | \nu \rangle = 2^N. \quad (11.9)$$

Here the last equality follows from the fact that the average of  $s_{mx}s_{nx} + s_{my}s_{ny}$  terms is always zero, because the enclosed field operators involve a spin flip. The non-spin-flipping terms  $\sum_\nu \sum_{\langle m,n \rangle} s_{mz}s_{nz}$  vanish also. Consider a fixed pair  $n, m$  a sum over all configurations will on

average yield zero because the two terms  $\uparrow\uparrow$  and  $\downarrow\downarrow$  with a contribution of  $+1$ , are cancelled by  $\uparrow\downarrow$  and  $\downarrow\uparrow$  contributing  $-1$  each.

Next step is to evaluate the 0th order part of Eq. (11.5),

$$C'_{\parallel}(0)(\Delta\mathbf{k}) \approx \frac{1}{2^N} \frac{1}{N^2} \sum_{\nu} \sum_{ij} \langle \nu | n_{i\uparrow} n_{j\downarrow} | \nu \rangle \approx \frac{1}{2^N} \frac{1}{N^2} \sum_i 2^{N-2} (N-1) = \frac{1}{4} - \frac{1}{4N}. \quad (11.10)$$

Here we arrive at  $\sum_{\nu} \sum_{ij} n_{i\uparrow} n_{j\downarrow} = 2^{N-2} \sum_i (N-1)$  using the same type of argument as before. For a fixed  $i$  we may choose  $j$  from the remaining  $N-1$  sites (note that the  $i=j$  term is zero). Site  $i$  will need to be  $\uparrow$  while site  $j$  will need to be  $\downarrow$ , and the remaining  $N-2$  are free to do whatever.

Now consider the first order contribution of Eq. (11.5). The first term of Eq. (11.5) contains  $c_{i\uparrow}^{\dagger} c_{i\uparrow} c_{j\downarrow}^{\dagger} c_{j\downarrow}$ . This term does not perform any spin flips, and hence calculating the contribution from this term to first order in  $\beta J$  cannot involve  $H_{xy}$ .

Thus taking the average of this term with the  $H_z$  part only gives the result,

$$-d \frac{1}{4} \frac{1}{2^N} \frac{1}{N^2} \sum_{\nu} \sum_{i,j} \sum_{\langle m,n \rangle} \langle \nu | n_{i\uparrow} n_{j\downarrow} (n_{n\uparrow} - n_{n\downarrow}) (n_{m\uparrow} - n_{m\downarrow}) | \nu \rangle. \quad (11.11)$$

Consider a fixed nearest neighbour pair  $\langle m, n \rangle$ . Using the same reasoning as of Eq. (11.9) we argue that when summing all configurations, the term  $(n_{n\uparrow} - n_{n\downarrow})(n_{m\uparrow} - n_{m\downarrow})$  will yield zero on average. So considering fixed  $i$ , fixed  $j$  and a fixed pair  $\langle m, n \rangle$  the sum evaluates to zero whenever  $i, j$  and  $\langle m, n \rangle$  concern all different sites.

If e.g.  $i$  coincides with one site in the pair  $\langle m, n \rangle$  while  $j$  doesn't, the sum will also yield zero, because in the contribution from  $H_z$  the  $\uparrow\downarrow$  contribution cancels the  $\uparrow\uparrow$  contribution.

So it turns out that in order to obtain a non-zero result, site  $i$  and site  $j$  must coincide with the nearest neighbour pair  $\langle m, n \rangle$ . Assuming periodic boundary conditions for the lattice, each  $i$  has exactly  $z$  nearest neighbours, thus the contribution from the first term of Eq. (11.5) evaluates to

$$-d \frac{1}{4} \frac{1}{2^N} \frac{1}{N^2} \sum_i 2^{N-2} \cdot z \cdot -1 = \frac{dz}{16N}.$$

The second term of Eq. (11.5) contains  $c_{i\uparrow}^{\dagger} c_{j\uparrow} c_{j\downarrow}^{\dagger} c_{i\downarrow}$  and involves a double spin flip. Hence only corrections arising from the  $H_{xy}$  part of the Hamiltonian will contribute to this sum. By noting that terms with  $i=j$  yield zero we obtain

$$\begin{aligned} & -\frac{1}{2^N} \frac{1}{N^2} \sum_{\nu} \langle \nu | \sum_{i \neq j} c_{i\uparrow}^{\dagger} c_{j\uparrow} c_{j\downarrow}^{\dagger} c_{i\downarrow} \frac{1}{2} \sum_{\langle m,n \rangle} \left( c_{m\downarrow}^{\dagger} c_{m\uparrow} c_{n\uparrow}^{\dagger} c_{n\downarrow} + c_{m\uparrow}^{\dagger} c_{m\downarrow} c_{n\downarrow}^{\dagger} c_{n\uparrow} \right) e^{i\Delta\mathbf{k}r_i} e^{i\Delta\mathbf{k}r_j} | \nu \rangle \\ & = \frac{1}{2^{N+1}} \frac{1}{N^2} \sum_{\nu} \langle \nu | \sum_{i \neq j} c_{i\uparrow}^{\dagger} c_{i\downarrow} c_{j\downarrow}^{\dagger} c_{j\uparrow} \sum_{\langle m,n \rangle} \left( c_{m\downarrow}^{\dagger} c_{m\uparrow} c_{n\uparrow}^{\dagger} c_{n\downarrow} + c_{m\uparrow}^{\dagger} c_{m\downarrow} c_{n\downarrow}^{\dagger} c_{n\uparrow} \right) e^{i\Delta\mathbf{k}r_i} e^{i\Delta\mathbf{k}r_j} | \nu \rangle. \end{aligned}$$

For simplicity we have removed terms like  $c_{i\uparrow}^{\dagger} c_{i\downarrow} c_{m\uparrow}^{\dagger} c_{m\downarrow} c_{n\downarrow}^{\dagger} c_{n\downarrow}$  which arises when commuting  $c_{j\downarrow} c_{j\downarrow}^{\dagger}$ . This term contains an odd number of spin flips, making it impossible to return to the state  $|\nu\rangle$ .

This term then turns out to be simpler than before. It is obvious that we will not obtain a non-zero result unless  $i, j$  reflip the spins flipped by  $H_{xy}$ , and thus  $i, j$  must coincide with  $\langle m, n \rangle$ . Thus the second term evaluates to,

$$\frac{1}{2^{N+1}} \frac{1}{N^2} \sum_i 2^{N-2} \cdot 2 \cdot \sum_{i=1}^D \cos(\Delta k_i a) = \frac{D}{4N} \gamma_{\Delta\mathbf{k}}. \quad (11.12)$$

where we have introduced  $\gamma_{\Delta\mathbf{k}} = \frac{1}{D} \sum_{i=1}^D \cos(\Delta k_i a)$ .

To first order in  $\beta J$  we obtain for large values of  $\tilde{T} = 1/\beta J$ , that

$$C_{\parallel}(\Delta\mathbf{k}) = -\frac{1}{4N} + \left[ \frac{dD}{8N} + \frac{D}{4N} \gamma_{\Delta\mathbf{k}} \right] \tilde{T}^{-1}. \quad (11.13)$$

### 11.1.2 Low Temperature Approximations

Again the calculations are founded in Eq. (11.4), which we restate below

$$C'_{\parallel}(\Delta\mathbf{k}) = \frac{1}{N^2} \sum_{ij} \left\{ \langle c_{i\uparrow}^{\dagger} c_{i\uparrow} c_{j\downarrow}^{\dagger} c_{j\downarrow} \rangle + \langle c_{i\uparrow}^{\dagger} c_{j\uparrow} c_{j\downarrow}^{\dagger} c_{i\downarrow} \rangle e^{-i(\mathbf{k}-\mathbf{k}')\mathbf{r}_i} e^{-i(\mathbf{k}'-\mathbf{k})\mathbf{r}_j} \right\}. \quad (11.14)$$

Consider for a moment the first term, as it can be rewritten with relative ease,

$$\begin{aligned} \frac{1}{N^2} \sum_{ij} \langle c_{i\uparrow}^{\dagger} c_{i\uparrow} c_{j\downarrow}^{\dagger} c_{j\downarrow} \rangle &= \frac{1}{N^2} \sum_{ij} \langle \hat{n}_{i\uparrow} \hat{n}_{j\downarrow} \rangle \\ &= \frac{1}{2N^2} \sum_{ij} [\langle \hat{n}_{i\uparrow} \hat{n}_{j\downarrow} \rangle + \langle \hat{n}_{i\downarrow} \hat{n}_{j\uparrow} \rangle] \\ &= \frac{1}{4N^2} \sum_{ij} \langle (\hat{n}_{i\uparrow} + \hat{n}_{i\downarrow})(\hat{n}_{j\uparrow} + \hat{n}_{j\downarrow}) \rangle - \frac{1}{4N^2} \sum_{ij} \langle (\hat{n}_{i\uparrow} - \hat{n}_{i\downarrow})(\hat{n}_{j\uparrow} - \hat{n}_{j\downarrow}) \rangle \\ &= \frac{1}{4} - \frac{1}{N^2} \langle S_z S_z \rangle. \end{aligned} \quad (11.15)$$

Since we have earlier in Eq. (10.31) derived an expression for  $\langle S_z S_z \rangle$  we can in principle evaluate this term. All the trouble is thus left in the second term,

$$\begin{aligned} \frac{1}{N^2} \sum_{ij} \langle c_{i\uparrow}^{\dagger} c_{j\uparrow} c_{j\downarrow}^{\dagger} c_{i\downarrow} \rangle e^{-i(\mathbf{k}-\mathbf{k}')\mathbf{r}_i} e^{-i(\mathbf{k}'-\mathbf{k})\mathbf{r}_j} &= \frac{1}{N^2} \sum_{ij} \langle c_{i\uparrow}^{\dagger} c_{j\uparrow} (\delta_{ij} - c_{i\downarrow}^{\dagger} c_{j\downarrow}) \rangle e^{-i\Delta\mathbf{k}\mathbf{r}_i} e^{i\Delta\mathbf{k}\mathbf{r}_j} \\ &= \frac{1}{N^2} \sum_i \langle c_{i\uparrow}^{\dagger} c_{i\uparrow} \rangle - \frac{1}{N^2} \sum_{ij} \langle c_{i\uparrow}^{\dagger} c_{j\uparrow} c_{i\downarrow}^{\dagger} c_{j\downarrow} \rangle e^{-i\Delta\mathbf{k}\mathbf{r}_i} e^{i\Delta\mathbf{k}\mathbf{r}_j} \\ &= \frac{1}{2N} - \frac{1}{N^2} \sum_{ij} \langle s_{i+} s_{j-} \rangle e^{-i\Delta\mathbf{k}\mathbf{r}_i} e^{i\Delta\mathbf{k}\mathbf{r}_j}. \end{aligned} \quad (11.16)$$

We can calculate the last term in spin wave theory. Split the cubic lattice in two sublattices, and represent points on one sublattice by  $j$  and points on the other sublattice by  $l$ . In the section on linear spin wave theory we introduced the Bose operators  $a_j$  and  $b_l$ . For the assumed spin  $\frac{1}{2}$  we have,

$$\begin{aligned} s_{j+} &= a_j + \mathcal{O}(a^2), & s_{l+} &= b_l^{\dagger} + \mathcal{O}(b^2) \\ s_{j-} &= a_j^{\dagger} + \mathcal{O}(a^2), & s_{l-} &= b_l + \mathcal{O}(b^2). \end{aligned}$$



Keeping terms up to quadratic order in the Bose operators we obtain

$$\begin{aligned} \frac{1}{N^2} \sum_{ij} \langle s_{i+} s_{j-} \rangle e^{-i\Delta\mathbf{k}\mathbf{r}_i} e^{i\Delta\mathbf{k}\mathbf{r}_j} = \frac{1}{N^2} \left[ \sum_{jj'} \langle a_j a_{j'}^\dagger \rangle e^{-i\Delta\mathbf{k}\mathbf{r}_j} e^{i\Delta\mathbf{k}\mathbf{r}_{j'}} + \sum_{l'} \langle b_l^\dagger b_{l'} \rangle e^{-i\Delta\mathbf{k}\mathbf{r}_l} e^{i\Delta\mathbf{k}\mathbf{r}_{l'}} \right. \\ \left. + \sum_{j'} \langle a_j b_{j'} \rangle e^{-i\Delta\mathbf{k}\mathbf{r}_j} e^{i\Delta\mathbf{k}\mathbf{r}_{j'}} + \sum_{lj'} \langle b_l^\dagger a_{j'}^\dagger \rangle e^{-i\Delta\mathbf{k}\mathbf{r}_l} e^{i\Delta\mathbf{k}\mathbf{r}_{j'}} \right]. \end{aligned} \quad (11.17)$$

Let us write  $\Delta\mathbf{k} = n\mathbf{Q} + \Delta\mathbf{k}_1$ , where  $\mathbf{Q}$  is a reciprocal lattice vector of a sublattice,  $n$  is any integer, and  $\Delta\mathbf{k}_1$  lies within the First Brillouin Zone (FBZ) of the sublattice. Then for some  $m, n$ ,

$$e^{i\Delta\mathbf{k}(\mathbf{r}_m - \mathbf{r}_n)} = e^{i\Delta\mathbf{k}_1(\mathbf{r}_m - \mathbf{r}_n)} e^{in\mathbf{Q}(\mathbf{r}_m - \mathbf{r}_n)}. \quad (11.18)$$

When  $m$  and  $n$  both belong to the same sublattices,  $\mathbf{r}_m - \mathbf{r}_n$  is a lattice vector of the sublattice and thus  $e^{in\mathbf{Q}(\mathbf{r}_m - \mathbf{r}_n)} = 1$ . When  $m, n$  belong to two different sublattices  $|\mathbf{r}_m - \mathbf{r}_n| = pa$  with  $p$  odd, and  $e^{in\mathbf{Q}(\mathbf{r}_m - \mathbf{r}_n)} = (-1)^n$ . These considerations allow us to write,

$$\begin{aligned} \frac{1}{N^2} \sum_{ij} \langle s_{i+} s_{j-} \rangle e^{-i\Delta\mathbf{k}\mathbf{r}_i} e^{i\Delta\mathbf{k}\mathbf{r}_j} = \frac{1}{2N} \left[ \langle a_{\Delta\mathbf{k}_1} a_{\Delta\mathbf{k}_1}^\dagger \rangle + \langle b_{\Delta\mathbf{k}_1}^\dagger b_{\Delta\mathbf{k}_1} \rangle \right. \\ \left. + (-1)^n \langle a_{\Delta\mathbf{k}_1} b_{\Delta\mathbf{k}_1} \rangle + (-1)^n \langle b_{\Delta\mathbf{k}_1}^\dagger a_{\Delta\mathbf{k}_1}^\dagger \rangle \right]. \end{aligned} \quad (11.19)$$

Then apply the Bogoliubov rotation of Eq. (10.27)

$$\begin{aligned} a_{\mathbf{u}} &= \alpha_{\mathbf{u}} \cosh \Theta_{\mathbf{u}} - \beta_{\mathbf{u}}^\dagger \sinh \Theta_{\mathbf{u}}, \\ b_{\mathbf{u}} &= -\alpha_{\mathbf{u}}^\dagger \sinh \Theta_{\mathbf{u}} + \beta_{\mathbf{u}} \cosh \Theta_{\mathbf{u}}, \end{aligned}$$

with  $\tanh 2\Theta_{\mathbf{u}} = \frac{1}{d}\gamma_{\mathbf{u}} = \frac{1}{dD} \sum_{i=1}^D \cos(u_i a)$ . We are now left with,

$$\begin{aligned} \frac{1}{N^2} \sum_{ij} \langle s_{i+} s_{j-} \rangle e^{-i\Delta\mathbf{k}\mathbf{r}_i} e^{i\Delta\mathbf{k}\mathbf{r}_j} = \frac{1}{2N} \left[ \langle \alpha_{\Delta\mathbf{k}_1} \alpha_{\Delta\mathbf{k}_1}^\dagger \rangle + \langle \beta_{\Delta\mathbf{k}_1}^\dagger \beta_{\Delta\mathbf{k}_1} \rangle \right. \\ \left. + \langle \alpha_{\Delta\mathbf{k}_1} \beta_{\Delta\mathbf{k}_1} \rangle + \langle \beta_{\Delta\mathbf{k}_1}^\dagger \alpha_{\Delta\mathbf{k}_1}^\dagger \rangle \right] e^{(-1)^{n+1} 2\Theta_{\Delta\mathbf{k}_1}}. \end{aligned} \quad (11.20)$$

Since only the first two terms yield a non-zero result, we arrive at

$$\begin{aligned} \frac{1}{N^2} \sum_{ij} \langle s_{i+} s_{j-} \rangle e^{-i\Delta\mathbf{k}\mathbf{r}_i} e^{i\Delta\mathbf{k}\mathbf{r}_j} &= \frac{1}{2N} [1 + 2n_B(\Delta\mathbf{k}_1)] e^{(-1)^{n+1} 2\Theta_{\Delta\mathbf{k}_1}} \\ &= \frac{1}{2N} \frac{e^{\beta\omega_{\Delta\mathbf{k}_1}} + 1}{e^{\beta\omega_{\Delta\mathbf{k}_1}} - 1} e^{(-1)^{n+1} 2\Theta_{\Delta\mathbf{k}_1}}. \end{aligned} \quad (11.21)$$

The final result in the low temperature limit  $T \approx 0$  is thus,

$$C_{\parallel}(\delta\mathbf{k}) = \frac{1}{2N} - \frac{1}{N^2} \langle S_z S_z \rangle - \frac{1}{2N} \frac{e^{\beta\omega_{\Delta\mathbf{k}_1}} + 1}{e^{\beta\omega_{\Delta\mathbf{k}_1}} - 1} e^{(-1)^{n+1} 2\Theta_{\Delta\mathbf{k}_1}}. \quad (11.22)$$

Note that in general this correlation is of the order of  $\mathcal{O}(1/N)$ .

## 11.2 Transverse Spin Correlations

When calculating the low temperature behaviour of the parallel spin correlations we implicitly assumed that the magnetic field applied after release of the optical lattice was parallel to the direction of the antiferromagnetic ordering. However if the spin ordering direction is assumed perpendicular to the ordering direction, we encounter the transverse spin correlation function  $C_{\perp}(\Delta\mathbf{k})$ .

In fact it is not necessary to literally change the direction of the applied magnetic field. Applying a  $\pi/2$  pulse immediately before the release of the optical lattice would effectively turn the spin ordering direction [52].

Since we only change the direction of the measured spin the high temperature result is identical to the case of parallel spin correlations.

### 11.2.1 Low Temperature Approximation

The expression for the transverse spin noise may be derived from the expression for  $C_{\parallel}(\Delta\mathbf{k})$  of Eq. (11.14) by interchanging spatial co-ordinates, i.e.

$$C_{\perp}(\Delta\mathbf{k}) = \frac{1}{2N} - \frac{1}{N^2} \langle S_x S_x \rangle - \frac{1}{N^2} \sum_{ij} \langle s_{iy} s_{jy} \rangle e^{-i\Delta\mathbf{k}(\mathbf{r}_j - \mathbf{r}_i)} - \frac{1}{N^2} \sum_{ij} \langle s_{iz} s_{jz} \rangle e^{-i\Delta\mathbf{k}(\mathbf{r}_j - \mathbf{r}_i)}. \quad (11.23)$$

Note that

$$\begin{aligned} \frac{1}{N^2} \sum_{ij} \langle s_{iy} s_{jy} \rangle e^{-i\Delta\mathbf{k}(\mathbf{r}_j - \mathbf{r}_i)} &= \frac{1}{4N^2} \sum_{ij} \langle s_{i+} s_{j+} + s_{i-} s_{j-} + s_{i+} s_{j-} + s_{i-} s_{j+} \rangle e^{-i\Delta\mathbf{k}(\mathbf{r}_j - \mathbf{r}_i)} \\ &= \frac{1}{2N^2} \sum_{ij} \langle s_{i+} s_{j-} \rangle e^{-i\Delta\mathbf{k}(\mathbf{r}_j - \mathbf{r}_i)}. \end{aligned}$$

This expression has already been calculated earlier in Eq. (11.22). For  $\langle S_x S_x \rangle$  we obtain

$$\frac{1}{N^2} \langle S_x S_x \rangle = \frac{1}{2N^2} \sum_{ij} \langle s_{i+} s_{j-} \rangle,$$

which can be derived from the previous result setting  $\Delta\mathbf{k} = \mathbf{0}$ . The most complicated term is  $\sum_{ij} \langle s_{iz} s_{jz} \rangle e^{-i\Delta\mathbf{k}(\mathbf{r}_j - \mathbf{r}_i)}$ . In order to deal with this expression, consider

$$\frac{1}{N} \sum_i e^{-i\Delta\mathbf{k}\mathbf{r}_i} s_{iz} = \sum_j (s - a_j^\dagger a_j) e^{-i\Delta\mathbf{k}\mathbf{r}_j} + \sum_l (-s + b_l^\dagger b_l) e^{-i\Delta\mathbf{k}\mathbf{r}_l} \quad (11.24)$$

$$= \frac{2}{N^2} \left( - \sum_j e^{-i\Delta\mathbf{k}\mathbf{r}_j} \sum_{\mathbf{u}\mathbf{u}'} e^{-i\mathbf{u}\mathbf{r}_j} a_{\mathbf{u}}^\dagger e^{i\mathbf{u}'\mathbf{r}_j} a_{\mathbf{u}'} + \sum_l e^{-i\Delta\mathbf{k}\mathbf{r}_l} \sum_{\mathbf{u}\mathbf{u}'} e^{i\mathbf{u}\mathbf{r}_l} b_{\mathbf{u}}^\dagger e^{-i\mathbf{u}'\mathbf{r}_l} b_{\mathbf{u}'} \right)$$

$$+ \frac{s}{N} \left( \sum_j e^{-i\Delta\mathbf{k}\mathbf{r}_j} - \sum_l e^{-i\Delta\mathbf{k}\mathbf{r}_l} \right)$$

$$= \frac{2}{N} \left( -a_{\mathbf{u}}^\dagger a_{\mathbf{u}-\Delta\mathbf{k}} + (-1)^n b_{\mathbf{u}}^\dagger b_{\mathbf{u}-\Delta\mathbf{k}} \right) + \frac{s}{N} \left( \sum_j e^{-i\Delta\mathbf{k}\mathbf{r}_j} - \sum_l e^{-i\Delta\mathbf{k}\mathbf{r}_l} \right).$$

(11.25)

Here we have remembered that  $\mathbf{u} - \mathbf{k}$  can lie outside the FBZ, and again the number of necessary lattice vector translations enters through the factor  $(-1)^n$ . A similar derivation shows that

$$\sum_j e^{i\Delta\mathbf{k}\mathbf{r}_j} s_{jz} = \frac{2}{N} \left( -(-1)^n a_{\mathbf{v}}^\dagger a_{\mathbf{v}+\Delta\mathbf{k}} + b_{\mathbf{v}}^\dagger b_{\mathbf{v}+\Delta\mathbf{k}} \right) + \frac{s}{N} \left( \sum_j e^{i\Delta\mathbf{k}\mathbf{r}_j} - \sum_l e^{i\Delta\mathbf{k}\mathbf{r}_l} \right). \quad (11.26)$$

Assume that  $\Delta\mathbf{k} \neq \mathbf{0}$ . In the case of zero  $\Delta\mathbf{k}$  the total expression for  $\frac{1}{N^2} \left\langle \sum_{ij} \langle s_{iz} s_{jz} \rangle e^{-i\Delta\mathbf{k}(\mathbf{r}_j - \mathbf{r}_i)} \right\rangle$  reduces to the result of Eq. (10.31).

Since  $a_{-\Delta\mathbf{k}}^\dagger = a_{\Delta\mathbf{k}}^\dagger$  the averaging of the multiplicity of those expression to second order in the field operators, we end up with two terms,

$$\frac{1}{N^2} \left\langle \sum_{ij} \langle s_{iz} s_{jz} \rangle e^{-i\Delta\mathbf{k}(\mathbf{r}_j - \mathbf{r}_i)} \right\rangle = K_1(\Delta\mathbf{k}) + K_2(\Delta\mathbf{k}) + K_3(\Delta\mathbf{k}).$$

Here

$$K_1(\Delta\mathbf{k}) = \frac{s^2}{N^2} \left( \sum_j e^{-i\Delta\mathbf{k}\mathbf{r}_j} - \sum_l e^{-i\Delta\mathbf{k}\mathbf{r}_l} \right)^2 \quad (11.27)$$

$$K_2(\Delta\mathbf{k}) = \frac{2s}{N^2} \left( \sum_j e^{-i\Delta\mathbf{k}\mathbf{r}_j} - \sum_l e^{-i\Delta\mathbf{k}\mathbf{r}_l} \right) \sum_{\mathbf{u}\mathbf{v}} \left\langle -a_{\mathbf{u}}^\dagger a_{\mathbf{u}-\Delta\mathbf{k}} + (-1)^n b_{\mathbf{u}}^\dagger b_{\mathbf{u}-\Delta\mathbf{k}} \right\rangle \\ + \frac{2s}{N^2} \left( \sum_j e^{-i\Delta\mathbf{k}\mathbf{r}_j} - \sum_l e^{-i\Delta\mathbf{k}\mathbf{r}_l} \right) \sum_{\mathbf{u}\mathbf{v}} \left\langle -a_{\mathbf{v}}^\dagger a_{\mathbf{v}+\Delta\mathbf{k}} + (-1)^n b_{\mathbf{v}}^\dagger b_{\mathbf{v}+\Delta\mathbf{k}} \right\rangle. \quad (11.28)$$

Summing the random phases of  $K_1(\Delta\mathbf{k})$  normally yields zero except in the case when  $\Delta\mathbf{k}_\pi = \pi \sum_{i=1}^D (\pm \hat{e}_i)/a$ , where the phases add up constructively yielding  $K_1(\Delta\mathbf{k}_\pi) = s^2$ . Likewise  $K_2(\Delta\mathbf{k})$  sum to zero except at  $\Delta\mathbf{k}_\pi$ . Inserting the appropriate Bose field operators we obtain the result

$$K_2(\Delta\mathbf{k}_\pi) = \frac{4s}{N} \sum_{\mathbf{u}} (n_{\mathbf{u}} \cosh^2 \theta_{\mathbf{u}} + (1 - n_{\mathbf{u}}) \sinh^2 \theta_{\mathbf{u}}). \quad (11.29)$$

Hence for  $\Delta\mathbf{k} \neq \Delta\mathbf{k}_\pi$  we obtain for  $\frac{1}{2}$  particles,

$$C_{\perp}(\Delta\mathbf{k}) = \frac{1}{2N} - \frac{1}{4N} \frac{e^{\beta\omega_{\Delta\mathbf{k}_1}} + 1}{e^{\beta\omega_{\Delta\mathbf{k}_1}} - 1} e^{(-1)^{n+1} 2\Theta_{\Delta\mathbf{k}_1}} - \frac{1}{2N} \frac{e^{\beta\omega_0} + 1}{e^{\beta\omega_0} - 1} e^{(-1)^{n+1} 2\Theta_0}. \quad (11.30a)$$

And for  $\Delta\mathbf{k} = \Delta\mathbf{k}_\pi$  we may ignore the above contribution in comparison with,

$$C_{\perp}(\Delta\mathbf{k}_\pi) = \frac{1}{2N} - \frac{1}{4} - \frac{2}{N} \sum_{\mathbf{u}} (n_{\mathbf{u}} \cosh^2 \theta_{\mathbf{u}} + (1 - n_{\mathbf{u}}) \sinh^2 \theta_{\mathbf{u}}). \quad (11.30b)$$

Note that away from  $\Delta\mathbf{k}_\pi$  the correlation function scale as  $\mathcal{O}(1/N)$  while at  $\Delta\mathbf{k}_\pi$  it is of order  $\mathcal{O}(1)$ .

### 11.3 Density-Density Correlation Function

The last correlation function we will consider here is already mentioned density-density correlation function.

$$C_{nn}(\Delta\mathbf{k}) = \sum_{\sigma\sigma'} \langle \hat{n}_{\sigma} \hat{n}_{\sigma'} \rangle - [\langle \hat{n}_{\sigma} \rangle]^2 = \frac{1}{N} - \frac{1}{2} \delta_{\Delta\mathbf{k}, \mathbf{Q}} - 2 \frac{1}{N^2} \sum_{ij} \langle \mathbf{s}_i \cdot \mathbf{s}_j \rangle e^{-i\Delta\mathbf{k}(\mathbf{r}_j - \mathbf{r}_i)}, \quad (11.31)$$

where  $\mathbf{Q}$  is a reciprocal lattice vector of the sublattice.

### 11.3.1 High Temperature Expansion

An analytical expression for the high temperature behaviour of the density-density correlation function has been derived by Bruun [53]. For a three dimensional lattice the result is

$$C_{nn}(\Delta\mathbf{k}) = -\frac{1}{2}\delta_{\Delta\mathbf{k},\mathbf{Q}} - \frac{1}{2N} + \beta J \frac{3}{8N} z\gamma_{\Delta\mathbf{k}}. \quad (11.32)$$

### 11.3.2 Low Temperature Expansion

An expression for the low temperature expansion can be pieced together from the already obtained results for different spin correlation functions.

$$C_{nn}(\Delta\mathbf{k}) = \frac{1}{N} - \frac{2}{N^2} \sum_{ij} \langle s_{i+} s_{j-} \rangle e^{-i\Delta\mathbf{k}(\mathbf{r}_j - \mathbf{r}_i)} - \frac{2}{N^2} \langle s_{iz} s_{jz} \rangle e^{-i\Delta\mathbf{k}(\mathbf{r}_j - \mathbf{r}_i)}. \quad (11.33)$$

For  $\Delta\mathbf{k} \neq \Delta\mathbf{k}_\pi$  this reduces to

$$C_{nn}(\Delta\mathbf{k}) = \frac{1}{N} - \frac{1}{N} \frac{e^{\beta\omega_{\Delta\mathbf{k}_1}} + 1}{e^{\beta\omega_{\Delta\mathbf{k}_1}} - 1} e^{(-1)^{n+1} 2\Theta_{\Delta\mathbf{k}_1}}. \quad (11.34a)$$

For  $\Delta\mathbf{k} = \Delta\mathbf{k}_\pi$  we get

$$C_{nn}(\Delta\mathbf{k}) = \frac{1}{N} - \frac{1}{2} - \frac{4}{N} \sum_{\mathbf{u}} (n_{\mathbf{u}} \cosh^2 \theta_{\mathbf{u}} + (1 - n_{\mathbf{u}}) \sinh^2 \theta_{\mathbf{u}}). \quad (11.34b)$$

As for the transverse spin noise the density-density correlation function scales as  $\mathcal{O}(1)$  at  $\Delta\mathbf{k}_\pi$  and as  $\mathcal{O}(1/N)$  for all other reciprocal lattice vectors.

Having calculated analytical expressions for the both parallel, transverse and density-density correlation functions we will need to compute those for a relevant optical lattice system. Here we will in short explain the computation in terms of a 3D cubic lattice containing  $N = N_x \times N_y \times N_z$  lattice sites separated by a lattice constant  $a$ .

The first Brillouin zone of this lattice contains  $8N$  reciprocal lattice points, described by:

$$\mathbf{k} = \left( \frac{\pi n_x}{a N_x}, \frac{\pi n_y}{a N_y}, \frac{\pi n_z}{a N_z} \right), \quad (12.1)$$

where  $n_x$  run from  $-N_x$  to  $N_x$ ,  $n_y$  from  $-N_y$  to  $N_y$  etc.

The two sublattices for spin  $\uparrow$  and spin  $\downarrow$  respectively consists of two interlacing *fcc* sublattices of side length  $2a$  each containing a total of  $N/2$  lattice sites. The corresponding reciprocal lattice has a *bcc* structure, and the first Brillouin zone for such a structure is a that of a truncated octahedron with side length  $2\pi/a$ .

For the low temperature correlation function behaviour we have obtained results of varying magnitude. To sum up both  $C_{nn}$  and  $C_{\perp}$  has correlations of size  $\mathcal{O}(1)$  at the reciprocal lattice point  $\Delta\mathbf{k}_{\pi}$ , while all correlation functions scale as  $\mathcal{O}(1/N)$  away from this point .

Experiments only measure the two-dimensional projection of the summed correlation functions in  $\Delta\mathbf{k}$  space. Hence summing the correlation functions in one direction (e.g. the z-direction),

$$C(\Delta\mathbf{k}_{\perp}) = \sum_{n_z=-N_z}^{N_z} C(\Delta\mathbf{k}_{bot} + n_z\pi\hat{e}_z/(N_z a)), \quad (12.2)$$

where  $\mathbf{k}_{\perp} = (k_x, k_y)$  is a two-dimensional vector. The solution of the two-dimensional array of detectors used for obtaining the density measurements is currently not good enough as to resolve the correlation functions for single reciprocal lattice vectors. Instead experiments concern the Gaussian smoothed correlation functions [49], given by

$$C^{exp}(\Delta\mathbf{k}_{\perp}) = \frac{1}{4\pi N\kappa^2} \sum_{\Delta\mathbf{k}'} e^{-\frac{1}{4\kappa^2} \frac{1}{(2\pi)^2} (\Delta\mathbf{k}'_{\perp} - \Delta\mathbf{k}_{\perp})^2} C(\Delta\mathbf{k}'). \quad (12.3)$$

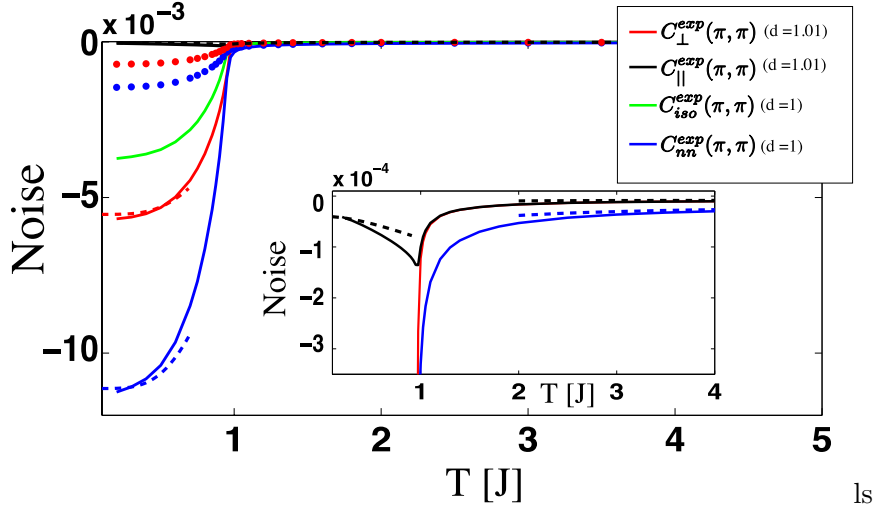


**Figure 12.1:** Noise correlation functions as a function of temperature  $T$  at  $\mathbf{k}_\perp = (\pi/a, \pi/a)$ . The solid lines represent the  $\Delta\mathbf{k}_z$  summed correlations while the dotted lines are the Gaussian smoothed results at  $\kappa = 1/40$ . The dashed line are the  $\Delta\mathbf{k}_z$  analytical results of Eqs. (11.22), (11.30) and (11.34).

Here  $\kappa = w/l$  with  $l = 2\pi t/ma$ ,  $t$  the atomic cloud expansion time and  $w$  is a width depending on detector resolution.

Regarding  $C_{nn}$  and  $C_\perp$  the dip at  $\Delta\mathbf{k}_\pi$  is greatly affected by this Gaussian smoothing. At the two-dimensional projection  $\Delta\mathbf{k}_\pi$  at  $\Delta\mathbf{k}_{\perp\pi} = (\pi/a, \pi/a)$  the dip is now of order  $\mathcal{O}(1/\kappa^2 N)$ . At other reciprocal lattice vectors the correlations are less affected by the Gaussian smoothing.

For a given system size the correlation functions are simply calculated by straightforward computation in terms of the dimensionless variables, i.e.

$$\tilde{T} = T/J, \quad \tilde{\omega}_\mathbf{u} = \frac{\omega_\mathbf{u}}{J} \quad (12.4)$$

An example of the applied MATLAB scripts calculating the components of the correlation functions is presented in Appendix C. The correlation functions  $C_{||}(\Delta\mathbf{k})$ ,  $C_\perp(\Delta\mathbf{k})$  and  $C_{nn}(\Delta\mathbf{k})$  can be computed for any  $\Delta\mathbf{k}$ .

Olav Syljuåsen from the University of Oslo simulated the three-dimensional Heisenberg system using a Quantum Monte Carlo method. From the simulated data a critical temperature  $\tilde{T}_N = 0.945$  was extracted.

For a system of size  $N = 32 \times 32 \times 32$  we present the results of our calculation in Figure 12.1 at  $\Delta\mathbf{k}_\perp = (\pi/a, \pi/a)$ . The inset shows a zoom of the plot close to  $\tilde{T}_N$ . Note the good agreement between analytical and simulated results.

The large correlations  $C_{nn}$  and  $C_\perp$  are anti-bunching dips of the period-doubled antiferromagnetically ordered lattice. While period doubling may stem from various physical effects. In order to guarantee that the period doubling is a feature of the spin ordering it is necessary to measure the spin resolved  $C_\perp$  or  $C_{||}$ .

One may note that the calculated correlations are small even for the macroscopic dips of  $C_\perp$  and  $C_{nn}$  the correlations is of order  $10^{-3}$  when including the Gaussian smoothing. In general they scale like  $1/N$ . Experimentally Fölling et al. has measured correlations of order  $C_{nn} \sim 10^{-4}$  for a slightly larger system. Even above the critical temperature  $T_N$  the correlations are within experimental grasp, i.e., for  $T = 2J$  we see that  $C_{nn}^{exp} \approx 6 \cdot 10^{-5}$  (which scales as

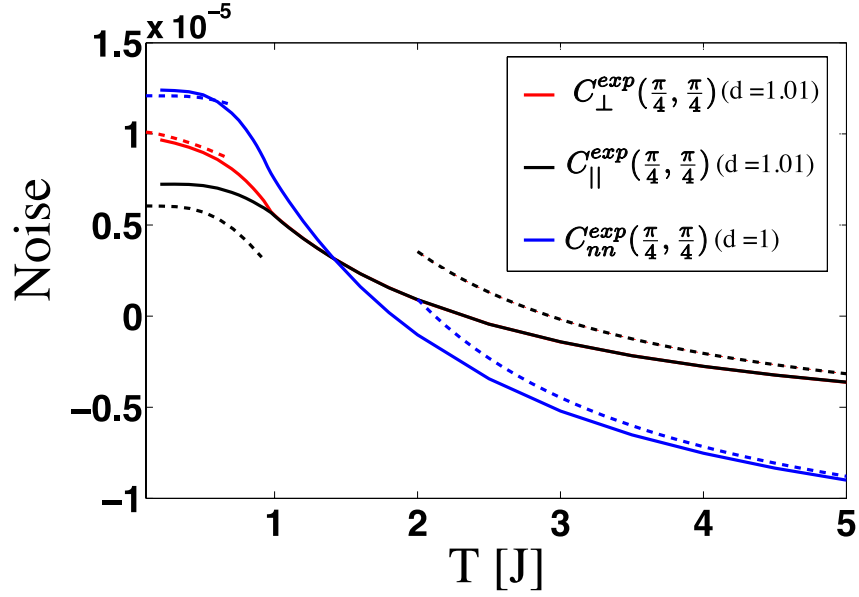


**Figure 12.2:** Noise correlation functions as a function of temperature  $T$  at  $\Delta\mathbf{k}_\perp = (\pi/4a, \pi/4a)$ . The solid lines represent the  $\Delta\mathbf{k}_z$  summed correlations. The dashed line are the  $\Delta\mathbf{k}_z$  analytical results of Eqs. (11.22), (11.30) and (11.34).

$1/N$ ). The conclusion then is that the measurement of noise correlations can be used to detect the onset of antiferromagnetic order even above  $T_N$ . For current experiments the actual spin temperature is uncertain. Measuring the noise correlation, the detailed spin noise behaviour presented here would provide a means of assessing the spin temperature in the experiments. [52].

We also show the calculated results for reciprocal lattice point  $\Delta\mathbf{k}_\perp = (\pi/4a, \pi/4a, \pi/4a)$  in Figure 12.2. Here the effect of Gaussian smoothening is negligible and has thus been left out.

Note that the correlation functions behaves differently from the case of  $k_\perp = (\pi/a, \pi/a)$ . They now decrease in absolute value for high temperatures and even change sign above the critical temperature  $T_N$ . Because the noise is of order  $\mathcal{O}(1/N)$ , a measurement requires higher experimental resolution than what is presently available [52].





## Conclusion

---

In this part of the thesis we have investigated a novel time-of-flight method for detecting anti-ferromagnetic correlations for spinfull fermionic particles in an optical lattice.

We have obtained analytical results for both spin resolved correlation functions as well as the density-density correlations in both the high-temperature and low-temperature regimes. Direct computations for a specific three dimensional optical lattice system show excellent agreement with Quantum Monte Carlo simulated data. The calculations have been based on experimentally relevant parameters, and by comparison to recent experiments it has been assessed that the correlations considered here lie within the current experimental solution.

In conclusion the spin-resolved noise correlations considered here possess valuable information about the antiferromagnetic correlations above as well as below the critical temperature.



# Bibliography

---

- [1] R. D. Mattuck, *A Guide to Feynman Diagrams in the Many-Body Problem*, (McGraw-Hill 1967).
- [2] A. P. Jauho, *Introduction to the Non-equilibrium Green's function technique*, (unpublished).
- [3] A. C. Hewson, *The Kondo Problem to Heavy Fermions*, (Cambridge University Press 1993).
- [4] P. W. Anderson, *Basic Notions of Condensed Matter Physics*, (Addison-Wesley 1984).
- [5] M. E. Peskin, and D. V. Schroeder, *An introduction to Quantum Field Theory* (Westview 1995).
- [6] K. Yosida, *Theory of Magnetism* (Springer Verlag 1996).
- [7] John Cardy, *Scaling and Renormalisation in Statistical Physics*, Cambridge University Press 1996.
- [8] A. Auerbach, *Interacting Electrons and Quantum Magnetism* (Springer Verlag 1998).
- [9] M. P. Marder, *Condensed Matter Physics*, (John Wiley & Sons Inc, 2000).
- [10] Henrik Bruus and Karsten Flensberg, *Many-Body Quantum Theory in Condensed Matter Physics*, (Oxford University Press 2004).
- [11] Jørgen Rammer, *Quantum Field Theory of Non-equilibrium States*, (Cambridge University Press 2007).
- [12] W. J. de Haas, J. H. de Boer, and G. J. van den Berg, *The electrical resistance of gold, copper and lead at low temperatures*, *Physica*, **1**, 1115 (1934).
- [13] J. Kondo, *Resistance Minimum in Dilute Magnetic Alloys*, *Progress of Theoretical Physics*, Vol. **32**, No. 1 (1964).
- [14] A. A. Abrikosov, *Influence of impurity ferromagnetism and the external magnetic field on the resistance of a metal with magnetic impurities*, *Physics* Vol. **2**, No. 2, pp. 61-69 (1965).
- [15] J. A. Schrieffer, P. A. Wolff, *Relation between the Anderson and Kondo Hamiltonians*, *Phys. Rev.* **149**, 491 - 492 (1966).

- [16] P. W. Anderson, *A poor man's derivation of scaling laws for the Kondo problem*, J. Phys. C: Solid St. Phys. **3**, 2436-41 (1970).
- [17] A. A. Abrikosov, and A. A. Migdal, *On the theory of the Kondo effect*, J. Low. Temp. Phys., Vol. **3**, No. 5 (1970).
- [18] M. Fowler, and A. Zawadowski, *Scaling and the renormalization group in the kondo effect*, Solid State Commun., Vol. **9**, 471—476 (1971).
- [19] M. Fowler, *Renormalization-Group Techniques in the Kondo Effect*, Phys. Rev. B. **6**, 3422-26 (1972).
- [20] J. Sólyom, and A. Zawadowski, *Are the scaling laws for the Kondo problem exact?*, J. Phys. F: Metal Phys. Vol. **4** (1974).
- [21] J. Sólyom, *Renormalization and scaling in the X-ray absorption and Kondo problems*, J. Phys. F: Met. Phys. **4** 2269 (1974).
- [22] N. Andrei, K. Furuya and J. H. Lowenstein, *Solution of the Kondo problem*, Rev. Mod. Phys., Vol. **55**, No. 2 (1983).
- [23] J. Rammer, and H. Smith, *Quantum field-theoretical methods in transport theory of metals*, Rev. Mod. Phys., Vol. **58**, No. 2 (1986).
- [24] D. Goldhaber-Gordon, Hadas Shtrikman, D. Mahalu, David Abusch-Magder, U. Meirav, and M. A. Kastner, *Kondo effect in a single-electron transistor*, Nature **391**, 156-159 (1998).
- [25] S. M. Cronenwett, T. H. Oosterkamp, Leo P. Kouwenhoven, *A Tunable Kondo Effect in Quantum Dots*, Science Vol. **281**. no. 5376, pp. 540 - 544 (1998).
- [26] A. Kaminski, Yu. V. Nazarov, and L. I. Glazman, *Universality of the Kondo effect in a quantum dot out of equilibrium*, Phys. Rev. B **62**, 8154 (2000).
- [27] Herbert Schoeller, and Jürgen König, *Real-Time Renormalization Group and Charge Fluctuations in Quantum Dots*, Phys. Rev. Lett. **84**, 3686 (2000).
- [28] Jesper Nygaard, David Henry Cobden, and Poul Erik Lindelof, *Kondo physics in carbon nanotubes*, Nature **408**, 342-346 (2000).
- [29] W. G. van der Wiel, S. De Franceschi, T. Fujisawa, J. M. Elzerman, S. Tarucha, L. P. Kouwenhoven, *The Kondo Effect in the Unitary Limit*, Science Vol. **289**. no. 5487, pp. 2105 - 2108 (2000).
- [30] P. Coleman, C. Hooley, and O. Parcollet, *Is the Quantum Dot at Large Bias a Weak-Coupling Problem?*, Phys. Rev. Lett. **86**, 4088 (2001).
- [31] A. Rosch, J. Kroha, and P. Wölfle, *Kondo Effect in Quantum Dots at High Voltage: Universality and Scaling*, Phys. Rev. Lett. **87**, 156802 (2001).
- [32] A. Rosch, J. Paaske, J. Kroha, and P. Wölfe, *Nonequilibrium Transport through a Kondo Dot in a Magnetic Field: Perturbation Theory and Poor Man's Scaling*, Phys. Rev. Lett. **90**, 076804 (2003).

- [33] M. Pustilnik, and L. I. Glazman, *Kondo effect in quantum dots*, J. Phys.: Cond. Matt. **13**, R513–R537 (2004).
- [34] J. Paaske, A. Rosch, and P. Wölfle, *Nonequilibrium transport through a Kondo dot in a magnetic field: Perturbation theory*, Phys. Rev. B **69**, 155330 (2004).
- [35] J. Paaske, A. Rosch, J. Kroha, and P. Wölfle, *Nonequilibrium transport through a Kondo dot: Decoherence effects*, Phys. Rev. B **70**, 155301 (2004).
- [36] A. Rosch, J. Paaske, J. Kroha, and P. Wölfle, *The Kondo Effect in Non-equilibrium Quantum Dots: Perturbative Renormalization Group*, Journal of the Physical Society of Japan, Vol. **74**, 118-126 (2005).
- [37] J. Paaske, and K. Flensberg, *Vibrational Sidebands and the Kondo Effect in Molecular Transistors*, Phys. Rev. Lett. **94**, 176801 (2005).
- [38] M. Pustilnik, *Kondo effect in nanostructures*, Phys. Stat. Sol. (a) **203**, No. 6, 1137-1147 (2006).
- [39] M. Grobis, I. G. Rau, R. M. Potok, and D. Goldhaber-Gordon, *Kondo Effect in Mesoscopic Quantum Dots*, arXiv:cond-mat/0611480v1 (2006).
- [40] P. Mehta and N. Andrei, *Nonequilibrium Transport in Quantum Impurity Models: The Bethe Ansatz for Open Systems*, Phys. Rev. Lett. **96**, 156802 (2006).
- [41] B. Doyon, and N. Andrei, *Universal aspects of nonequilibrium currents in a quantum dot*, Phys. Rev. B **73**, 245326 (2006).
- [42] P. Fritsch, and S. Kehrein, *Non-equilibrium scaling analysis of the Kondo model*, Annals of Physics **324**, 1105–1135 (2009).
- [43] Herbert Schoeller, *A perturbative nonequilibrium renormalization group method for dissipative quantum mechanics*, Eur. Phys. J. Special Topics **168**, 179–266 (2009).
- [44] S. Schmaus, V. Koerting, Paaske, T. S. Jespersen, J. Nygård, and P. Wölfle, *Nonequilibrium cotunneling through a three-level quantum dot*, Phys. Rev. B. **79**, 045105 (2009).
- [45] D. Jaksch, C. Bruder, J. I. Cirac, C. W. Gardiner, and P. Zoller, *Cold Bosonic Atoms in Optical Lattices*, Phys. Rev. Lett. **81**, 3108 (1998).
- [46] W. Hofstetter, J. I. Cirac, P. Zoller, E. Demler, and M. D. Lukin, *High-Temperature Superfluidity of Fermionic Atoms in Optical Lattices*, Phys. Rev. Lett. **89**, 220407 (2002).
- [47] E. Altman, E. Demler, and M. D. Lukin, *Probing many-body states of ultracold atoms via noise correlations*, Phys. Rev. A **70**, 013603 (2004).
- [48] T. Rom, Th. Best, D. van Oosten, U. Schneider, S. Fölling, B. Paredes and I. Bloch, *Free fermion antibunching in a degenerate atomic Fermi gas released from an optical lattice*, T. Rom, Th. Best, D. van Oosten, U. Schneider, S. Fölling, B. Paredes and I. Bloch, Nature **444**, 733-736 (2006).
- [49] S. Fölling, S. Trotzky, P. Cheinet, M. Feld, R. Saers, A. Widera, T. Müller, and I. Bloch, *Direct observation of second-order atom tunnelling*, Nature **431**, 481 (2007).

- [50] I. Bloch, J. Dalibard, and W. Zwerger, *Many-body physics with ultracold gases*, Rev. Mod. Phys. **80**, 885 (2008).
- [51] G. M. Bruun, Brian M. Andersen, Eugene Demler, and Anders S. Sørensen, *Probing Spatial Spin Correlations of Ultracold Gases by Quantum Noise Spectroscopy*, Phys Rev. Lett. **102**, 030401 (2009).
- [52] G. M. Bruun, O. F. Syljuasen, K. G. L. Pedersen, B. M. Andersen, E. Demler, A. S. Sørensen, *Antiferromagnetic noise correlations in optical lattices*, <http://arxiv.org/abs/0907.0652> (2009)
- [53] G. M. Bruun, *Density-density correlations for high temperatures*, unpublished (2009).

## The Scaling Equations for $J_{\pm}$

---

This calculation outlines roughly the steps of the procedure in obtaining the scaling equation Eq. (6.38). In order to keep the notation to a minimum we will in general write  $\gamma B$  simply as  $B$ . To keep equations lean any unused or unimportant sums or integrals are in general not written explicitly, and we count on the reader to refer back to the relevant equations if doubt should arise.

As of Eq. (6.20),

$$S_-^{(2)} = -\frac{1}{2}T_c \sum_{a'ab'b} \int_c d\tau \int_c d\tau' J_{a'a}^{\pm} J_{b'b}^z S^+(\tau) S^z(\tau') s_{a'a}^-(\tau) s_{b'b}^z(\tau') \quad (\text{A.1})$$

$$S_+^{(2)} = -\frac{1}{2}T_c \sum_{a'ab'b} \int_c d\tau \int_c d\tau' J_{a'a}^{\pm} J_{b'b}^z S^-(\tau) S^z(\tau') s_{a'a}^+(\tau) s_{b'b}^z(\tau') \quad (\text{A.2})$$

Average these expressions to obtain the the effective  $S$ -matrix for each  $\tilde{S}_-^{(2)}$ ,

$$\begin{aligned} \tilde{S}_-^{(2)} &= \frac{i}{2} J_{a'a}^{\pm} J_{ab}^z S^+(\tau) S^z(\tau') c_{a'\downarrow}^{\dagger}(\tau) c_{b\uparrow}(\tau') G_a^{(0)}(\tau, \tau') \\ &\quad - \frac{1}{2} i J_{ba}^{\pm} J_{b'b}^z S^+(\tau') S^z(\tau) c_{b'\downarrow}^{\dagger}(\tau) c_{a\uparrow}(\tau') G_b^{(0)}(\tau, \tau') \end{aligned} \quad (\text{A.3})$$

Where the time-ordering operator, the time-integration and the momentum sums are contained implicitly. Likewise for  $\tilde{S}_+^{(2)}$ ,

$$\begin{aligned} \tilde{S}_+^{(2)} &= -\frac{i}{2} J_{a'a}^{\pm} J_{ab}^z S^-(\tau) S^z(\tau') c_{a'\downarrow}^{\dagger}(\tau) c_{b\uparrow}(\tau') G_a^{(0)}(\tau, \tau') \\ &\quad + \frac{1}{2} i J_{ba}^{\pm} J_{b'b}^z S^-(\tau') S^z(\tau) c_{b'\uparrow}^{\dagger}(\tau) c_{a\downarrow}(\tau') G_b^{(0)}(\tau, \tau') \end{aligned} \quad (\text{A.4})$$

In the coming we will only consider the first diagonal term in the Schwinger-Keldysh representation. Thus for  $\tilde{S}_-^{(2)}$  we find that,

$$\begin{aligned} \tau >_c \tau' : \frac{i}{2} \int_{-\infty}^{\infty} dt \int_{-\infty}^t dt' & \left[ J_{a'a}^{\pm} J_{ab}^z S^+(t) S^z(t') c_{a'\downarrow}^{\dagger}(t) c_{b\uparrow}(t') G_a^{(0)>}(t, t') \right. \\ & \left. - J_{ba}^{\pm} J_{b'b}^z S^z(t) S^+(t') c_{b'\downarrow}^{\dagger}(t) c_{a\uparrow}(t') G_b^{(0)>}(t, t') \right] \end{aligned} \quad (\text{A.5})$$

$$\begin{aligned} \tau <_c \tau' : -\frac{1}{2} i \int_{-\infty}^{\infty} dt \int_t^{\infty} dt' & \left[ J_{a'a}^{\pm} J_{ab}^z S^z(t') S^+(t) c_{b\uparrow}(t') c_{a'\downarrow}^{\dagger}(t) G_a^{(0)<}(t, t') \right. \\ & \left. - J_{ba}^{\pm} J_{b'b}^z S^+(t') S^z(t) c_{a\uparrow}(t') c_{b'\downarrow}^{\dagger}(t) G_b^{(0)<}(t, t') \right] \end{aligned} \quad (\text{A.6})$$

and for  $\tilde{S}_+^{(2)}$ ,

$$\begin{aligned} \tau >_c \tau' : -\frac{1}{2} i \int_{-\infty}^{\infty} dt \int_t^{\infty} dt' & \left[ J_{a'a}^{\pm} J_{ab}^z S^-(t) S^z(t') c_{a'\downarrow}^{\dagger}(t) c_{b\uparrow}(t') G_a^{(0)>}(t, t') \right. \\ & \left. - J_{ba}^{\pm} J_{b'b}^z S^z(t) S^-(t') c_{b'\uparrow}^{\dagger}(t) c_{a\downarrow}(t') G_b^{(0)>}(t, t') \right] \end{aligned} \quad (\text{A.7})$$

$$\begin{aligned} \tau <_c \tau' : \frac{i}{2} \int_{-\infty}^{\infty} dt \int_{-\infty}^t dt' & \left[ J_{a'a}^{\pm} J_{ab}^z S^z(t') S^-(t) c_{b\uparrow}(t') c_{a'\downarrow}^{\dagger}(t) G_a^{(0)<}(t, t') \right. \\ & \left. - J_{ba}^{\pm} J_{b'b}^z S^-(t') S^z(t) c_{a\downarrow}(t') c_{b'\uparrow}^{\dagger}(t) G_b^{(0)<}(t, t') \right] \end{aligned} \quad (\text{A.8})$$

Utilize the general spin 1/2 relations,

$$\begin{aligned} S^+ S^- &= \frac{1}{2} + S^z & S^- S^+ &= \frac{1}{2} - S^z \\ S^- S^z &= -S^z S^- = \frac{1}{2} S^- & S^+ S^z &= -\frac{1}{2} S^+ = -S^z S^+ \\ S^z S^z &= \frac{1}{4} \end{aligned}$$

Starting with the first ordering of  $\tilde{S}_-^{(2)}$ , where we have changed the limit of one integral from  $\infty$  to  $-\infty$ . Such a change will only influence the real part of the effective  $S$  matrix, which will not be considered here.

$$\frac{i}{2} \int_{-\infty}^t dt' c_{a'\downarrow}^{\dagger}(t) c_{b\uparrow}(t') J_{a'a}^{\pm} J_{ab}^z e^{-iBt} \left[ S^+ S^z G_a^{(0)>}(t, t') - S^z S^+ G_a^{(0)<}(t, t') \right] \quad (\text{A.9})$$

$$-\frac{i}{4} \int_{-\infty}^t dt' c_{a'\downarrow}^{\dagger}(t) c_{b\uparrow}(t') J_{a'a}^{\pm} J_{ab}^z e^{-iBt} \left[ S^+ G_a^{(0)>}(t, t') + S^+ G_a^{(0)<}(t, t') \right] \quad (\text{A.10})$$

and then the  $\tilde{S}_-^{(2)}$  last ordering

$$-\frac{i}{2} \int_{-\infty}^t dt' c_{b'\downarrow}^{\dagger}(t) c_{a\uparrow}(t') J_{ba}^{\pm} J_{b'b}^z e^{-iBt'} \left[ S^z S^+ G_b^{(0)>}(t, t') - S^+ S^z G_b^{(0)<}(t, t') \right] \quad (\text{A.11})$$

$$\frac{i}{4} \int_{-\infty}^t dt' c_{b'\downarrow}^{\dagger}(t) c_{a\uparrow}(t') J_{ba}^{\pm} J_{b'b}^z e^{-iBt'} \left[ S^+ G_b^{(0)<}(t, t') + S^+ G_b^{(0)>}(t, t') \right] \quad (\text{A.12})$$

Then turn to  $\tilde{S}_+^{(2)}$  first ordering,

$$\frac{i}{2} \int_{-\infty}^t dt' c_{a'\downarrow}^{\dagger}(t) c_{b\uparrow}(t') J_{a'a}^{\pm} J_{ab}^z e^{iBt} \left[ S^- S^z G_a^{(0)>}(t, t') - S^z S^- G_a^{(0)<}(t, t') \right] \quad (\text{A.13})$$

$$-\frac{i}{4} \int_{-\infty}^t dt' c_{a'\downarrow}^{\dagger}(t) c_{b\uparrow}(t') J_{a'a}^{\pm} J_{ab}^z e^{iBt} \left[ S^- G_b^{(0)>}(t, t') + S^- G_b^{(0)<}(t, t') \right] \quad (\text{A.14})$$



and then  $\tilde{S}_+^{(2)}$ , last ordering

$$-\frac{i}{2} \int_{-\infty}^t dt' c_{b'\uparrow}^\dagger(t) c_{a\downarrow}(t') J_{ab}^\pm J_{a'a}^z e^{iBt'} \left[ S^z S^- G_a^{(0)>}(t, t') - S^- S^z G_a^{(0)<}(t, t') \right] \quad (\text{A.15})$$

$$\frac{i}{4} \int_{-\infty}^t dt' c_{b'\uparrow}^\dagger(t) c_{a\downarrow}(t') J_{ab}^\pm J_{a'a}^z e^{iBt'} \left[ S^- G_a^{(0)>}(t, t') + S^- G_a^{(0)<}(t, t') \right] \quad (\text{A.16})$$

We will go by a little different approach here but the overall result is still valid. Instead of performing the time-integration directly we insert the Fourier transforms of the field operators and perform the time integrals. The included frequency  $\varepsilon$  will then play the rôle of the incoming state energy. For  $\tilde{S}_-^{(2)}$  we have that,

$$\int_{-\infty}^t dt' \int \frac{d\omega}{2\pi} \int \frac{d\varepsilon}{2\pi} c_{a'\downarrow}^\dagger(\omega) c_{b\uparrow}(\varepsilon) \left[ -J_{ab}^\pm J_{a'a}^z S^+ e^{-iBt} + J_{a'a}^\pm J_{ab}^z S^+ e^{-iBt'} \right] \\ \times (1 - 2f(\xi_a)) e^{-i\xi_a(t-t')} e^{-i\omega t} e^{i\varepsilon t'}. \quad (\text{A.17})$$

There is two relevant time integrations contained in this expressions

$$e^{-iBt} e^{-i\omega t} \int_{-\infty}^t dt' e^{-i\xi_a(t-t')} e^{i\varepsilon t'} = e^{-iBt} e^{i(\varepsilon-\omega)t} \frac{i}{\xi_a + \varepsilon - i0_+} \quad (\text{A.18})$$

and

$$e^{-i\omega t} \int_{-\infty}^t dt' e^{-i\xi_a(t-t')} e^{i\varepsilon t'} e^{-iBt'} = e^{-iBt} e^{i(\varepsilon-\omega)t} \frac{-i}{\xi_a - \varepsilon - B + i0_+} \quad (\text{A.19})$$

While for  $\tilde{S}_+^{(2)}$ ,

$$\int_{-\infty}^t dt' \int \frac{d\omega}{2\pi} \int \frac{d\varepsilon}{2\pi} c_{a'\downarrow}^\dagger(t) c_{b\uparrow}(t') \left[ -J_{a'a}^\pm J_{ab}^z S^- e^{iBt} + J_{ab}^\pm J_{a'a}^z S^- e^{iBt'} \right] \\ \times (1 - 2f(\xi_a)) e^{-i\xi_a(t-t')} e^{-i\omega t} e^{i\varepsilon t'} \quad (\text{A.20})$$

Which contain the same relevant time integrals. For  $\delta_D \tilde{S}_-^{(2)}$  and  $\delta_D \tilde{S}_+^{(2)}$  (and ignoring imaginary parts),

$$\int_{\square} \nu_F d\varepsilon_a \frac{\text{sgn}(\varepsilon_a - \mu_a)}{\varepsilon_a - \mu_a + \varepsilon} \\ = \nu_F \frac{\delta D}{D - \mu_a + \varepsilon} - \nu_F \frac{\delta D}{-D - \mu_a + \varepsilon} \\ = \nu_F \frac{\delta D}{D} \frac{2D^2}{(\varepsilon - \mu_a)^2 - D^2} \quad (\text{A.21})$$

and

$$\int_{\square} \nu_F d\varepsilon_a \frac{\text{sgn}(\varepsilon_a - \mu_a)}{\varepsilon_a \mu_a - \varepsilon - B} \\ = \nu_F \frac{\delta D}{D - \mu_a + \varepsilon - B} - \nu_F \frac{\delta D}{D - \mu_a + \varepsilon - B} \\ = \nu_F \frac{\delta D}{D} \frac{2D^2}{(\varepsilon - \mu_a - B)^2 - D^2} \quad (\text{A.22})$$

Collecting all the terms and inserting into the scaling equations of chapter 5 leaves one with,

$$\frac{\delta J_{\alpha'\beta}^{\pm}}{\delta \ln D} = \frac{1}{2} \nu_F \sum_{\alpha} \left( J_{\alpha'\alpha}^z J_{\alpha\beta}^{\pm} + J_{\alpha'\alpha}^{\pm} J_{\alpha\beta}^z \right) \left( \frac{D^2}{D^2 - (\varepsilon - \mu_{\alpha})^2} + \frac{D^2}{D^2 - (\varepsilon - \mu_{\alpha} - B)^2} \right) \quad (\text{A.23})$$

APPENDIX B

# Time Ordering on the Keldysh Contour for 2-loop Calculations

---

Time ordering an expression of the form

$$T_c \int_c d\tau \int_c d\tau' \int_c d\tau'' H'(\tau) H'(\tau') H'(\tau'') \quad (\text{B.1})$$

In this case we don't distinguish between cases when  $\tau$  reside on the upper or lower contour. This gives rise to the  $3! = 6$  different time-orderings presented in Figure B.1.

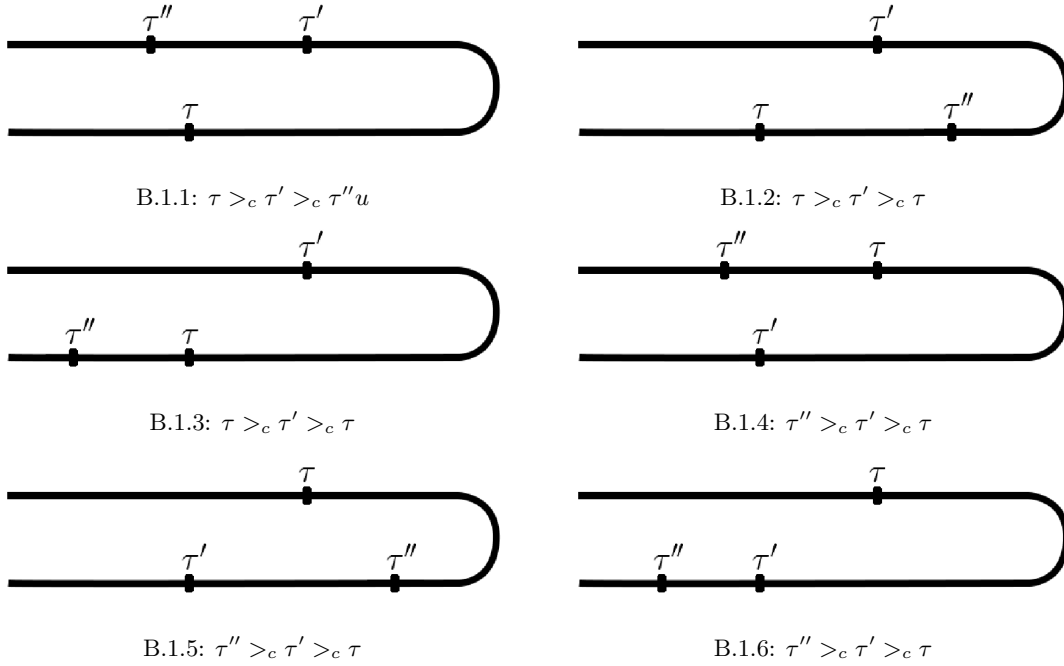


**Figure B.1:** Keldysh time ordering of three different times  $\tau$ ,  $\tau'$  and  $\tau''$ .



# Matlab code

---

```

1 function ss = szsz(T)
2     Nx=16;
3     Ny=16;
4     Nz=16;
5
6     d = 1.01;
7     D=3;
8     z=2*D;
9
10    for t = 1:length(T),
11        ssi = 0;
12        for nx = -Nx:1:Nx,
13            for ny = -Ny:1:Ny,
14                for nz = -Nz:1:Nz,
15                    dk = [nx/Nx,ny/Ny,nz/Nz];
16                    if ((sum(dk.^2) <= sum((abs(dk) - [1,1,1]).^2)) && (dk(1)<=1) ...
17                        && (dk(2)<=1) && (dk(3)<=1)), % includes only FBZ
18                        gamma = 1/D*sum(cos(dk*pi));
19                        omega = z*1/2*sqrt(d^2-gamma^2);
20                        ssi = ssi + 1/(2*sinh(omega/(2*T(t)))^2);
21                    end
22                end
23            end
24        ss(t) = ssi/((2*Nx+1)*(2*Ny+1)*(2*Nz+1))^2;
25    end
26
27 function ss = spsm(T,q)
28     Nx=16;
29     Ny=16;
30     Nz=16;
31     N=8*Nx*Ny*Nz;
32
33     qx = q(1);
34     qy = q(2);
35     qz = q(3);

```

```

36
37     D = 3;
38     z = 2*D;
39     d = 1.01;
40
41     for t=1:length(T),
42         dq = [qx/Nx, qy/Ny, qz/Nz];
43         sgn = 1;
44         if (sum(dq.*dq) > sum([1,1,1]-abs(dq)).^2),
45             dq = dq-sign(dq+ones(1,3)*1E-12);
46             sgn = -1; % Determining the sign of (-1)^n
47         end
48         gamma = 1/D*sum(cos(dq*pi));
49         omega = z*1/2*sqrt(d^2-gamma^2);
50         ss(t) = 1/(2*N)*(1+exp(-omega/T(t)))/(1-exp(-omega/T(t)))*sqrt((1-sgn*...
51             gamma/d)/(1+sgn*gamma/d));
52
53 function [ sxsx, qss ] = sxsx( T , q )
54
55     Nx = 16;
56     Ny = 16;
57     Nz = 16;
58
59     N = 8*Nx*Ny*Nz;
60
61     dq = [q(1)/Nx, q(2)/Ny, q(3)/Nz];
62
63     D = 3;
64     z = 2*D;
65     d = 1.01;
66
67     ss = 0;
68     for nx = 0:(2*Nx-1),
69         for ny = 0:(2*Ny-1),
70             for nz = 0:(2*Nz-1),
71                 n = [nx, ny, nz];
72                 if (mod(nx+ny+nz,2)==0)
73                     ss = ss + exp(i*sum(dq.*n)*pi);
74                 else
75                     ss = ss - exp(i*sum(dq.*n)*pi);
76                 end
77             end
78         end
79     end
80     ss = real(ss);
81
82     qss = zeros(size(T));
83     if (q == [16, 16, 16]),
84         for nx = -Nx:Nx,
85             for ny = -Ny:Ny,
86                 for nz = -Nz:Nz,
87                     dk = [nx/Nx, ny/Ny, nz/Nz];
88                     if ((sum(dk.^2) <= sum([1,1,1]).^2) && (dk(1)<=1) ...
89                         && (dk(2)<=1) && (dk(3)<=1))
90                         gammak = 1/D*sum(cos(dk*pi));
91                         thetak = .5*atanh(gammak/d);
92                         omegak = z*1/2*sqrt(d^2-gammak^2);
93                         for t=1:length(T),

```

---

```
92         nk = 1/(exp(omegak/T(t))-1);
93         qss(t) = qss(t) + 2*nk*cosh(thetak)^2+2*(1-nk)*sinh(...
          thetak)^2;
94     end
95     end
96     end
97     end
98     end
99     end
100
101     sxx = 1/N^2*(0.5*ss)^2*ones(size(T)) - 2/N^2*.5*ss*qss;
```





APPENDIX D

**Article**

---

Antiferromagnetic noise correlations in optical lattices

arXiv:0907.0652v1

Authors: G. M. Bruun, O. F. Syljuåsen, K. G. L. Pedersen, B. M. Andersen,  
E. Demler, A. S. Sørensen

# Antiferromagnetic noise correlations in optical lattices

G. M. Bruun<sup>1,2</sup>, O. F. Syljuåsen<sup>3</sup>, K. G. L. Pedersen<sup>4</sup>, B. M. Andersen<sup>4</sup>, E. Demler<sup>5</sup>, A. S. Sørensen<sup>4</sup>

<sup>1</sup>*Niels Bohr International Academy, University of Copenhagen, DK-2100 Copenhagen Ø, Denmark*

<sup>2</sup>*Mathematical Physics, Lund Institute of Technology, P. O. Box 118, SE-22100 Lund, Sweden*

<sup>3</sup>*Department of Physics, University of Oslo, P. O. Box 1048 Blindern, N-0316 Oslo, Norway*

<sup>4</sup>*Niels Bohr Institute, University of Copenhagen, DK-2100 Copenhagen Ø, Denmark*

<sup>5</sup>*Department of Physics, Harvard University, Cambridge, Massachusetts 02138, USA*

(Dated: July 3, 2009)

We analyze how noise correlations probed by time-of-flight (TOF) experiments reveal antiferromagnetic (AF) correlations of fermionic atoms in two-dimensional (2D) and three-dimensional (3D) optical lattices. Combining analytical and quantum Monte Carlo (QMC) calculations using experimentally realistic parameters, we show that AF correlations can be detected for temperatures above and below the critical temperature for AF ordering. It is demonstrated that spin-resolved noise correlations yield important information about the spin ordering. Finally, we show how to extract the spin correlation length and the related critical exponent of the AF transition from the noise.

PACS numbers: 05.40.Ca, 37.10.Jk, 75.40.Cx, 75.50.Ee

Atoms in optical lattices hold the potential to unravel the fundamental physics of phenomena related to quantum systems in periodic potentials including spin phases and high- $T_c$  superconductors [1]. One has already observed the Mott insulator transition for bosons [2], the emergence of superexchange interactions [3], the transition between metallic, band-insulator and Mott phases for fermions [4, 5], and fermionic pairing [6]. In addition to creating these lattice systems at sufficiently low temperatures  $T$ , a major challenge is how to detect the various phases predicted theoretically. These phases can be investigated via higher order correlation functions which only show up as quantum noise in most experiments. Quantum spin noise spectroscopy [7, 8] and the measurement of correlations of the momentum distribution of the atoms after release from the lattice (TOF experiments) are two ways to probe these correlation functions [9]. TOF experiments have already been used to detect pairing correlations in a Fermi gas [10], bosonic bunching and fermionic anti-bunching of atoms in optical lattices [11], the Mott-superfluid transition for bosons [12], and the effects of disorder in the Mott phase [13].

Here, we show how AF correlations of fermionic atoms in optical lattices give rise to distinct measurable signals in TOF experiments even above the critical temperature for magnetic ordering. Spin-resolved experiments are demonstrated to yield additional information which can be used to identify the magnetic ordering and broken symmetry axis. The main results are illustrated in Figs. 1-2 which show noise correlations in the momentum distributions after expansion as a function of temperature and momentum. We finally discuss how the spin correlation length and the related critical exponent  $\nu$  can be extracted experimentally from the noise.

We consider a two-component Fermi gas in an optical lattice of size  $N = N_x N_y N_z$ . In the limit of strong repulsion the gas is in the Mott phase for low  $T$  at half-filling

and can be described by the Heisenberg model

$$\hat{H} = J \sum_{\langle l, m \rangle} [\hat{s}_l^x \hat{s}_m^x + \hat{s}_l^y \hat{s}_m^y + (1 + \Delta) \hat{s}_l^z \hat{s}_m^z]. \quad (1)$$

Here  $\hat{s}_l$  is the spin-1/2 operator for atoms at site  $\mathbf{r}_l$  and  $\langle l, m \rangle$  denotes neighboring pairs. The interaction is  $J = 4t_\uparrow t_\downarrow / U$ , with  $U > 0$  the on-site repulsion between atoms and  $t_\sigma$  the spin-dependent tunneling matrix element. The anisotropy parameter is  $\Delta = -(t_\uparrow - t_\downarrow)^2 / (t_\uparrow^2 + t_\downarrow^2)$ . Below we consider both cubic (3D) and square (2D) lattices with lattice constant  $a$  of unity. We do not include any effects of a trapping potential.

A major experimental goal is to detect the onset of AF correlations with decreasing  $T$ . TOF experiments probe correlation functions of the form [11]

$$C_{AB}(\mathbf{r} - \mathbf{r}') = \frac{\langle \hat{A}(\mathbf{r}) \hat{B}(\mathbf{r}') \rangle - \langle \hat{A}(\mathbf{r}) \rangle \langle \hat{B}(\mathbf{r}') \rangle}{\langle \hat{A}(\mathbf{r}) \rangle \langle \hat{B}(\mathbf{r}') \rangle}, \quad (2)$$

where  $\hat{A}(\mathbf{r})$  and  $\hat{B}(\mathbf{r})$  are atomic observables measured at  $\mathbf{r}$  after expansion. In Refs. 10, 11, the atomic density correlations  $C_{nn}(\mathbf{d})$  were measured with  $\hat{A}(\mathbf{r}) = \hat{B}(\mathbf{r}) = \sum_\sigma \hat{n}_\sigma(\mathbf{r})$  the density operator of the atoms. Here  $\hat{n}_\sigma(\mathbf{r}) = \hat{\psi}_\sigma^\dagger(\mathbf{r}) \hat{\psi}_\sigma(\mathbf{r})$  with  $\hat{\psi}_\sigma(\mathbf{r})$  the field operator for atoms in spin state  $\sigma$ . We also consider the correlations between images of each of the spin components  $C_{\parallel}(\mathbf{d})$  corresponding to  $\hat{A}(\mathbf{r}) = \hat{n}_\uparrow(\mathbf{r})$  and  $\hat{B}(\mathbf{r}) = \hat{n}_\downarrow(\mathbf{r})$ . This may be achieved by, e.g., spatially separating the two atomic spin states using a Stern-Gerlach technique [14]. By applying a  $\pi/2$  pulse before the expansion one can also gain access to the spin noise perpendicular to the  $z$  component  $C_{\perp}(\mathbf{d})$  corresponding to  $\hat{A}(\mathbf{r}) = \exp(i\hat{s}^y \pi/2) \hat{n}_\uparrow(\mathbf{r}) \exp(-i\hat{s}^y \pi/2)$  and  $\hat{B}(\mathbf{r}) = \exp(i\hat{s}^y \pi/2) \hat{n}_\downarrow(\mathbf{r}) \exp(-i\hat{s}^y \pi/2)$ .

After normal ordering and expansion of the field oper-

ators in the lowest band Wannier states, we obtain

$$C_{\text{nn}}(\mathbf{k}) = \frac{1}{N} - \frac{1}{2}\delta_{\mathbf{k},\mathbf{K}} - 2\langle\hat{\mathbf{s}}_{\mathbf{k}} \cdot \hat{\mathbf{s}}_{-\mathbf{k}}\rangle, \quad (3)$$

$$C_{\parallel}(\mathbf{k}) = \frac{1}{2N} - \langle\hat{s}_0^z \hat{s}_0^z\rangle - \langle\hat{s}_{\mathbf{k}}^x \hat{s}_{-\mathbf{k}}^x\rangle - \langle\hat{s}_{\mathbf{k}}^y \hat{s}_{-\mathbf{k}}^y\rangle, \quad (4)$$

$$C_{\perp}(\mathbf{k}) = \frac{1}{2N} - \langle\hat{s}_0^x \hat{s}_0^x\rangle - \langle\hat{s}_{\mathbf{k}}^y \hat{s}_{-\mathbf{k}}^y\rangle - \langle\hat{s}_{\mathbf{k}}^z \hat{s}_{-\mathbf{k}}^z\rangle, \quad (5)$$

where  $\mathbf{K}$  is a reciprocal lattice vector, and  $\hat{\mathbf{s}}_{\mathbf{k}} = N^{-1} \sum_l \hat{s}_l e^{-i\mathbf{k}\cdot\mathbf{r}_l}$ . We assume free expansion of the atoms for a duration  $t$ , neglect autocorrelation terms  $\propto \delta(\mathbf{d})$  in (3)-(5), and express  $C$  in terms of the momentum  $\mathbf{k} = m\mathbf{d}/t$  ( $\hbar = 1$  throughout). These correlation functions have contributions with different scalings. For 3D systems, the spins order below the Néel temperature  $T_N$ . Assuming the broken symmetry axis along the  $z$  axis,  $C_{\text{nn}}$  and  $C_{\perp}$  have a contribution from  $\langle\hat{s}_{\mathbf{k}}^z \hat{s}_{-\mathbf{k}}^z\rangle \sim \mathcal{O}(1)$  at  $\mathbf{k} = (\pi, \pi, \pi)$  for  $T < T_N$ . At other momenta or for  $T > T_N$  the correlation functions scale as  $1/N$ . Note that we will perform calculations where the total spin  $\propto \hat{s}_0^z$  of the lattice is allowed to fluctuate, which is different from the experimental situation where the number of particles in each spin state is fixed. This may give rise to different momentum independent terms in (3)-(5) for the experiment, but the  $k$  dependent part should be accurately captured by our calculations.

Experiments take 2D column density images of the expanding cloud corresponding to integrating over  $z$  and  $z'$  in both the numerator and denominator in (2). The cameras also introduce a smoothening in the  $xy$ -plane, which can be modeled by convolution with a Gaussian [11]. In total, the experimental procedure corresponds to measuring the averaged correlation function

$$C^{\text{exp}}(\mathbf{k}_{\perp}) = \frac{1}{4\pi N \kappa^2} \sum_{\mathbf{k}'} e^{-\frac{1}{4\kappa^2} \frac{1}{(2\pi)^2} (\mathbf{k}'_{\perp} - \mathbf{k}_{\perp})^2} C(\mathbf{k}'), \quad (6)$$

where  $\mathbf{k}_{\perp} = (k_x, k_y)$  and  $\kappa = w/l$  with  $l = 2\pi t/ma$  (keeping  $a$  for clarity) and  $w$  a width depending on the pixel resolution of the CCD camera. The averaging in the  $z$ -direction reduces the contributions to  $C_{\text{nn}}$  and  $C_{\perp}$  at  $\mathbf{k} = (\pi, \pi, \pi)$  from  $\mathcal{O}(1)$  for  $T < T_N$  to  $1/N_z$  and the Gaussian smoothening further reduces it to  $\mathcal{O}(1/\kappa^2 N)$ . This reduction happens because the correlations are restricted to a single point  $\mathbf{k} = (\pi, \pi, \pi)$  and we are averaging over  $N_z \cdot N_x N_y / \kappa^2$  points. Away from  $\mathbf{k}_{\perp} = (\pi, \pi)$  or for  $T > T_N$  the correlations have a wider distribution and they are less affected by the averaging.

We plot in Fig. 1  $C_{\text{nn}}^{\text{exp}}(k, k)$  as a function of  $k = k_x = k_y$  and  $T$  for a 3D lattice of size  $N = 32^3$ . The spin correlation functions  $\langle\hat{\mathbf{s}}_{\mathbf{k}} \cdot \hat{\mathbf{s}}_{-\mathbf{k}}\rangle$  were calculated using QMC simulations using the Stochastic Series Expansion method [15] with directed-loop updates [16]. This method is very efficient for Heisenberg models and gives accurate results for a wide range of  $T$  for large systems. For the isotropic Heisenberg model, the QMC calculations yield  $T_N \simeq 0.945J$  in agreement with Ref. 18.  $C_{\text{nn}}^{\text{exp}}$

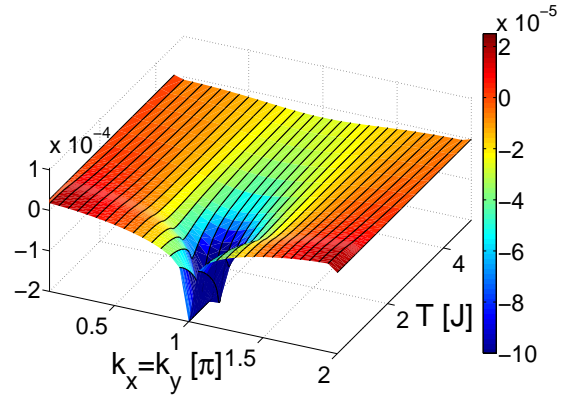


FIG. 1: (Color online) Plot of  $C_{\text{nn}}^{\text{exp}}(\mathbf{k}_{\perp})$  versus temperature  $T$  and momentum along a diagonal cut  $k = k_x = k_y$ .

was then calculated from (3) with the  $k_z$  average in (6) included to simulate the experimentally relevant situation [11]. The main feature of the plot is the dip at  $k = \pi$  coming from AF ordering. For  $T < T_N$ , this gives rise to a large Bragg dip at  $k_x = k_y = \pi$  [9, 17]. We see that the Bragg dip remains also above  $T_N$  but has a larger width due to AF correlations without long range order. The spin correlation length  $\xi$  can be extracted directly from the width of the dip which decreases with decreasing  $T - T_N$  reflecting that  $\xi$  increases as  $\xi \sim 1/|T - T_N|^{\nu}$  for  $T \rightarrow T_N^+$ . We show below how the noise indeed can be used to extract the critical exponent  $\nu$ . At high  $T$  the AF correlations lead to singlet formation of neighboring spins. This gives rise to a precursor of the Bragg peak at  $k_x = k_y = \pi$  and an equal signal of opposite sign at  $\mathbf{k}_{\perp} = 0$  [see (7)]. These momentum correlations can be understood by noting that two fermions in a singlet are more (less) likely to have the same (opposite) momentum due to the Pauli exclusion principle. The uniform spin noise case  $k = 0$  was also considered in [8].

In the high- $T$  limit  $J/T = 1/\tilde{T} \ll 1$  ( $k_B = 1$ ), controlled analytical results for the correlation functions (3)-(5) may be obtained by expanding in  $\tilde{T}^{-1}$ . We obtain

$$C_{\text{nn}}(\mathbf{k}) = -\frac{1}{2}\delta_{\mathbf{k},\mathbf{K}} - \frac{1}{2N} + \frac{3Z\gamma_{\mathbf{k}}}{8N\tilde{T}} + \mathcal{O}(\tilde{T}^{-2}), \quad (7)$$

$$C_{\parallel}(\mathbf{k}) = C_{\perp}(\mathbf{k}) = -\frac{1}{4N} + \frac{Z}{8N\tilde{T}}\left(\frac{1}{2} + \gamma_{\mathbf{k}}\right) + \mathcal{O}(\tilde{T}^{-2}) \quad (8)$$

with  $Z = 4(6)$  for 2D(3D) lattices. For simplicity we have taken  $\Delta = 0$  and  $\gamma_{\mathbf{k}} = Z^{-1} \sum_{\mathbf{a}} 2 \cos(\mathbf{k} \cdot \mathbf{a})$  where  $\sum_{\mathbf{a}}$  sums over the unit vectors spanning the lattice. The average of (7) and (8) over  $z$  can be obtained by simply omitting the  $z$  direction in the sum.

To obtain analytic expressions for low  $T$ , we perform a spin-wave calculation, which should be fairly accurate for a 3D system at  $T \ll T_N$ . This yields after some algebra

$$C_{\parallel}(\mathbf{k}) = \frac{1}{2N} - \langle\hat{s}_0^z \hat{s}_0^z\rangle - \frac{1}{2N}(1 + 2f_{\mathbf{k}})e^{-2\Theta_{\mathbf{k}}}, \quad (9)$$

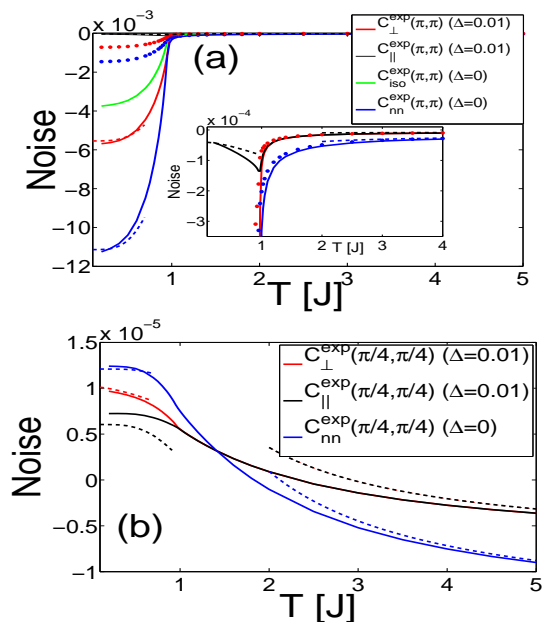


FIG. 2: (Color online) Noise correlation functions  $C_{\perp}^{\text{exp}}(\mathbf{k}_{\perp})$  (red),  $C_{\parallel}^{\text{exp}}(\mathbf{k}_{\perp})$  (black),  $C_{\text{iso}}^{\text{exp}}(\mathbf{k}_{\perp})$  (green), and  $C_{\text{nn}}^{\text{exp}}(\mathbf{k}_{\perp})$  (blue) versus  $T$  at  $\mathbf{k}_{\perp} = (\pi, \pi)$  (a) and  $\mathbf{k}_{\perp} = (\pi/4, \pi/4)$  (b). The dotted (solid) lines are with (without) Gaussian smearing ( $\kappa = 1/40$ ). Dashed lines show the analytical results (7)-(9). Inset (a): same plot but zoomed in near  $T_N$ .

where  $\tanh 2\Theta_{\mathbf{k}} = \gamma_{\mathbf{k}}/(1 + \Delta)$  and  $f_{\mathbf{k}} = [\exp \omega_{\mathbf{k}}/T - 1]^{-1}$  is the Bose distribution function for the spin-waves with energy  $\omega_{\mathbf{k}} = 3J\sqrt{(1 + \Delta)^2 - \gamma_{\mathbf{k}}^2}$ . We also have  $\langle \hat{s}_{\mathbf{k}}^z \hat{s}_{-\mathbf{k}}^z \rangle = \sum_{\mathbf{k}'} \sinh^{-2}(\beta\omega_{\mathbf{k}}/2)/2N^2$  where the sum extends over the AF reduced Brillouin zone [8]. A similar but somewhat more lengthy expression can be derived for  $C_{\perp}(\mathbf{k})$ .

We plot in Fig. 2  $C_{\text{nn}}^{\text{exp}}(\mathbf{k}_{\perp})$ ,  $C_{\parallel}^{\text{exp}}(\mathbf{k}_{\perp})$ , and  $C_{\perp}^{\text{exp}}(\mathbf{k}_{\perp})$  as a function of  $T$  for  $\mathbf{k}_{\perp} = (\pi, \pi)$  (a) and  $\mathbf{k}_{\perp} = (\pi/4, \pi/4)$  (b) for the same parameters as above. The solid curves include the average over  $k_z$  only and the dotted curves include a Gaussian smearing in the  $(k_x, k_y)$  plane as well. The values for  $T \rightarrow 0$  with Gaussian smearing are consistent with the results of Refs. [11] given the different system size and slightly different measured quantities. For simplicity we have excluded the Gaussian averaging for  $\mathbf{k}_{\perp} = (\pi/4, \pi/4)$  since it [contrary to the  $\mathbf{k}_{\perp} = (\pi, \pi)$  case] leads to only negligible changes. We trigger the AF ordering along the  $z$ -direction for  $T < T_N$  by including a small anisotropy  $\Delta = 0.01$  for  $C_{\parallel}^{\text{exp}}$  and  $C_{\perp}^{\text{exp}}$ .

Figure 2(a) shows the Bragg dip for  $T < T_N$  coming from  $\langle \hat{s}_{\mathbf{k}}^z \hat{s}_{-\mathbf{k}}^z \rangle \approx |\langle s_i^z \rangle|^2$  for  $\mathbf{k} = (\pi, \pi, \pi)$  with  $|\langle s_i^z \rangle| > 0$ . Extrapolating to  $T = 0$  we have  $|\langle s_i^z \rangle| \simeq 0.43 \pm 0.01$ , a value reduced from  $1/2$  by quantum fluctuations. On the other hand the spin noise parallel to the broken symmetry axis  $C_{\parallel}$  is reduced with the onset of magnetic ordering for  $T < T_N$  as can be seen from the inset in Fig. 2(a). (The minimal value of  $C_{\parallel}$  at  $T_N$  is dependent on the anisotropy  $\Delta$ .) Note that even though the density correlations are

larger and hence more easily measurable, the spin resolved measurements are crucial in verifying e.g. whether the correlation dip is indeed due to magnetic ordering and not caused, for example, by formation of a period-doubled charge-density wave. The difference between  $C_{\parallel}$  and  $C_{\perp}$  for  $\Delta > 0$  can furthermore be used to identify the broken symmetry axis. In the isotropic case, there is no broken symmetry axis and  $C_{\parallel}^{\text{exp}} = C_{\perp}^{\text{exp}} = C_{\text{iso}}^{\text{exp}}$  for  $\Delta \rightarrow 0$ , as can be seen from the green curve in Fig. 2(a).

The calculated correlations are rather small even for the quantities including the macroscopic contribution  $\langle \hat{s}_{\mathbf{k}}^z \hat{s}_{-\mathbf{k}}^z \rangle \approx |\langle s_i^z \rangle|^2$  at  $\mathbf{k} = (\pi, \pi, \pi)$ , e.g., for low temperatures  $T \lesssim J/2$   $C_{\text{nn}}^{\text{exp}} \approx 10^{-2}$  ( $10^{-3}$ ) without (with) Gaussian smearing and scales like  $1/N_z$  ( $1/N$ ). This is, however, still significantly larger than the correlations of order  $C_{\text{nn}} \sim 10^{-4}$  which were recently measured with slightly bigger system sizes [11]. The correlations are also close to the measured experimental values even for temperatures above  $T_N$ , i.e., for  $T = 2J$  we have  $C_{\text{nn}}^{\text{exp}} \approx 6 \cdot 10^{-5}$  (scaling as  $1/N$ ), which is comparable to the recent experiments [11]. The measurement of noise correlations can thus be used to show the onset of AF order even above the critical temperature. Furthermore, for current experiments the spin temperature is uncertain because there are no sensitive probes. If the noise correlations are measured, the detailed theoretical curves presented here would provide a means of assessing the spin temperature in the experiments.

The density and spin noise at  $\mathbf{k}_{\perp} = (\pi/4, \pi/4)$  depicted in Fig. 2(b) exhibit a different behavior from that at  $\mathbf{k}_{\perp} = (\pi, \pi)$ : it now decreases in numerical value for high  $T$  and even changes sign above  $T_N$ . This unusual behavior is a geometric effect of the lattice. Note that since the noise scales as  $1/N$  away from the Bragg point, a measurement requires higher experimental resolution than what is presently available or more sensitive detection methods such as spin noise spectroscopy [8].

Atomic gases are well suited to study fundamental problems in 2D physics as the observation of the Berezinskii-Kosterlitz-Thouless transition illustrates [19]. Recently, single layer 2D atomic gases have been produced which avoids the averaging over  $z$  discussed above [20]. We now study the Mott phase at half-filling for a 2D square lattice. In 2D there is no ordered phase for  $T > 0$  due to fluctuations, but there are still significant AF correlations [21]. This is illustrated in Fig. 3(a), which shows  $C_{\text{iso}}^{\text{exp}}(\mathbf{k}_{\perp})$  and  $C_{\text{nn}}^{\text{exp}}(\mathbf{k}_{\perp})$  as a function of  $T$ . The AF correlations give rise to a large dip for  $\mathbf{k}_{\perp} = (\pi, \pi)$  both in the density and spin noise which is a precursor of the AF ordered state at  $T = 0$ . Since there is no averaging over the  $z$ -direction, the correlations are much stronger than for a 3D system above  $T_N$ . Figure 3 illustrates that the noise exhibits the same non-trivial features as a function of  $k$  and  $T$  as the 3D case.

Critical exponents characterizing continuous phase transitions are often difficult to measure. We now demon-

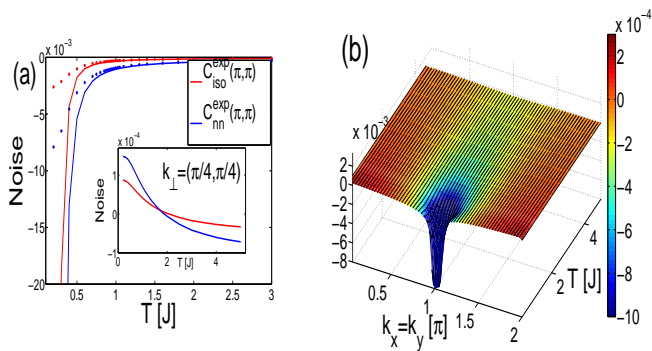


FIG. 3: (Color online) (a) Noise correlation functions  $C_{\text{iso}}^{\text{exp}}(\mathbf{k}_{\perp})$  (red) and  $C_{\text{nn}}^{\text{exp}}(\mathbf{k}_{\perp})$  (blue) versus  $T$  at  $\mathbf{k}_{\perp} = (\pi, \pi)$  for a 2D lattice. The curves are obtained from QMC simulations on  $64 \times 64$  lattices. The dotted (solid) lines are with (without) Gaussian smearing using  $\kappa = 1/40$ . Inset: same as solid lines in main panel except at  $\mathbf{k}_{\perp} = (\pi/4, \pi/4)$ . (b) Same as Fig. 1 but for a 2D system without the  $k_z$  summation.

strate how noise measurements can be used to obtain the critical exponent  $\nu$ . The correlation length  $\xi$  can be extracted from the width of the AF dip in the 3D resolved function  $C_{\text{nn}}(\mathbf{k})$  at  $\mathbf{k} = (\pi, \pi, \pi)$ . We find that this yields a critical exponent  $\nu \approx 0.70$  as expected for a 3D Heisenberg model [22]. Importantly,  $\nu$  can also be extracted from the experimentally relevant  $k_z$ -summed correlation function  $C_{\text{nn}}^{\text{exp}}$ . Figure 4(a-c) show  $C_{\text{nn}}^{\text{exp}}(\mathbf{k}_{\perp})$  at three fixed temperatures above  $T_N$ . To obtain  $\nu$ , we fit  $C_{\text{nn}}^{\text{exp}}(\mathbf{k}_{\perp})$  to a summed lattice propagator of the form  $\sum_{k_z} [2(3 - \sum_{\alpha=x,y,z} \cos(k_{\alpha} - \pi))\xi^2 + 1]^{-1}$  with  $k_z = 2\pi n_z/N_z$ . Figure 4(d) shows the extracted correlation length  $\xi$  for various system sizes. One clearly sees the finite-size effects setting in at decreasing  $T - T_N$ . The

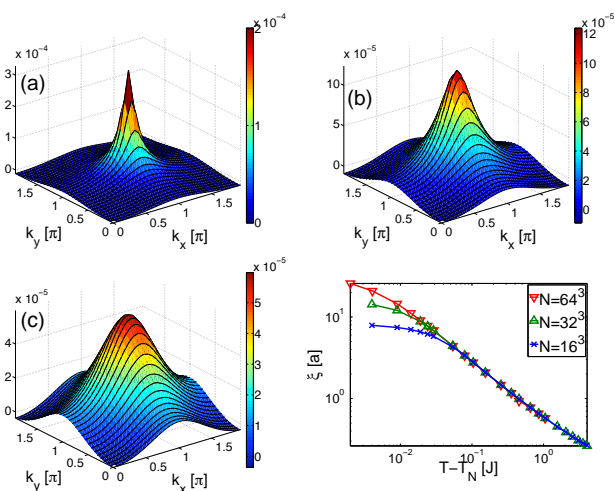


FIG. 4: (Color online) Panels (a-c) show  $(-1)C_{\text{nn}}^{\text{exp}}(\mathbf{k}_{\perp})$  at  $T/J = 1.0$  (a),  $T/J = 1.2$  (b), and  $T/J = 1.6$  (c). (d) Log-log plot of extracted correlation length  $\xi$  versus  $|T - T_N|$  displaying the power-law behavior  $\xi \sim |T - T_N|^{-0.70}$ .

extracted power-law yields  $\nu \approx 0.70$ . To obtain a robust value for  $\nu$  one needs to probe the noise for temperatures where it is somewhat smaller than what has been measured to date. This would however enable one to probe the critical properties of the AF transition.

In summary, we performed analytic and numerical calculations modeling TOF experiments for repulsive fermionic atoms in optical lattices using experimentally realistic parameters. This demonstrated that such experiments are well suited to detect AF correlations both below and above the critical temperature. Spin-resolved measurements were shown to yield valuable additional information and we finally discussed how to extract the critical exponent governing the correlation length close to the AF transition from the noise.

We thank H. Moritz for the suggestion to look at TOF experiments. The QMC simulations were carried out using resources provided by the NOTUR project of the Norwegian Research Council. B. M. A. acknowledges support from the Villum Kann Rasmussen foundation and E. D. from NSF DMR-0705472, CUA, DARPA, MURI.

- 
- [1] W. Hofstetter *et al.*, Phys. Rev. Lett. **89**, 220407 (2002); L.-M. Duan, E. Demler, and M. D. Lukin *ibid.*, **91**, 090402 (2003).
  - [2] M. Greiner *et al.*, Nature **415**, 39 (2002).
  - [3] S. Trotzky *et al.*, Science **319**, 295 (2008).
  - [4] R. Jördens *et al.*, Nature **455**, 204 (2008).
  - [5] U. Schneider *et al.*, Science **322**, 1520 (2008).
  - [6] J. K. Chin *et al.*, Nature **443**, 961 (2006).
  - [7] K. Eckert *et al.* Nat. Phys. **4**, 50 (2007).
  - [8] G. M. Bruun *et al.* Phys. Rev. Lett. **102**, 030401 (2009).
  - [9] E. Altman, E. Demler, and M. D. Lukin, Phys. Rev. A **70**, 013603 (2004).
  - [10] M. Greiner *et al.* Phys. Rev. Lett. **94** 110401 (2005).
  - [11] S. Fölling *et al.*, Nature **434**, 481 (2005); T. Rom *et al.*, *ibid* **444**, 733 (2006).
  - [12] I. B. Spielman, W. D. Phillips, and J. V. Porto, Phys. Rev. Lett. **98**, 080404 (2007).
  - [13] V. Guarrera *et al.*, Phys. Rev. Lett. **100**, 250403 (2008).
  - [14] T. Esslinger, private communication.
  - [15] A. W. Sandvik and J. Kurkijärvi, Phys. Rev. B **43**, 5950 (1991).
  - [16] O. F. Syljuåsen and A. W. Sandvik, Phys. Rev. E **66**, 046701 (2002).
  - [17] B. M. Andersen and G. M. Bruun, Phys. Rev. A **76**, 041602 (2007).
  - [18] A. W. Sandvik, Phys. Rev. Lett. **80**, 5196 (1998).
  - [19] Z. Hadzibabic *et al.*, Nature **441**, 1118 (2006); V. Schweikhard, S. Tung, and E. A. Cornell, Phys. Rev. Lett. **99**, 030401 (2007); P. Cladé *et al.*, arXiv:0805.3519.
  - [20] N. Gemelke *et al.* arXiv:0904.1532; J. I. Gillen *et al.*, arXiv:0812.3630.
  - [21] A. Auerbach, *Interacting Electrons and Quantum Magnetism*, (Springer Verlag, 1998).
  - [22] A. Pelissetto and E. Vicari, Phys. Rep. **368**, 549 (2002).

**[nano.ku.dk/english/research/nanotheory](https://nano.ku.dk/english/research/nanotheory)**

Theory for Nanosystems

Niels Bohr Institute

Copenhagen University

H. C. Ørsted Institutet, Bygning D Universitetsparken 5

DK-2100 København N

Denmark